THE VIBRATION CHARACTERISTICS

OF

PACKAGES OF THICK, PRETWISTED

TURBINE BLADES

N. D. COGGER, B.Sc., M.I.O.A., A.M.R.Ae.S.

Kingston Polytechnic

in collaboration with the University of Surrey

April 1979

Submitted in partial fulfilment of the requirements for

the Degree of Doctor of Philosophy

VOLUME CONTAINS CLEAR OVERLAYS

OVERLAYS HAVE BEEN SCANNED SEPERATELY AND THEN AGAIN OVER THE RELEVANT PAGE

A B S T R A C T

THE VIBRATION CHARACTERISTICS OF PACKAGES OF THICK, PRETWISTED TURBINE BLADES

N. D. Cogger

A consideration of the working environment of turbine blade assemblies demonstrates the necessity for preventing vibration induced fatigue failures and this study seeks to establish an adaptable and efficient method to enable the designer to predict the frequencies at which such failures could arise.

Exact mathematical solutions to the problem are not, generally, possible and thus recourse must be made to approximation techniques, such as lumped parameter and finite element modelling. In this study, a survey of such techniques shows that although a finite element model may be more accurate than a lumped parameter solution for the two dimensional analysis of untwisted blade packages the latter is more amenable to the modifications required by the three dimensional analysis of pretwisted blading. It is also demonstrated that the inclusion of such factors as non-uniform blading, rotation of the bladed disc assembly and improvements in the accuracy of the model do not generally increase the complexity of the problem when such a technique is employed.

The Myklestad lumped mass model for the analysis of beams has, therefore, been adapted to turbine blade packages enabling tangential, torsional, axial and longitudinal modes to be calculated.

Concomitant experimental analyses of simplified blade package models have been undertaken using Laser holographic and interferometric techniques to assess the accuracy of predicted vibration frequencies and modal shapes. Good agreement is shown to exist and where differences have occurred improvements in the model have shown to amend the solution.

It is concluded that lumped parameter modelling is capable of providing a flexible, perspicuous and economic tool for use in the design of turbine blade packages. The simplicity of the basic model allows the effect of modifications to be easily assessed. whilst the accuracy is considered to remain within the limits imposed by manufacturing tolerances.

CONTENTS

CONTENTS

CONTENTS

LIST OF TABLES

LIST OF FIGURES

LIST OF FIGURES

NOMENCLATURE

(i) Theoretical Analysis

A Cross-sectional area; a coefficient

[A] Matrix of influence coefficients

a Coefficient

B Substitution for bending moment, $(X''/EI)(L/N)^2$; a constant

C Coefficient

{C} Eigenvector, $[M]^{\frac{1}{2}}\{X\}$

D Substitution for slope, $X'(L/N)$

E Young's modulus

F Shear force at point z

F_c Centrifugal force

f Natural frequency of vibration of a beam

G Modulus of rigidity

H Ratio of major and minor second moments of area; axis

[H] Symmetrical matrix, $[L]^{-1}[M][L]^{-1T}$

I Second moment of area of cross-section

I_p Polar moment of inertia

J Inertia of beam; torsional constant

j Dimensions defining the junction of a blade and shroud in a package

K Shear stress distribution factor

[K] Stiffness matrix

L Length of beam

[L] Matrix with zero coefficients above the diagonal

M Bending moment at point z

[M] Mass matrix

m Elemental mass

NOMENCLATURE

N Number of elements, or subdivisions of beam

n Constant

P Load; axial tensile force; a coefficient

p Parameter defining taper; number

Q Coefficient

q Parameter defining taper

R Residual parameter; axis

r Constant

S Substitution for shear force, $(X'''/EI)(L/N)^3$

s Constant

T Kinetic energy; thickness of beam; torque

[T] Symmetrical matrix, $[M]^{\frac{1}{2}}[A][M]^{\frac{1}{2}}$

t Time

U Strain energy

u Longitudinal deformation

V Dimensionless frequency parameter, $L(m\omega^2/EIL)^{\frac{1}{4}}$; potential potential energy; axis

v Transverse deformation

W Dimensionless frequency parameter, $(V/N)^4$

X Amplitude of displacement x

x Displacement of beam at point z at time t; length

Y Amplitude of displacement y

y Displacement of beam in the "stiff" direction

Z Amplitude of longitudinal displacement at point z

{Z} Column matrix, $[L]^T\{\delta_0\}$

z Distance measured along beam from one end; element length

NOMENCLATURE

α Dimensionless constant, $T^2/12L^2$ or I/AL^2

β $(\mu^2 + \nu^2)^{\frac{1}{2}}$

γ Dimensionless constant, KE/G

Δ Small change in ....; $X_B' X_S - X_B X_S'$

δ Displacement; infinitesimal change in ....

ε $(\mu^2 - \nu^2)^{\frac{1}{2}}$

ε' $(\nu^2 - \mu^2)^{\frac{1}{2}}$

θ Pretwist of cross-section; angular displacement of an element

Λ Dimensionless parameter, $(m\omega^2 L/EA)^{\frac{1}{2}}$

λ Function of circular frequency, $1/\omega^2$

μ Frequency parameter (V/L)

ν Parameter defining taper, $\nu = p/2 = q/2$

ρ Mass/unit length

Ψ $((I\rho/GJ)\, L^2\omega^2)^{\frac{1}{2}}$

Ω Rotational speed

ω Circular frequency

(ii) Experimental Analysis

a Amplitude of light

d Object displacement

I Intensity of light

i Suffix denoting image

o Suffix denoting object

p Suffix denoting hologram plate

r Suffix denoting reference beam

T Exposure time of photographic plate

NOMENCLATURE

t	Time
x	variable
α	Angle of illumination
β	Angle of observation
Δ	Small change in ....
λ	Wavelength of light
Φ	Vibration amplitude term, $(2\pi/\lambda)\ 2d_o$
ϕ	Phase of light
ω	Circular frequency

1. THE THEORETICAL ANALYSIS OF TURBINE BLADES AND ASSEMBLIES

1.1 Introduction

The design engineer seeks to protect a component from in-service failure due to stress, temperature, corrosion and any other environmental effect by a combination of the methods of isolation and selection. When isolation is not possible the component properties must be selected so that the effects of the environment are most effectively resisted.

To avoid some groups of fatigue failures components must be designed such that certain frequencies of excitation will not give rise to excessive amplitudes of vibration. Often, these prohibited frequencies are known in advance of the initial design, the nature of the environment being sufficiently predictable, but in others the presence of an unsuspected source of vibration is not revealed until a prototype fails. In both instances it is important that the natural frequencies of vibration of the component be known, primarily to avoid dangerous excitations and secondly to aid the identification of the source of the failure.

Unless it can be readily established that only the fundamental frequency of a component is of significance, the analytical computation required for all but the simplest components requires the use of a digital computer to solve the relevant equations. In the study of the transverse vibrations of beams (in which domain can be included a wide range of design components) analytical solutions do exist, but only for the uniform case and certain mathematically contrived cases. In all

probability the typical designer has a limited knowledge of numerical methods of solution and only those engineers who specialise in vibration analysis have an opportunity to appreciate the many refinements of the basic methods.

The present work, therefore, seeks to establish a method to predict the natural frequencies of vibration of thick, pretwisted beams, with varying cross-section (in which category fall turbine blade packages). The work forms a natural extension to that by Allen (1), both in the theoretical analysis and the development of experimental techniques, using Laser holography, to assess the accuracy of the numerical solutions.

The importance of turbine disc vibration may be judged not only from the considerable amount of research undertaken in this field, but also by consideration of the working environment of the component. In addition to the torsional stresses of the disc, imposed by the transmission of torque from the blades to the shaft of the turbine,the blades themselves are subject to rapid, pulsating forces generated by the working fluid issuing from the stator. In general these forces may be considered as having axial and tangential components, but an additional radial component is provided by centrifugal forces, which can be considerable in present day high speed turbo-machinery. Temperature effects and imbalance of components can also add to this hostile environment, although the latter may be minimised by good manufacturing technique.

Since the failure of even a single blade can cause additional damage and the whole machine to be rendered inoperative it is of prime importance to prevent vibration induced fatigue

failure by careful design. Indeed, although improved materials and prediction methods have made rare failures due to static overloading, the demand for greater reliability with increased loads has meant that vibration induced fatigue failure remains a severe problem (2).

Although it can be shown that attaching turbine blades to a flexible disc can give rise to more complex vibration characteristics than if the blade is considered as a single cantilever (3) it is the blade which is most seriously affected by the intermittent forces of the working fluid and any vibration of the turbine assembly.

Consequently, this work aims to provide an adaptable, efficient and perspicuous method for prediction of the vibration characteristics of cantilevered turbine blades, including the effect of joining the blade tips with a shroud. Although this precludes a detailed study of the vibration of disc assemblies, consideration of this aspect will be given in the following discussion.

1.2 Approximation Techniques

1.2.1 Introduction

The analysis of a dynamic structural problem is more complex and time consuming than the static problem for two main reasons. The loading and the response to this loading vary with time and a succession of solutions corresponding to all times of interest in the response history needs to be established. Also, a dynamic load on a structure causes displacements associated with accelerations,which in turn produce inertia forces resisting these accelerations. It can easily be deduced that the displacements which cause the inertia forces are themselves affected by the magnitudes of these forces and thus the motion can only be described in terms of differential equations.

These differential equations of motion are generally not amenable to exact solution, except in a few simple, or mathematically contrived,cases. Additionally in most structures, whether based on plates or beams the mass and, therefore, the inertia forces are distributed continuously, giving rise to a system with an infinite number of degrees of freedom and thus an infinite number of resonant frequencies.

It is therefore necessary to approximate the real system to enable the required number of modes to be extracted with a suitable degree of efficiency and accuracy. Obviously this represents a compromise and several methods have been developed to facilitate an

expedient solution.

In order to derive a prediction method to enable the designer to establish the resonant frequencies of packages of pretwisted turbine blades it has been necessary to make an assessment of the approximation techniques currently available and develop that considered most suitable. Since the method is intended for use at the basic design stage it is considered that flexibility and ease of manipulation would be at least as important as accuracy and the discussion of the approximation techniques has been biased by this factor.

1.2.2 Lumped Parameter Modelling

From the preceding discussion it has been seen that, since a beam generally has a continuously distributed mass an infinite number of degrees of freedom and hence modal shapes is possible. In order to make the problem more tractable,one solution is to reduce the number of masses and therefore the inertia forces,by concentrating them at a finite number of discrete points, while the elastic properties of the structure are retained by considering the masses to be joined by light, uniform beams giving the correct flexural constant (EI). The displacements and accelerations need then only be defined at these points. Further restrictions may be applied to constrain the directions of motion of the structure. The number of degrees of freedom (and thus the number of natural frequencies) of the system is then restricted to the product of the number of masses and the

directions in which they are permitted to move.

Having defined the model there still exist alternative arithmetical solutions for solving the problem, either using tabulation methods, matrix relaxation or matrix iteration and reduction. The latter two techniques involve setting up the necessary number of simultaneous equations of motion, expressed as a matrix equation,from which eigen-values and eigen-vectors may be extracted. The former method, which is frequency selective, requires that each element is analysed in turn to satisfy dynamic and elastic conditions determined by the assumed frequency. If the end conditions are not satisfied for the type of beam further trial frequencies are assumed, based on the results of previous estimates, until the end conditions are satisfied, the frequency at which this occurs being a natural frequency of the system. The tabulation method used in this study is that due to Myklestad (4),itself based on the Holzer method for close-coupled torsional systems (5).

Obviously the greater the number of masses the more accurate becomes the approximation and several workers have shown that for most cases the accuracy converges to that of an exact solution at the rate of N^{-2}, if the beam has one or both ends free, or N^{-4} if the ends are clamped or pinned, where N is the number of masses. It can be seen from this convergence rate that there is an economic limit to the number of parameters beyond which the improvement in accuracy is too small to justify the

increased calculation time.

Since the accuracy of this type of model is dependent on the number of masses rather than the actual method of solution, contrary to the requirements of economy, it would appear that an improvement in the type of discrete element would be advantageous. Leckie and Lindberg (6) compared four models:-

i) concentrated masses connected by light uniform beams of flexural constant EI (a "Myklestad" model).

ii) light, rigid beam elements, connected by springs representing the flexural constant, with mass concentrated at the joints.

iii) rigid beam elements with distributed mass, connected by springs representing the flexural constant.

iv) rigid beam elements with distributed mass, supported at discrete points on a massless continuous beam of flexural constant EI. Between the supports the deflection of the mass varied linearly.

In all cases a finite difference technique was used to provide a solution from these models for free-free, simply supported and clamped-clamped beams. It was concluded that "no single model is entirely satisfactory under all circumstances and hence no positive recommendation can be made as to the best model to adopt".

The basic Myklestad model (i) was shown to give good

results for simply supported and clamped models, with the error varying as N^{-4}, but when applied to the free-free beam the error increased to vary as N^{-2}. The simple finite difference model (ii) and the "refined" model (iv) both gave poor results with the error varying as N^{-2}.

It is difficult to extrapolate these results to apply to the analysis of turbine blades, which can generally be assumed to be cantilevers (i.e. clamped-free beams) since this case was not considered and also the method which gave the better solution for the clamped beam, (i), gave poor results for a free beam, whilst the reverse was true for model (iii).

Allen (1) considered further improvements to the basic concentrated mass model with particular reference to the cantilever. By positioning the mass at the centre of the beam element instead of at the junction it was found that the error in the frequency parameter for the first four modes was reduced by a factor of -0.5. Allen then argued that since the mass concentrations at the beginning, middle and end of a given step are (0.5, 0, 0.5) for the Myklestad model and (0, 1, 0) for the central mass model, giving an error ratio between the two of 2:-1 it would be logical to assume that an improved accuracy would be obtained by forming a mass distribution of (1/6, 4/6, 1/6). These figures will be recognised as the multipliers used for summation and integration by Simpson's rule. This principle was then further extended by considering that, although all three models represent the first moment of

mass correctly the second moment is represented correctly only by the so-called "Simpson-model".

Now, the pth moment, about an axis passing through the point Z = 0, of a distributed mass is given by the expression $\int_0^L ({}^m/_L)\, z^p dz$, while the equivalent for a discrete mass is $\sum_{r=0}^{n} \Delta m \, ({}^{rL}/_N)^p$. Thus,by a suitable distribution of mass it was possible to obtain a 10-step model in which the pth order moment of the discrete mass was the same as the pth order moment of a uniformly distributed mass, where $0 < p < 5$.

The corresponding 10th order model required that some of the masses be negative, which is obviously an unacceptable departure from the true state and therefore an equivalent model was derived with eleven masses (one at each end and one at each step junction,which satisfied three conditions:

i) the total of the discrete masses equalled the mass of the cantilever.

ii) the distribution was symmetrical.

iii) the first five solutions of the frequency parameter were required to agree with those of the exact theoretical solution.

It was shown that using ten step models only the last gave acceptable values for the fifth mode - this being predetermined - but on increasing the number of steps to twenty only the "Simpson model" gave consistently better results than the Myklestad model. It was then

necessary to establish whether any of these improved models were adequate for departures from the case of the thin uniform rod. Allowances were made for shear flexibility and rotary inertia, which become more significant as the thickness/length ratio of the beam increases, by applying lumped inertia coincidentally with each mass, for all but the "mid-point mass" model. In general it was demonstrated that the basic Myklestad model (of forty steps) and the "Simpson model" (of twenty steps) gave higher accuracy than the other for a variety of end conditions. In fact the Myklestad model tended to be marginally more accurate than the "Simpson model" and while a greater number of steps are used the simplicity of the basic lumped parameter model gives it an added advantage.

It may be concluded from this discussion that although it is tempting to improve a lumped parameter model to obtain greater accuracy with a smaller number of steps, in fact greater flexibility and economy, with accuracy,is gained by simply increasing the number of steps in a basic model.

1.2.3 Distributed Parameter Modelling

An approximation which could, intuitively,appear to be more accurate than the lumped parameter model, is that in which each element is considered to be subject to a distributed, rather than a discrete, load. Allen (1) investigated two models of this type.

In the first each element was assumed to be

subjected to a linearly varying distribution of transverse load, suitably adjusted to produce elastic and dynamic compatability over the length of the element. Although good results were obtained for the thin beam, with errors proportional to N^{-4} considerably higher errors were noted when allowance for thickness was included, errors in this case being proportional to N^{-2} for all end conditions.

The errors were shown to be reduced if, instead of considering an element subject to a linearly varying distributed load, a constant load was assumed to act in conjunction with a distributed moment. However, although errors were less, the convergence rate remained inversely proportional to the square of the number of elements.

In both cases solution of the model was by tabulation techniques in which each element was analysed to satisfy dynamic and elastic conditions determined from an assumed frequency. A consistent physical model does not exist for the distributed parameter approximation and thus a solution using a set of simultaneous equations is no longer possible.

1.2.4 Generalised Co-ordinates

For this approach the continuous distribution of mass in a beam is again approximated to a series of discrete masses (m_1, m_2, ..., m_n). It is then possible to form a series of simultaneous equations in terms of generalised co-ordinates given by the amplitudes of motion (x_1, x_2, ..., x_n) of the respective masses. The elastic

properties of the model may then be defined by a symmetrical array of coefficients, $[A]$, say, in which an element A_{rs} (equal to A_{sr}) is the displacement of mass r due to a unit force applied at s. Since the inertia force at any point, p, due to a vibratory motion of circular frequency ω is given by $\omega^2 m_p x_p$ the resultant from the actions of all n inertia forces is given by the matrix expression

$$[A][M]\omega^2 \{X\}$$

where M is a diagonal matrix of order n representing the masses (m)

and $\{X\}$ is a column vector of the displacements (x).

Since each mass is given the displacement assumed in computing the inertia forces the matrix equation

$$\omega^2 [A][M]\{X\} = \{X\} \qquad (1.1)$$

is valid.

It can be seen that there will be n solutions of the equation (1.1), where the eigen-values of the characteristic matrix $[A][M]$ are the values of ω^{-2} and $\{X\}$ is the eigen-vector giving the modal shape.

However, if the inertia per unit length is not constant (as will be the case with tapered and pretwisted beams) the characteristic matrix, $[A][M]$, will no longer be symmetrical. Obviously a solution is more efficient and computer storage requirements reduced if matrices are symmetrical. Additionally an evaluation technique, such as Jacobi's method, which is needed when close or equal roots are to be evaluated, can only be used on

symmetrical matrices.

It becomes necessary, therefore, to pre-multiply both sides of equation (1.1) by $[M]^{\frac{1}{2}}$ to give

$$[M]^{\frac{1}{2}}[A][M]^{\frac{1}{2}}[M]^{\frac{1}{2}}\{X\} = \omega^{-2}[M]^{\frac{1}{2}}\{X\}$$

which may be simplified by writing

$$[T]\{C\} = \omega^{-2}\{C\} \qquad (1.2)$$

where $[T] = [M]^{\frac{1}{2}}[A][M]^{\frac{1}{2}}$ and is symmetric

and $\{C\} = [M]^{\frac{1}{2}}\{X\}$

Each term in the eigen-vector {C} may be considered as a generalised co-ordinate.

Allen developed an analogous group of generalised co-ordinates which allowed the equations (1.1) and (1.2) to be replaced by a similar matrix equation, but of lower order than the discrete mass system, for a given accuracy. This involved setting up a series of linearly independent polynomials such that by a summation of scalar multiples of the polynomials any of the first five natural frequency modes of vibration could be represented with an acceptable error limit. By derivation from equation (1.2) each polynomial was interpreted as the product of the deflected form at any position along the beam and the square root of the mass per unit length.

It was shown that, for the case of the thin, uniform beam, the use of the ten functions to describe the deflected shape gave an accuracy comparable with a basic discrete mass model of forty steps.

However the inclusion of both shear flexibility and

rotary inertia to this solution, to cater for the thick beam, doubled the size of the matrices, since it is necessary to retain a set of co-ordinates to define the rotation of a transverse cross-section separate from the co-ordinates defining deflection. This is in contrast with the Myklestad model where the inclusion of terms to cater for thickness do not appreciably affect the size of the problem.

It was shown that the number of generalised co-ordinates required to maintain the accuracy obtained with the thin beam increased from ten to nineteen resulting in an increase in computer running time of between 3 and $3\frac{1}{2}$. To economise on computer usage it was shown to be possible to reduce the order of the matrix by an improvement in the set of polynomials, which more closely represented the end conditions of the beam under consideration. Although the use of thirteen generalised co-ordinates (seven representing deflection and six rotation) was shown to give acceptable errors in the case of the cantilever, the error increased for the pinned free beam.

Although this technique was shown to be applicable to pretwisted cantilevers the variations in error tended to be more random in comparison with the lumped and distributed parameter solutions, this being indicative of a loss of numerical consistency in the resolution of the matrix rather than an inherent failure in the method. It was also demonstrated that,

irrespective of the closeness of computation of the frequency parameter, the error in modal shape from the generalised co-ordinate model differed appreciably from that obtained by lumped and distributed parameter models.

1.2.5 Finite Element Analysis

The use of finite element techniques has become widespread in recent years and provides a convenient and reliable idealisation applicable to all types of structures, from those which may be considered as frameworks, consisting of, effectively, one-dimensional members, through two-dimensional plate and shell structures, to three-dimensional solids.

In essence the method consists of idealising the continuous structure to a finite number of elements, joined only at points referred to as nodes, where the forces and displacements are assumed to occur. The behaviour of each element may then be analysed using conventional techniques, taking into account equilibrium of forces, compatability of displacements and the laws governing the material behaviour. The individual contributions are added and the resulting set of matrix equations solved for the displacements and stresses.

It can easily be shown (7) that, assuming elastic behaviour of the element, the nodal forces and displacements of a statically loaded structure are related by the equation

$$[K]\{\delta\} = \{P\} \qquad (1.3)$$

where $[K]$ represents the stiffness of the structure

$\{\delta\}$ the nodal displacements

and $\{P\}$ the nodal loads.

In vibrational problems the principal of d'Alembert may be invoked to reduce the problem to a static one, provided that forces equal to the negative product of the masses and accelerations are introduced, in which case equation (1.3) becomes

$$[K]\{\delta\} = -([M_o]+[M])\{\ddot{\delta}\}+\{P\} \qquad (1.4)$$

where $[M_o]$ is a diagonal matrix of external masses attached to the nodes

and $[M]$ is the overall mass matrix assembled from the element mass matrices.

However, the general equation (1.4) may be simplified if there are no external forces ($\{P\}$) and the elements are considered to have distributed mass only, giving

$$[K]\{\delta\} = -[M]\{\ddot{\delta}\} \qquad (1.5)$$

For vibration at a natural frequency with all points moving in phase

$$\{\delta\} = \{\delta_o\} \sin \omega t$$

$$\text{and thus } \{\ddot{\delta}\} = -\omega^2 \{\delta_o\} \sin \omega t$$

and by substitution equation (1.5) becomes

$$([K]-\omega^2 [M])\{\delta\} = 0 \qquad (1.6)$$

which will be recognised as a typical eigen-value problem for which several methods of solution exist.

If $[K]$ and $[M]$ are of order n there will be, in general, n values of ω which satisfy equation (1.6).

Most standard eigen-value problems are presented for solution in the form

$$[H]\{X\} = \lambda \{X\}$$

where the matrix $[H]$ is symmetrical.

Now, it is convenient to write $\lambda = {}^{1}/_{\omega^2}$ since most iteration procedures yield the largest eigen-value λ and this definition will, therefore, provide, initially, the lowest natural frequency. Equation (1.6) can, then, be written in the form

$$[K]^{-1}[M]\{\delta\} = \lambda \{\delta\} \qquad (1.7)$$

However, $[K]^{-1}[M]$ will not, generally, be symmetrical and it is necessary to rewrite $[K]$ in triangular form in terms of a new matrix $[L]$ having zero coefficients above the diagonal, where

$$[K] = [L][L]^T$$

Thus, if equation (1.7) is multipled by $[L]^{-1}$ it can be rewritten as

$$[L]^{-1}[M]\{\delta\} = \lambda[L]^T\{\delta\}$$

If the substitutions

$$\{Z\} = [L]^T \{\delta\}$$

$$\text{and } [H] = [L]^{-1}[M][L]^{-1T}$$

are made the problem can be expressed in the required form, with $[H]$ symmetrical, that is

$$[H]\{Z\} = \lambda \{Z\} \qquad (1.8)$$

Values of λ may then be determined and the modes ($\{Z\}$) from which the actual modes $\{\delta\}$ are available.

Although the basis of this method is shown to be

straightforward the problem arises in defining a suitable element which best meets the often conflicting requirements of a practical problem.

1.2.6 Conclusions

A survey of techniques enabling a continuous structure to be approximated to a model with a finite number of degrees of freedom, to allow a dynamic analysis to be made, has been presented. It is admitted that the survey is by no means exhaustive, but only those methods which show potential suitability for application to turbine blade package analysis have been discussed.

In the following section (1.3) the general approach of this section is replaced by a more detailed discussion of the use of these techniques in order to arrive at the most suitable approximation for the three dimensional dynamic analysis of blade packages.

1.3 The Application of Approximation Methods to the Dynamic Analysis of Turbine Blades and Packages

1.3.1 Introduction

In the preceding section an outline of four methods of approximating the continuous structure of the beam to a structure with a finite number of degrees of freedom was given. These methods will now be discussed in detail in relation to their application to the specific problem of the vibration of turbine blades, with reference to the solutions of other workers in this field.

1.3.2 Method of Analysis

One of the first analyses of the bending vibration of beams for which there is no exact solution was that due to Myklestad (4), based on Holzer's method for finding natural modes of torsional vibration (5). Both are based on the fact that, at a natural frequency and with a finite vibration amplitude the shaking force becomes zero. Whilst the technique is more complex when considering flexural vibration, since the number of degrees of freedom is increased from one to at least two, the methods are essentially similar and suited to a tabulation solution, this being necessary prior to the introduction of digital computers. Indeed, two advantages claimed by Myklestad for his method were that the technique was simple enough to be used by inexperienced labour and that, since the results were plotted graphically,even closely grouped frequencies would not be overlooked. The latter was considered to

be an important aspect in the analysis of aircraft wings with flexibly mounted engines, for which the method was originally developed. It is perhaps surprising that Myklestad's analysis was restricted to slender beams, since allowance for thickness is easily included by an additional term representing inertia in the equation relating moments and an additional term representing shear flexibility in the displacement equation. Prohl (8) extended this analysis of single beams to include the effect of fitting a shroud to the blade tips, earlier shown by Smith (9) to introduce additional groups of natural frequencies which cannot be predicted by consideration of only the blades. Again, however, Prohl omitted to include an allowance for blade thickness and retained Smith's assumptions that the shroud would be adequately represented by an additional mass at the blade tip and that the blades were inextensional. But, Prohl did include axial and torsional as well as flexural vibration.

The adaptability of the Myklestad method was appreciated by Prohl, who indicated that the blades need not be uniform and that flexural and torsional flexibility at the blade root could be included. A digital computer was used for the calculations, in place of the graphical method of Myklestad.

The introduction of digital computers to perform automatically a series of Myklestad tabulation routines

precludes the use of graphical methods to aid the selection of a suitable frequency to converge on a solution. Mahalingam (10) showed that the model could be easily improved to give a fast convergence rate when using computers. The selection of a new estimate of the natural frequency was obtained by considering a small change in either a lumped mass, or the elasticity of an element, depending on the boundary conditions of the beam being considered. The relevant parameter change was defined as that required to give correct boundary conditions and thus the frequency estimate becomes the natural frequency of the modified system. The modified system is then converted to the real system, with a corresponding change in frequency, giving an improved second estimate of frequency. Other workers have considerably improved on the basic Myklestad model for the single non-uniform beam, including Huang and Wu (11),Carnegie (12, 13) and Fu (14) who included the effects of centrifugal forces due to rotation of the disc assembly, pretwist and coupling effects caused by the centre of torsional flexure and the centroid not being coincident.

The validity, adaptability, accuracy and ease of solution of the lumped parameter model is clearly demonstrated in these references.

In his survey of approximation methods, which included lumped and distributed parameter models and the use of generalised co-ordinates to represent deflection, Allen (1) demonstrated that while suitably accurate

frequency results could be obtained for a thick pretwisted beam with all three models, in some cases the latter solution was less reliable at high frequencies due to inaccuracies in the solution of the matrix. Errors in modal shapes were also higher for the general co-ordinate model. Little advantage was shown to be gained by the use of a distributed parameter model rather than the simpler lumped parameter model. It was shown that the major difference between the tabulation and generalised co-ordinate (matrix) solutions was in the computer storage and running time required. Not only was the running time for the general co-ordinate method double that for the Myklestad model, but the storage requirement for floating point variables was increased by a factor of approximately seventeen. The approximations compared were a forty step Myklestad model and a model with a deflected form defined by thirteen orthogonal polynomials for each reference plane.

An additional advantageous feature of the lumped parameter solution arises from the fact that the evaluation of a trial frequency is independent of any other computation carried out at a different frequency. Thus, it is possible to perform a coarse search on a model of reduced accuracy, after which frequency ranges of interest can be searched with a discrete mass model of greater accuracy than that used for less significant areas. Indeed, areas of no importance need not be examined at all. This approach may even be more economical than the technique described by Mahalingam (ibid) to achieve improved convergence.

When considering an extension of the model to the more complicated blade package the use of generalised co-ordinates becomes excessively unwieldy, especially when axial, torsional and longitudinal motion are being considered in addition to tangential motion and it may be concluded that of the models discussed the lumped parameter and finite element models only provide suitable techniques for the analysis of a package.

Since, as has been discussed previously, the solution to a finite element approximation is a standard eigenvalue problem the accuracy of the solution depends primarily on the element used, provided the computer has sufficient resolving power to enable the matrices to be solved accurately. The definition of the element is, therefore, of prime importance to enable the problem to be solved not only accurately, but also economically.

Several investigators have derived elements considered suitable to define the vibration of a "Timoshenko beam", that is, in which the effect of thickness has been included, but it has been shown to be difficult to incorporate all of the boundary conditions associated with beams. It will be recalled that those for the cantilever are zero displacement and bending slope at the built-in end and zero bending moment and shear force at the free end.

Several formulations have been based on the element due to McCalley (15, 16) in which only two nodal degrees of freedom are considered, displacement and bending slope, from which consistent mass and stiffness matrices can be

derived. While this fulfils the requirements of an encastré beam the representation of boundary conditions at the free end is not possible. Carnegie, Thomas and Dokumaci (17) developed an element with two degrees of freedom (displacement and bending slope) at each of four equispaced nodes, which generally gives improved results for thicker beams than that due to McCalley, since representation of shear deformation and rotary inertia is better. However, when considering a slender beam, more accurate results are obtained from the element of McCalley since that due to Carnegie et al tends to "waste" degrees of freedom which are put to better use to improve the representation of bending in the simpler element.

Thomas and Abbas (18) developed a further element with four nodal degrees of freedom (deflection, total slope, bending slope and its first derivative) at each of two nodes. It was claimed that this enabled all boundary conditions to be satisfied at either end of a beam. However, whilst this element is most conveniently used with continuity of the four degrees of freedom across the element boundaries, difficulties are introduced at changes of section, or at the junctions of beams. It is also argued by Thomas D. (19) that greater accuracy is obtained if these constraints are not applied, since the finite element solution finds the distribution of bending moment, shear force and displacement over the whole structure which corresponds to the state of minimum potential energy, subject to the constraints imposed by the element displacement functions and the geometrical boundary

conditions. It is shown that, normally, bending moment and shear force at a free end, say, are, approximations to zero of the same order of accuracy as at any other points on the structure. *If, by using the element of Thomas and* Abbas, these conditions are artificially constrained to be exactly zero, the accuracy at other points along the structure tends to be worse, since the potential energy is higher, which, in turn, increases the natural frequency.

For general purposes Thomas D. (19) concludes that the simpler element of Carnegie, Thomas and Dokumaci is better, because, with only two degrees of freedom per node it is not necessary to consider the extra constraints which need to be imposed on the total slope and the first derivative of the bending slope at boundaries and across elements. Additionally this element has a faster convergence rate than that due to Thomas and Abbas.

It should be noted that the restriction on the number of degrees of freedom per node precludes the use of all these elements for the dynamic analysis of the pretwisted beam.

In a recent paper Thomas and Belek (20) extended the use of finite element analysis to the free vibration of blade packages. The packages investigated were idealised using rectangular cross-section elements with three degrees of freedom at each of two nodes, allowing flexural and longitudinal movement. The motion was thus restricted to the plane of the package. The system considered was similar to that of Smith (9) in which the shroud cross-sectional area was small and the blade motion described by

the Bernoulli-Euler theory, applicable to the slender beam. The effect of blade thickness and finite shroud width can be shown to have opposing effects on the frequency and thus the results are, fortunately, more accurate than may be expected. As with most blade package investigations the disc to which the blades were considered to be attached was assumed to have infinite radius and infinite rigidity, but it was claimed that both disc flexibility and greater complexity of the blade configuration could be taken into account.

The solution of this model was based on the theory of stationary potential energy, in which the potential energy (V) is given by

$$V = U - \omega^2 T \tag{1.9}$$

where U is the time independent strain energy

T is the time independent kinetic energy

and ω is the free vibration frequency

The strain and kinetic energies are related to the stiffness and mass matrices by the nodal displacements, that is

$$U = \tfrac{1}{2} \{\delta\}^T [k] \{\delta\} \tag{1.10}$$

$$T = \tfrac{1}{2} \{\delta\}^T [m] \{\delta\} \tag{1.11}$$

Substitution of these expressions in equation (1.9) and invoking the condition of stationary potential energy yields a standard eigen-value problem of the form

$$([K] - \lambda [M])\{\delta\} = 0$$

Now, from the Bernoulli-Euler theory of flexural vibration the energy of an element can be obtained from

$$U = \tfrac{1}{2} EI \int_0^1 \left(\frac{\partial^2 v}{\partial z^2}\right)^2 dz + \tfrac{1}{2} EA \int_0^1 \left(\frac{\partial u}{\partial z}\right)^2 dz \quad (1.12)$$

$$T = \tfrac{1}{2} \rho A \int_0^1 (\dot{u}^2 + \dot{v}^2)\, dz \quad (1.13)$$

where u is the longitudinal deformation

v is the transverse deformation

and z the element length

Thomas and Belek considered that the flexural and longitudinal displacement states within an element could then be approximated by a cubic and a linear polynomial respectively, with respect to z. Substitution of these polynomials into equations (1.12) and (1.13) enabled the stiffness and mass matrices to be derived from equations *(1.10 and (1.11)*.

By careful numbering of the nodes when building the blade packet from the elements, the stiffness and mass matrices will be found to have a banded configuration. Although the overall size of the matrices is obviously a function of the number of blades, elements and degrees of freedom, the bandwidth can be shown to be independent of the number of blades. It is more efficient to utilise this banded configuration for solution of the matrices, rather than transforming them into symmetrical form and Thomas and Belek used an algorithm developed by Gupta (21) to extract the eigen-values and eigen-vectors for the model. A comparison of results from a forty step Myklestad tabulation solution for one of the packages

investigated theoretically and experimentally by Thomas and Belek is shown in Table 1. It can be seen that in all cases the finite element solution is more accurate than the lumped parameter solution, although there is a sudden increase in the error of the finite element model for the second batch modes. This would appear to indicate that the limit of this idealisation has been reached and that a larger number of elements, or an improved element with an allowance for thickness would be required to solve for modes higher than the second with any confidence.

Whilst this model was shown to give suitably accurate results for slender blades it is necessary to consider its extension to deal with the vibration of tapered, pretwisted blade packages.

Improvement of the element to one with six degrees of freedom per node would allow calculation of torsional and axial modes with a consequent doubling of the order and the bandwidth of the mass and stiffness matrices. However, the effects of shear flexibility and rotary inertia (necessary when calculating the axial modes), pretwist and taper would require a redefinition of the element itself with a subsequent increase in the complexity of the displacement functions.

It was stated earlier that the Thomas and Belek model, with a shroud of small cross-sectional area, could be compared to that of Smith (9), in which the blade/shroud junction is considerably simplified. A full width shroud, which would cause an increase in the vibration frequency,

would require an improved model of the junction to cater for the effect, further increasing the complexity of the problem.

A comparison of the lumped parameter idealisation with the finite element model shows the advantages of the former in these respects. While the size of the problem is doubled in both cases when extending the number of degrees of freedom from three to six the definition of the lumped parameter model itself remains the same. Taper is adequately described by relevant, simple changes in the mass and flexural constant of the beam elements and pretwist by considering each element as being without pretwist, but successive elements rotated bodily by an amount equal to the total pretwist of the previous elemental length. Since the number of elements in a finite element model is necessarily much smaller this type of approximation is obviously inadequate.

Whilst the reactions at the blade/shroud junction of a lumped parameter model are still assumed to act as points the forces are considered in conjunction with the moments which make an allowance for the thickness of the blade and shroud. In fact, by introducing a suitable factor the "effective thickness" at the junction may be varied easily to effect a suitable allowance for the efficiency of the joint.

It is also pertinent to consider the effect of increasing the accuracy of the models. An increase in the number of elements in a finite element model of a given number of blades will increase the bandwidth of the

mass and stiffness matrices by at least the number of nodal degrees of freedom, increasing the computer storage requirement, while an improvement in the element itself will involve an increase in the calculation effort required to produce these matrices and may also involve an increase in the order if the number of modes is greater.

Whilst a lumped parameter model will require a larger number of (simple) elements to attain reasonable accuracy it has been shown that an increase in the number of masses is generally better than an improvement in the type of parameter. This increase in the number of masses only affects the number of times the four equations of equilibrium and compatability require to be solved and does not increase the core storage requirement, since only the final end conditions for each blade are stored. The array, whose determinant is required to be zero for the boundary conditions to be satisfied, can only be of the order given by the product of the number of degrees of freedom and the number of blades. Indeed, the storage requirement for a lumped parameter model is minimal compared with that needed by a finite element solution.

In a comparison of finite element and lumped parameter solutions for vibration in beam systems Henshell and Warburton (22) compared the time taken to solve models of an equal number of elements using an Atlas computer and Atlas Autocode, a high level scientific language. It was shown that the lumped parameter model (solved using a matrix solution rather than tabulation) was three times as fast as,

but less accurate than,the finite element method. However, this comparison tends to emphasise the advantages of using a tabulation solution to a Myklestad model rather than matrix methods. In all the Myklestad models considered the number of masses was kept low, and of the same order as the number of finite elements. It should be remembered that such a coarse approximation with a simple idealisation cannot be compared directly with a finite element solution using a model which is inherently more accurate due to its greater complexity. However, when using a matrix solution it is necessary to minimise the number of lumped parameters to maintain an economic matrix order. The number of eigen-values found is generally the same as the order of the matrix and thus a more accurate Myklestad model, using the optimum number of steps (of the order forty, say) will be uneconomic and solve for a large number of unwanted frequencies. It has been indicated previously that a tabulation solution is frequency selective and that limited bandwidths covering important frequencies can be solved economically with an accurate model, with a large number of masses, independently of any other frequency range. None of the other models considered in this investigation is capable of solution only in a particular area of interest, since the number of eigen-values will always be directly related to the total number of degrees of freedom of the model. Indeed, it is generally true that only a limited number of modes is of interest, as was demonstrated by Armstrong and Stevenson (23)

who found that "By fairly rigorous endurance testing, backed by strain gauging, it has been shown that more than 90% of these (compressor blade) failures can be attributed to vibration in the first or second flexural mode, the first torsional mode and the first edgewise mode".

1.3.3 Conclusions

Of the approximations of beam systems considered in section 1.2 it has been shown that two are appropriate to the solution of blade packages, a finite element model and the tabulation solution of the lumped parameter model of Myklestad. Whilst the latter solution tends to be less accurate than the former it can be shown to be more amenable to modification to cater for non-uniformity of the blades and the complexity of the blade/shroud junction, without an undue increase in the size of the problem or the computer effort required to solve it. In addition the Myklestad tabulation method is shown to be the only idealisation capable of a frequency selective solution, which can offer considerable improvements in the economy of a model with a large number of elements.

1.4 The Vibration of Bladed Disc Assemblies

As was mentioned in the introduction (1.1) Ewins has shown that consideration of the complete turbine disc assembly can introduce further natural frequencies of vibration in addition to those predicted under the assumption that the disc on which the blades are mounted is of infinite radius and stiffness. This thesis has been supported by experimental evidence and theoretical calculation (3).

Two basic methods may be applied to model the basic assembly, a receptance coupling procedure, which enables the constituent parts of the assembly to be combined, and the use of finite elements.

The latter approach presupposes the form of the vibration of the assembly and requires the solution of high order matrices. The former analysis has, however, been developed by Ewins to provide a general analysis for bladed disc vibration, which will cope with assemblies of any number of non-identical blades without any assumptions as to the modal shape. The basis of receptance coupling is the application of dynamic equilibrium and compatability at the junction between two connected components. Individual analyses of the components provide the so-called receptance functions which relate the forces and displacements at the junctions. In general , since forces and displacements can exist in three translational and three rotational directions, six equations of compatability and equilibrium will be required for each junction and thus the receptance will be described by a sixth order matrix of individual functions. However, in particular cases a reduction in the number of degrees of freedom is possible to derive a more efficient analysis (24).

In the analyses described in references (3) and (24) a simple model consisting of a uniform disc fitted with uniform, untwisted blades of constant cross-section, joined at their tips by a uniform straight shroud was investigated. Whilst this is sufficient to demonstrate the validity of the approach it is considered that application to an assembly of pretwisted, tapered, shrouded blades would considerably increase the complexity of the problem, since the necessary expressions for receptance data for this type of blading are not readily available.

Disc induced vibration will affect mainly the axial rather than the longitudinal, tangential and torsional modes and it has been shown that the axial vibration tends asymptotically to the natural frequency of the cantilever blade as the number of nodal diameters increases (3). In fact, while assemblies with small blades show largely disc controlled axial modes there is shown to be a trend to blade controlled modes as the blade size increases relative to the disc.

In the present study, whilst axial motion has been included the emphasis is placed on the tangential vibration modes, in which direction the disc can be considered infinitely stiff. The blade dimensions are also such that the axial modes are considered to be "blade-controlled".

It has been decided, therefore, that the assumption of an infinitely stiff disc of infinite radius remains valid and the effects of the disc will not be included in the approximate model.

1.5 Concluding the Survey of Blade Package Approximation Techniques

In this chapter a survey has been undertaken of the approximation techniques applicable to the analysis of continuous structures with particular reference to the analysis of thick, pretwisted turbine blade packages. Although the effects of a flexible disc have been studied it has been concluded that, for the purposes of the current analysis the relative blade/disc dimensions will be such as to give "blade controlled" axial vibration and thus the disc itself has been assumed to be of infinite stiffness and radius and only the motion of the blades and shroud will be included.

Of the methods available to approximate the continuous structure of the beam it has been concluded that only two are applicable to the analysis of blade packages, these being the simple model of Myklestad with a tabulation solution and the use of finite elements.

Whilst it can be shown that the finite element approximation provides a better representation of a package of beams undergoing free vibration,the application of this to a package of thick, non-uniform beams, with inclusion of pretwist,cannot be undertaken without a fundamental improvement in the elements. The addition of a complex blade/shroud junction further increases the complexity of the model. The inclusion of all six degrees of freedom and an increase in the number of elements to cope with the complexities of the pretwisted blade package lead to a considerable increase in the order of the mass and stiffness matrices.

Whilst large, modern computers will easily cope with high order matrix operations the core storage and time requirements

will also be high. It is possible to partition large matrices and solve only part of the problem at a time, storing the partitioned matrices not currently being analysed on disc, but while this reduces the core storage requirement (making it suitable for smaller computers) the core to disc transfer also becomes time consuming. In general it may be concluded that a finite element solution can give good accuracy, but requires considerably more computer time and core storage than the lumped parameter solution. It should also be remembered that all the eigen-values available from an approximation with a given number of degrees of freedom require to be solved, whereas in many cases only the low modes are required.

Since the tabulation method due to Myklestad solves the problem for a selected frequency independently of any other frequencies only those frequency ranges of interest need be examined. It has been shown that the accuracy of the model is independent of the size of the determinant relating the end conditions, whose solution is required to test whether a given frequency is a natural frequency, this only being a function of the number of blades (N) and the number of degrees of freedom, giving a maximum order of (6 x N). This implies that an improvement in the accuracy of the model by increasing the number of masses does not involve a proportional increase in the time taken to find a solution. The simplicity of the model allows a variety of end conditions to be investigated, without a change in the fundamental model.

When considering the application of a method to provide basic design criteria it is important that the method be flexible,

to allow the effect of modifications to be assessed easily. It is considered that in this respect the lumped parameter solution offers considerable advantages over the finite element analysis. Although the former method is less accurate it is considered that the accuracy remains within the limits imposed by manufacturing tolerances.

It has been concluded, therefore, that taking into account efficiency and adaptability as well as accuracy the lumped parameter method due to Myklestad is best suited for extension to cover the analysis of blade packages consisting of non-uniform, pretwisted beams.

In the following chapters the Myklestad method is developed from the basic model to that suitable for the analysis of complex blade packages. A parallel experimental analysis, using Laser techniques enables an assessment of the accuracy of the frequencies and modal shapes to be made, considering tangential, torsional and axial vibration.

2. THE MYKLESTAD METHOD APPLIED TO THE VIBRATION OF THICK CANTILEVERS

2.1 Introduction

In the previous chapter it was shown that the lumped parameter method for the prediction of turbine blade vibration characteristics offered the advantages of adaptability and economy when compared with other solutions to the problem. It is now proposed to show in detail how the technique due to Myklestad may be developed from the analysis of single beams to that of a package of pretwisted, shrouded blades capable of movement in three mutually perpendicular planes. The effects of taper and of centrifugal forces due to rotation of the blade will also be considered.

In order to restrict the number of parameters it has been found necessary to make certain assumptions, though it is considered that these limitations affect only the detail and not the general principles of the analysis.

In considering a beam with a high thickness/length ratio it has been assumed that unstrained transverse sections through it remain plane when subject to vibratory conditions, as defined by Timoshenko (25). In addition the flexural and torsional neutral axes for any cross section have been assumed to be concurrent and the common neutral axis thus formed to be straight. Cross sections have also been considered as rectangular to enable the relationship between shear flexibility and flexural flexibility to be a constant.

Whilst it is common for the cross section of a turbine blade to be unsymmetrical with respect to the principal axes of inertia, giving rise to additional flexural-torsional coupling, this effect will be negligible for tangential vibration and of only minor significance for many of the axial and torsional modes of

vibration, when considering blades of normal proportions. It is considered, therefore, that, for the purposes of this investigation, an adequate representation of turbine blading is retained.

Although a practical turbine blade package would, obviously, have the blade longitudinal axes radiating from the turbine axis those of the packages analysed in this investigation have been assumed to be co-planar, parallel and equispaced and any difference due the fan effect of the former has been assumed insignificant.

Both blades and shrouds are considered to be of the same, homogeneous material and the junctions between them to be identical. Although it is not essential to the method, the roots of the blades have been assumed to be fully encastre with the exception of the analysis of the tapered beam when ascertaining the effectiveness of the clamp used on the experimental rig.

The fundamental principle has necessarily been accepted that in a free vibration the motion can be considered as the sum of a series of separate motions in any one of which all parts move with the same frequency and pass through their mid positions simultaneously.

2.2 The Single Cantilever

2.2.1 The Myklestad Model

The conventional lumped parameter model is shown in Figure 1(a) from which it can be seen that the beam is subdivided into a number of parts, half of the mass of any part being considered as concentrated at each end. The remaining light portion of the beam is treated as having a uniform flexural constant. It is obvious that each junction has two associated concentrations of mass and thus it is convenient to consider each step as consisting of a mass of Δm at the end z, but no mass at the other end $(z + \Delta z)$. A typical element, with the variables used to define its motion, is shown in Figure 1(b).

If the thickness of the beam is significant then a discrete inertia ΔJ is also required at position z, the magnitude being given by the expression:

$$\Delta J = \Delta m \left(T^2/_{12}\right)$$

Application of d'Alembert's Principle gives both an inertia force (of magnitude $-\Delta m \left(\frac{d^2x}{dt^2}\right)$) in the x direction and an inertia couple (of magnitude $-\Delta J \left(\frac{d^2x'}{dt^2}\right)$ in the x' direction. If the circular frequency of vibration is ω then the substitution $x = X \cos \omega t$ may be made and all the terms shown in Figure 1(b) contain the factor $\cos \omega t$. The equations of equilibrium and compatability may now be established and since $\cos \omega t$ is not normally zero it can be extracted as a factor, leaving:

$$F + \Delta F = F + \omega^2 \Delta m.X \qquad (2.1)$$

$$M + \Delta M = M + (F + \Delta F)\,\Delta z - \omega^2 \Delta J X' \qquad (2.2)$$

$$X' + \Delta X' = X' + \{(M + \Delta M)\,\Delta z - (F+\Delta F)\,\frac{\Delta z^2}{2}\}/EI \qquad (2.3)$$

$$X + \Delta X = X + X'\Delta z + \{(M+\Delta M)\,\frac{\Delta z^2}{2} - (F+\Delta F)\,\frac{\Delta z^3}{3}\}/EI$$
$$- (F+\Delta F)\,\Delta z\,(K/GA) \qquad (2.4)$$

The final negative expressions in equations (2.2) and (2.4) are, respectively, the rotary inertia and shear flexibility terms introduced to cater for thickness.

The general equations (2.1) to (2.4) may be further developed to provide a more efficient analysis of the uniform beam. If the equations are rearranged and divided by Δz then, since in the limit $\Delta m/\Delta z$ tends to m/L and $\Delta J/\Delta z$ tends to $(M/L)(T^2/12)$, for the uniform case, the following set of equations is obtained:

$$F' = \omega^2\,(m/L)\,X_{total} \qquad (2.5)$$

$$M' = F - \omega^2\,(m/L)(T^2/12)\,X'_{rotat} \qquad (2.6)$$

$$(X'_{rotat})' = M/EI \qquad (2.7)$$

$$X'_{total} = X'_{rotat} - F(K/GA) \qquad (2.8)$$

Elimination of F,M and X' from these equations gives rise to the characteristic equation:

$$EIX^{iv} + \frac{m\omega^2}{L}\left(\frac{KEI}{GA} + \frac{T^2}{12}\right) X'' - \frac{m\omega^2}{L}\left(1 - \frac{m\omega^2}{L} \cdot \frac{K}{GA} \cdot \frac{T^2}{12}\right)X = 0 \qquad (2.9)$$

Equation (2.9) may be more conveniently expressed in terms of a non-dimensional frequency parameter, V, related

to the actual frequency by the expression:

$$f = \frac{\omega}{2\pi} = \frac{V^2}{2\pi} \left(\frac{EI}{mL^3}\right)^{\frac{1}{2}} \qquad (2.10)$$

This results in the characteristic equation (2.9) becoming:

$$X^{iv} + \frac{V^4}{L^4}\left(\frac{KEI}{GA} + \frac{T^2}{12}\right) X'' - \frac{V^4}{L^4}\left\{1 - \frac{V^4}{L^4}\left(\frac{KEI}{GA}\right)\left(\frac{T^2}{12}\right)\right\} X = 0 \qquad (2.11)$$

Further simplification may be achieved by introducing dimensionless parameters representing the bending and shear flexibilities of the beam $\left(\frac{KE}{G}\cdot\frac{I}{A}\right)$ and the term $(T^2/12)$, which for a rectangular cross-section is derived directly from (I/A). Thus:

$$\alpha = T^2/12L^2 = I/AL^2$$

$$\gamma = KE/G$$

resulting in equation (2.11) becoming:

$$X^{iv} + \frac{V^4}{L^2}\,\alpha\,(\gamma + 1)\,X'' - \frac{V^4}{L^4}\,(1 - V^4\,\gamma\,\alpha^2)\,X = 0 \qquad (2.12)$$

It is because this equation is not generally amenable to an exact solution that the various numerical techniques, such as those discussed in Chapter 1, have been developed.

To return to the Myklestad solution to this problem it can be seen from Figure 1 that it is convenient if, when progressing along the beam, transferring data to the next element, the overall length (L) be traversed in a

number of equal steps (N). Thus, each element is considered to have a mass $\Delta m = m/N$, half of which is placed at the end of each element. It can be deduced that, although the element shown in Figure 1(b) is suitable for contiguous, intermediate steps, the end steps must differ from these. Thus, if the beam is treated as having N identical steps an extra mass of m/2N occurs at the root and half of the mass of the tip element has not been included. The end steps, therefore need to be suitably modified by a "dummy" mass of magnitude (-m/2N) at the base and the mass of (m/2N) at the tip (Figure 1(c)).

The equations (2.1) to (2.4) may now be simplified to provide a suitable algorithm for automatic computing.

It is logical to replace the term $\omega^2 \Delta m$ in equation (2.1) by a function of the non-dimensional frequency parameter (V), defined in equation (2.10) and the number of steps (N), thus:

$$W = (V/N)^4 \qquad (2.13)$$

Also, with particular reference to equation (2.4), it is convenient to define the following variables

$$D = (L/N)\ X'; \qquad B = (L/N)^2\ M/EI;$$

$$S = (L/N)^3\ F/EI$$

Then, if the equations (2.1), (2.2) and (2.3) are multiplied by $(L/N)^3/EI$, $(L/N)^2/EI$ and (L/N) respectively and the new variables substituted the following equations are obtained:

$$S + \Delta S = S + WX \tag{2.14}$$

$$B + \Delta B = B + (S + \Delta S) - WD\ \alpha N^2 \tag{2.15}$$

$$X + \Delta X = X + D + \tfrac{1}{2}(B + \Delta B) - 1/3\ (S + \Delta S) - (S + \Delta S)\ \gamma \alpha N^2 \tag{2.16}$$

$$D + \Delta D = D + (B + \Delta B) - \tfrac{1}{2}(S + \Delta S) \tag{2.17}$$

It may be noted that the order of the last two equations has been reversed to give an algorithm in which the right hand sides contain the most recently calculated values of the variables S, B, X and D, thus providing a routine ideally suited to computation.

In fact equation (2.16) may be simplified further given the assumptions that:

i) $E = 8G/3$

ii) the bar is of rectangular cross section, for which $K = 1.2$ in which case

$$\gamma = KE/G = 3.2 \qquad \text{(Ref. 2.6)}$$

Thus the correction for shear flexibility is 3.2 times larger than that due to rotary inertia.

The equations (2.14) to (2.17) which form the basis of the Myklestad method can be solved as folows.

Two linearly independent sets of initial values for S, B, X and D at $z = 0$ are estimated, such that they are consistent with the end conditions for the beam. In the case of a cantilever, for example X_o and D_o must always be zero, while it is convenient for S_o to be finite and B_o zero for the first set and B_o finite with S_o zero for the second set. It must be remembered that the initial shear

force term requires an adjustment to allow for the "dummy" mass, as discussed previously.

A frequency is then assumed, the value being based on any information which may be available to define a range of interest. The equations (2.14) to (2.17) are then solved repeatedly, progressing from element to element along the beam, for the two sets of initial conditions. The final values of S, B, X and D may then be tested to establish whether a suitable combination of the two sets of initial values resulted in the final values satisfying the end conditions for the beam at $z = L$. In the case of the cantilever S_L and B_L must obviously be zero while X_L and/or D_L are finite. If this is so then the assumed frequency can be accepted as a resonant frequency. S_L will, in fact, differ from its true final value, again, due to the inclusion of the "extra" mass.

Usually the end conditions are not satisfied and it is then required to establish a measure of the error, which may be compared with previous errors to enable an improved estimate of the frequency to be made. The choice of a residual parameter to represent the error is of prime importance, especially when using automatic computing rather than plotting the results by hand, as envisaged by Myklestad.

If, therefore, the residual parameter is defined by forming a linear combination of the two sets of final end conditions, related by the coefficients a_1 and a_2, say, then considering the example of the cantilever a convenient

expression for the residual is the matrix equation

$$\begin{bmatrix} M_1 & M_2 \\ F_1 & F_2 \end{bmatrix} \begin{bmatrix} a_1 \\ a_2 \end{bmatrix} = \underset{\sim}{R}$$

For a resonant frequency $\underset{\sim}{R}$ must be zero and the only non-trivial solution satisfying this requirement is that:

$$\det \begin{vmatrix} M_1 & M_2 \\ F_1 & F_2 \end{vmatrix} = 0$$

Thus it is required to test the value of the determinant of the (suitable) end conditions after each trial frequency.

Having defined a suitable residual parameter it is now necessary to develop a routine to interpret its value to enable rapid convergency to a sensibly zero value, thus establishing the resonant frequency.

2.2.2 Location of Roots

For the uniform, untwisted, single cantilever there is generally good separation between the solutions in the frequency parameter, V, for at least the first five natural frequencies and, provided that successive trials are made at intervals in V of not more than 1.0 the presence of a root may be detected by a change in sign of the residual. Successive linear interpolation, or, the "rule of false position" will then reveal a sensibly zero value for the residual and hence the frequency at which this occurs. However, while the location of roots is being discussed, it is pertinent to include extensions to this basic technique, which ensure that all roots, including

close pairs and double roots are found, with an economical search interval. However, it is generally true that these refinements are only necessary when pretwisted or packaged beams are being analysed.

A case in which the location of roots by a change in sign of the residual, R, is inadequate is exemplified by Figure 2, where four successive values of the frequency parameter all obtain positive values of R and thus the possibility of a root, or roots, between trials 2 and 3 is not detected. However, if the slopes of straight lines joining adjacent points are investigated a turning point can be identified. If this turning point is a minimum for a group of positive values of R, or a maximum for a group of negative values of R, then the presence of roots is implied. If the approximation is made that the curve of R against V is parabolic then the turning point can be defined. If vibration in both planes is being considered then a double root at the turning point can be identified. When the roots are a close pair a change in sign is detected and the two roots can be found by iteration.

Once a root has been disclosed as lying between two trial values then its actual position can be located in two ways. As discussed previously, the curve between the points can be approximated to a straight line to enable an improved value for V to be established. Secondly, the search interval between the two values can be subdivided and a finer search initiated from the first point. In

general it can be shown that the former procedure requires less trials than the latter, however there are some cases where repeated subdivision becomes more economical. Figure 3 illustrates a case where the rate of convergence is increased by subdivision. A change in sign has been detected between trials V_1 and V_2, but the presence of a root close to, though outside the range, has given rise to a low maximum value at the turning point. As is shown by Figure 3 the rate of convergence using successive iteration is slow, but if the interval is subdivided then the turning point can be located by comparison of the slopes. When the turning point and the root are not in the same subdivision (Figure 4(a)) then linear interpolation can again be used. If, however, they do occur in the same subdivision (Figure 4(b)) then greater economy is achieved by further subdivision and a repeat of the process. Allen (1) demonstrated that this method satisfactorily located all roots for the pretwisted beams considered in his investigation.

2.2.3 The Tapered Cantilever

The model described in section 2.2.1 may easily be extended to allow for taper in one or both planes by defining the mass and dimensions at each station as a function of a suitable linear or exponential equation. Within the current investigation both linear and exponential taper were considered, results for the latter being compared with an exact analysis, while those from the former were compared with experimental data.

In order to establish the accuracy of a lumped

parameter model of the Myklestad type the special case of the exponentially tapered cantilever was considered in some detail.

For the case of undamped vibration it is easy to show that the modal shape $x = f(z)$ associated with a natural frequency of $\omega/2\pi$ is obtained from the differential equation

$$\frac{d^2}{dz^2}\left(EI.\frac{d^2x}{dz^2}\right) - \rho\omega^2 x = 0 \qquad (2.18)$$

If the mass per unit length (ρ) or the flexural coefficient (EI) are functions of z then equation (2.18) is not, generally, amenable to analytical solution. However, various special cases exist, including the solution in which:

$$EI = (EI)_o e^{-pz} \text{ and } \rho = \rho_o e^{-qz}$$

the suffix o indicating values at $z = 0$.
Substitution of these values in equation (2.18), and rearrangement gives:

$$\frac{d^2}{dz^2}\left(e^{-pz}\frac{d^2x}{dz^2}\right) = \mu^4 e^{-qz} x \qquad (2.19)$$

where $\mu^4 = \left(\frac{\rho}{EI}\right)_o \omega^2$

(Comparison with equation (2.10) shows that $\mu^4 = \left(\frac{V}{L}\right)^4$)
Expanding (2.19) and using the notation $D \equiv \frac{d}{dx}$

$$D^2\left(e^{-pz}D^2x\right) = D\left(e^{-pz}D^3x - pe^{-pz}D^2x\right)$$
$$= e^{-qz}\mu^4 x \qquad (2.20)$$

Rewriting equation (2.20) two distinct solutions emerge

$$\{(D^2-pD) + \mu^2 e^{(p-q)z/2}\}\ x = 0 \qquad (2.21)$$

$$\{(D^2-pD) - \mu^2 e^{(p-q)z/2}\}\ x = 0 \qquad (2.22)$$

If, in order to validate an arithmetic approximation, the study is restricted to cantilevered blades of constant thickness, but of varying width, then considerable simplification is obtained and it can be seen that :

$$(\frac{\rho}{EI}) \text{ is a constant}$$

$$\text{and thus } p = q = 2\nu, \text{ say.}$$

Substituting these values in equations (2.21) and (2.22) leads to

$$(D^2 - 2\nu D + \mu^2)\ x = 0 \qquad (2.23)$$

$$(D^2 - 2\nu D - \mu^2)\ x = 0 \qquad (2.24)$$

The form of x is then seen to be

$$x = e^{\nu z} (A \cosh \beta z + B \sinh \beta z + P\cos \varepsilon z + Q \sin \varepsilon z) \qquad (2.25)$$

where $\beta^2 = \mu^2 + \nu^2$ (2.26)

$\varepsilon^2 = \mu^2 - \nu^2$ (2.27)

provided that p is less than 2μ.

If $z = 0$ defines the clamp and $z = 1$ the free end, then

$$x = Dx = 0 \text{ at } z = 0$$

$$(EI)D^2x = D(EI\ D^2x) = 0 \text{ at } z = 1$$

Then, conditions at the clamp readily produce the requirements that:

$$A + P = 0 \tag{2.28}$$

$$B\beta + Q\varepsilon = 0 \tag{2.29}$$

The tip conditions give the following equations, where

$$c = \cos\varepsilon z \qquad ch = \cosh\beta z$$

$$s = \sin\varepsilon z \qquad sh = \sinh\beta z$$

$$\{A(\nu^2 + \beta^2) + 2\nu\beta B\}ch + \{B(\nu^2 + \beta^2) + 2\nu\beta A\}sh$$
$$+ \{P(\nu^2 - \varepsilon^2) + 2\nu\varepsilon Q\}c + \{Q(\nu^2 - \varepsilon^2) - 2\nu\varepsilon P\}s = 0 \tag{2.30}$$

and

$$\{A\nu(\beta^2 - \nu^2) + B\beta(\beta^2 - \nu^2)\}ch$$
$$+ \{A\beta(\beta^2 - \nu^2) + B\nu(\beta^2 - \nu^2)\}sh$$
$$+ \{-P\nu(\varepsilon^2 + \nu^2) - Q\varepsilon(\varepsilon^2 + \nu^2)\}c$$
$$+ \{P\varepsilon(\varepsilon^2 + \nu^2) - Q\nu(\varepsilon^2 + \nu^2)\}s = 0 \tag{2.31}$$

Equation (2.31) may be abbreviated using equations (2.26) and (2.27), that is, $\beta^2 - \nu^2 = \varepsilon^2 + \nu^2 = \mu^2$ and then dividing through by μ^2, hence:

$$\{A\nu + B\beta\}ch + \{A\beta + B\nu\}sh$$
$$- \{P\nu + Q\varepsilon\}s + \{P\varepsilon - Q\nu\}s = 0 \tag{2.32}$$

Equations (2.28), (2.29), (2.30) and (2.32) are compatible if, and only if, the determinant of the coefficients of A, B, P, Q in the set is zero.

That is,

$$\det\begin{vmatrix} 1 & 0 & 1 & 0 \\ 0 & \beta & 0 & \varepsilon \\ (\nu^2+\beta^2)ch & (2\beta\nu)ch & (\nu^2-\varepsilon^2)c & (2\varepsilon\nu)c+ \\ +(2\beta\nu)sh & +(\nu^2+\beta^2)sh & -(2\varepsilon\nu)s & (\nu^2-\varepsilon^2)s \\ (\nu)ch+(\beta)sh & (\beta)ch+(\nu)sh & (-\nu)c+(\varepsilon)s & (-\varepsilon)c-(\nu)s \end{vmatrix} = 0$$

Evaluation of this determinant may be simplified by remembering that $P = -A$ and $Q\varepsilon = -B\beta$ from equations (2.28) and (2.29). Thus rows three and four can be reduced to

$$\begin{vmatrix} (\nu^2+\beta^2)ch+(2\beta\nu)sh & (2\beta\nu)ch+(\nu^2+\beta^2)sh \\ -(\nu^2-\varepsilon^2)c+(2\varepsilon\nu)s & -(2\beta\nu)c-\frac{\beta}{\varepsilon}(\nu^2-\varepsilon^2)s \\ (\nu)ch+(\beta)sh & (\beta)ch+(\nu)sh \\ +(\nu)c-(\varepsilon)s & +(\beta)c+(\frac{\beta}{\varepsilon}\nu)s \end{vmatrix}$$

which, when equal to zero provides the required solution.

It will be remembered that this solution of equations (2.23) and (2.24) depended on p being less than 2μ. However when p and thus ν, are large the correspondingly low value of μ would, theoretically, lead to ε values of less than zero from equation (2.27). Hence the form of equation (2.25) would change to:

$$x=e^{\nu z}(A\cosh\beta z+B\sinh\beta z+P\cosh\varepsilon' z+Q\sinh\varepsilon' z) \qquad (2.33)$$

where $(\varepsilon')^2 = \nu^2 - \mu^2$

At the clamp ($z = 0$) $x = Dx = 0$

so that equation (2.33) becomes:

$$x = A + P = 0 \tag{2.34}$$

and:

$$Dx=e^{\nu z}(A\beta\sinh\beta z+B\beta\cosh\beta z+P\varepsilon'\sinh\varepsilon' z+Q\varepsilon'\cosh\varepsilon' z)$$
$$+ \nu e^{\nu z}(A\cosh\beta z+B\sinh\beta z+P\cosh\varepsilon' z+Q\sinh\varepsilon' z) = 0$$

or
$$B\beta+Q\varepsilon'+\nu(A+P) = 0$$

which, using equation (2.34) is reduced to

$$B\beta+Q\varepsilon' = 0 \tag{2.35}$$

At the tip ($z = 1$) the bending moment and shear force must be zero hence:

$$(EI)D^2x=D\{(EI)D^2x\} = 0$$

and thus

$$\{A(\nu^2+\beta^2)+2\nu\beta B\}\cosh\beta z+\{B(\nu^2+\beta^2)+2\nu\beta A\}\sinh\beta z$$
$$+ \{P(\nu^2+\varepsilon'^2)+2\nu\varepsilon' Q\}\cosh\varepsilon' z+\{Q(\nu^2+\varepsilon'^2)+2\nu\varepsilon' P\}\sinh\varepsilon' z = 0 \tag{2.36}$$

and

$$\{A\nu(\nu^2+3\beta^2)+B\beta(3\nu^2+\beta^2)\}\cosh\beta z+\{A\beta(3\beta^2+\beta^2)+B\nu(\nu^2+3\beta^2)\}\sinh\beta z$$
$$+\{P\nu(\nu^2+3\varepsilon'^2)+Q\varepsilon'(3\nu^2+\varepsilon'^2)\}\cosh\varepsilon' z$$
$$+\{P\varepsilon'(3\nu^2+\varepsilon'^2)+Q\varepsilon'(\nu^2+3\varepsilon'^2)\}\sinh\varepsilon' z = 0 \tag{2.37}$$

Again, the equations (2.34) to (2.37) are compatible only if the determinant of the coefficients of A, B, P and Q in the set is zero. As with the preceding case the four by four determinant can be simplified using the relationships

$$P = -A \text{ and } Q\varepsilon' = B\beta$$

to give the determinant

$$\begin{vmatrix} 2\nu\beta sh\beta z+(\nu^2+\beta^2)ch\beta z & 2\nu\beta ch\beta z+(\nu^2+\beta^2)sh\beta z \\ -2\nu\varepsilon' sh\varepsilon' z-(\nu^2+\varepsilon'^2)ch\varepsilon' z & -2\nu\beta ch\varepsilon' z-\frac{B}{\varepsilon'}(\nu^2+\varepsilon'^2)sh\varepsilon' z \\ \\ \beta(3\nu^2+\beta^2)sh\beta z+\nu(\nu^2+3\beta^2)ch\beta z & \beta(3\nu^2+\beta^2)ch\beta z+\nu(\nu^2+3\beta^2)sh\beta z \\ -\varepsilon'(3\nu^2+\varepsilon'^2)sh\varepsilon' z-\nu(\nu^2+3\varepsilon'^2)ch\varepsilon' z & -\beta(3\nu^2+\varepsilon'^2)ch\varepsilon' z-\frac{\nu\beta}{\varepsilon'}(\nu^2+3\varepsilon'^2)sh\varepsilon' z \end{vmatrix}$$

Thus, the problem is reduced to finding a value of the frequency parameter μ for which either of the determinants, of order 2, above (the choice depending on whether p is less than or greater than 2μ) solve to give a zero value. As with the Myklestad solution, a value of μ is chosen and the determinant evaluated to give a residual parameter R. A similar iteration routine to that described in section 2.2.2 can then be used to determine a suitable μ value to give a zero residual, thus locating a root.

Solutions for the first five modes of vibration of exponentially tapered cantilevers were derived using the above analysis and compared with equivalent solutions from Myklestad routines with three degrees of approximation (ten, twenty and forty steps). A series of taper ratios was analysed with values for p within the range 0.0 to 8.0. A comparison of the values obtained from the exact and approximate analyses is given in Tables 2 and 3 and the graphs (Figures 5 and 6). The first graph (Figure 5) is a plot of the frequency parameter (defined here as μL)

against the taper, expressed as the exponent p, and compares values obtained from the theoretical analysis with the least accurate Myklestad model of ten steps, for the first five modes. Figure 6 is a carpet plot of the frequency parameter against error and taper for the ten and forty step solutions.

An interesting feature is highlighted by Figure 5 and is shown in the plot for the fifth mode. At high values of the frequency parameter solution of the determinant defining the residual (R) involves finding the difference between two very large numbers. If the discriminatory powers of the computer are insufficient to describe these numbers with adequate accuracy then round-off errors can give rise to spurious roots. To demonstrate this, the exact analysis was performed on a small computer (a Digital Equipment Corporation PDP-8/E) in which 24 bits are used to represent a floating point number and then on a larger machine (an Elliot 4120), which represents a real number with 48 bits. In the former case spurious solutions were found and are shown by the symbol ▲ on the graph, while the latter values denoted by the symbol •, give the correct solution. Although this effect was only shown up by the exact analysis it can also occur with the Myklestad method. However, if it is apparent that the computer does not adopt sufficient bits to describe a number for adequate discrimination then the choice of initial conditions at the root may be adjusted to improve the credibility of the residual.

It may be concluded from the above analysis that a lumped parameter model can be considered adequate to describe this type of dynamic system, provided that the degree of approximation is suitable. It is obvious that, if rapid changes in the beam dimensions are present and/or high order modes are required then a more accurate model with a larger number of elements is necessary.

In addition to the analysis of an exponentially tapered cantilever the Myklestad method was also used to derive the resonant frequencies and modal shapes of a linearly tapered cantilever, with varying end conditions. The data were compared with results obtained experimentally using laser image-speckle interferometry, as described in Chapter 3 and enabled the effectiveness of the clamp in providing a fully encastre end condition to be ascertained.

In the calculation it was assumed that the clamp and beam combination acted as a single structure. The end conditions at the base of the clamp were varied from those applying to a built-in structure (initial slope and deflection both zero) to those for a free-free beam (initial shear force and bending moment zero). The latter condition was included because the clamp was placed on a bonded rubber mat. In the extreme, rubber-in-shear could provide effectively free conditions at the base, although for this case it was considered improbable in practice. If the clamp was effective similar results should be obtained from all end conditions and these would agree with

the experimental values. Table 4 compares the results of the two extreme end conditions defined above, with those obtained experimentally, from which it may be concluded that the clamp provided suitably encastré conditions and also gave full vibration isolation of the model from the optical table.

2.2.3 The Pretwisted Beam

The lumped parameter model discussed in section 2.2.1 lends itself easily to being extended to deal with the effects of pretwist. If it is sufficient to consider the beam as being approximated by a lumped mass model then, by extension, it is also adequate to treat each element as being itself without pretwist, while contiguous elements are staggered. The discontinuity at the element junction is then such that the angle of stagger is equal to the pretwist of the previous elemental length. Thus the model developed in section 2.2.1 can be maintained, the only modification necessary being to calculate two new sets of variables at the end of an element, aligned with the next element. If the variables are defined as in Figure (7a) and the relative angular positions of the major and minor principal axes of adjacent elements are as in Figure (7b) then it is easily seen that the matrix relationship

$$\begin{bmatrix} X_1 & X_2 \\ X_1' & X_2' \\ M_1 & M_2 \\ F_1 & F_2 \end{bmatrix}_{\substack{\text{start of} \\ \text{element} \\ r+1}} = \begin{bmatrix} X_1 & X_2 \\ X_1' & X_2' \\ M_1 & M_2 \\ F_1 & F_2 \end{bmatrix}_{\substack{\text{end of} \\ \text{element} \\ r}} \begin{bmatrix} \cos\Delta\theta & \sin\Delta\theta \\ -\sin\Delta\theta & \cos\Delta\theta \end{bmatrix} \qquad (2.38)$$

defines the state at the beginning of element (r + 1) from that existing at the end of element r.

Now, it will be remembered that, when considering the thick beam, an inertia term, of magnitude $(^{I}/_{A})$ times the element mass and coincident with it was necessarily included. However, the angular displacement between the principal axes of the element cross-sections at the junctions of the pretwisted model does not allow these inertias to be added directly, although the masses may be combined as previously. Inertia moments affecting the bending moments M_1 and M_2 may be satisfactorily included by assuming that half the mass of each element is concentrated at the beginning of each element with coincident inertias of magnitude $(^{m}/_{2N})$ $(^{I1}/_{A})$ and $(^{m}/_{2N})$ $(^{I2}/_{A})$. The equations 2.1 to 2.4 may then be used to traverse the element for both planes of deflection with an additional two operations to correct shear force and bending moment so that the forces and moments arising from the lumped mass and inertias at the end of the element are included.

Simplification of the equations 2.1 - 2.4 is achieved, as before, by the use of the composite variables D, B, S, W, α and γ, but with the addition of a term $H = (^{I2}/_{I1})$ to allow for the elastic and dynamic differences between the reference planes.

For the transformation of equation 2.38 to be applicable it is obviously important that the variables $(D, B, S)_1$ are compatible with $(D, B, S)_2$. Thus it is

assumed that all these variables and the frequency parameter are defined in terms of the flexural coefficient $(EI)_1$, then corrected as necessary by the ratio of the second moments of area (H).

The Myklestad equations for the pretwisted beam may, therefore, be expressed as below, where the arrow indicates that the new value of the variable to the left is calculated from the expression to the right, using the current values for the variables.

$$S_1 \rightarrow S_1 + (W/2)\ X_1$$

$$S_2 \rightarrow S_2 + (W/2)\ X_2$$

$$M_1 \rightarrow M_1 + S_1 - (W\alpha N^2/2)\ D_1$$

$$M_2 \rightarrow M_2 + S_2 - (WH\alpha N^2/2)\ D_2$$

$$X_1 \rightarrow X_1 + D_1 + M_1/2 - S_1/3 - (\gamma\alpha N^2)\ S_1 \qquad (2.39)$$

$$X_2 \rightarrow X_2 + D_2 + (M_2/2 - S_2/3)/H - (\gamma\alpha N^2)\ S_2 \qquad (2.40)$$

$$D_1 \rightarrow D_1 + M_1 - S_1/2 \qquad (2.41)$$

$$D_2 \rightarrow D_2 + (M_2 - S_2/2)/H \qquad (2.42)$$

$$S_1 \rightarrow S_1 + (W/2)\ X_1 \qquad (2.43)$$

$$S_2 \rightarrow S_2 + (W/2)\ X_2 \qquad (2.44)$$

$$M_1 \rightarrow M_1 - (W\alpha N^2/2)\ D_1 \qquad (2.45)$$

$$M_2 \rightarrow M_2 - (WH\alpha N^2/2)\ D_2 \qquad (2.46)$$

It should be noted that, for the correct interpretation of these equations, they must be evaluated in the order shown. Since vibration in two planes is now being considered there will be a total of sixteen reactions at the blade tip, calculated from four linearly independent inputs at the base (two for each plane). The determinant of the tip

coefficients is thus of order four and a pivotal condensation technique, based on that due to Gauss, is required for its solution. A full description of the method used in this analysis appears in section 2.4.

2.2.4 Allowance for Centrifugal Forces on a Rotating Beam

Both in the preceding analysis of the single blade and the following analysis of blade packages the effects of rotation about an axis perpendicular to the longitudinal axis of the blades have been ignored. However it is clear that, since present day turbines rotate at high speeds, the centrifugal forces, which are a function of the square of the angular velocity, cannot be considered as negligible.

Basically, centrifugal forces cause an increase in the blade stiffness and a consequent reduction in movement and some workers, for example Huang and Wu (11), Fu (14) and Carnegie (12) have included a correction to account for this when estimating vibration frequencies. It can be shown that Myklestad method is particularly amenable to such a modification.

Figure 8 shows a typical Myklestad element with the addition of an angular velocity of rotation of Ω and the centrifugal forces F_c associated with it. It can be seen that the basic equations of compatability and equilibrium are now of the form:

$$X + \Delta X = X - X'\Delta z + \{M\frac{\Delta z^2}{2} - (F - F_c X')\frac{\Delta z^3}{3}\}/EI - (F - F_c X')\,\Delta z\,(\frac{K}{GA}) \qquad (2.47)$$

$$X' + \Delta X' = X' + \{M\Delta z - (F - F_c X') \frac{\Delta z^2}{2}\} / EI \qquad (2.48)$$

$$M + \Delta M = M - F\Delta z + F_c \Delta X - \omega^2 \Delta J \ (X' + \Delta X') \qquad (2.49)$$

$$F + \Delta F = F + \omega^2 \ \Delta m \ (X + \Delta X) \qquad (2.50)$$

$$F_c + \Delta F_c = F_c + \Delta m \ \Omega^2 \ (z + \Delta z) \qquad (2.51)$$

It will be seen that the model in Figure (8) and the order of the equations (2.47) to (2.51) are different from Figure 1 and the associated equations (2.1) to (2.4). This reversal of the direction of the algorithm is necessary to enable the moment of the centrifugal force to be calculated from the difference in the displacement of the ends of the element (Δm). Although this affects the detail of the method, the principle is retained and the application to blade packages follows similar arguments to those given earlier.

2.3 Analysis of Packages of Thick, Pretwisted Cantilever Blades

2.3.1 Introduction

In Chapter 1 the contributions of several authors on the analysis of blade packages were discussed in detail. Having shown that the lumped parameter approximate model originally due to Myklestad, but further developed by other workers, has certain advantages over the alternative methods, it is now proposed to extend the techniques developed in the preceding sections to cover the vibration of a series of cantilever blades joined at their tips by a shroud.

An early paper by Smith (9) applied the Myklestad technique to packages consisting of parallel, equispaced blades of uniform section vibrating only in the plane of the package. The blades were considered to be joined by inextensional bands, represented only by their centre lines, the mass of each band being concentrated at the blade tips. The former approximation obviously requires all blades to have the same displacement at the tips, while the latter restricted all motion of significance to a direction normal to the unstrained centre lines of the blades. The shrouds in this model do, however, introduce resistance to slope at the blade tips, while the effect of neglecting junction thickness (which tends to underestimate natural frequencies) and shear flexibility and rotary inertia (shown by Allen to cause overestimation of frequencies) are probably self-cancelling.

Prohl (8) extended Smith's model to include pretwist of the blades, but although torsional coupling of the blades and axial flexibility of the bands were included, shear flexibility, rotary inertia and an allowance for thickness at the blade/shroud junctions were, again, neglected.

Allen (1) also improved Smith's model, to include the effects due to thickness of both blades and shrouds, but restricted the analysis to blades vibrating in a single plane. Thus, torsional coupling of the blades, axial flexibility of the shrouds and pretwist were excluded. However, deformation due to axial forces was included for both blades and shrouds, thus permitting transverse coupling between the deflections arising from all the beams in the package. Additionally, since the pressure fluctuations giving rise to blade vibrations are also capable of exciting flexural vibration of the shroud (and, therefore the possibility of shroud failure) longitudinal vibration of the blade was also considered.

Shiga (27) modified the method due to Prohl and considered an unstaggered model similar to that of Allen. The principal axis of the blade cross section was considered to be parallel and perpendicular to the direction of rotation of the package and although tangential and axial vibration were calculated, flexural-flexural and flexural-torsional coupling and the effects of pretwist were omitted.

The purpose of the current investigation is,

therefore, to develop the basic analysis of previous workers to include the case where the blade principal axes are at an angle to the direction of rotation of the package. All blade/shroud coupling effects will also be introduced.

2.3.2 The Effect of Connecting Single Blades with Shroud Bands

The common practice of joining turbine blade tips with a shroud not only prevents leakage of the working fluid around the blade tip, but also provides increased resistance to displacement caused by blade vibrations. However, additional natural vibration frequencies, other than those of a single cantilever blade, are now permitted to occur due to coupling effects. Thus groups of distinct, but interrelated modal shapes, within a relatively narrow frequency band, are formed in addition to the "detached" frequencies of the separate blades.

The "detached" modes, consisting of the fundamental frequency and its harmonics, have deflection curves for each blade similar to that of the single blade with a free tip and encastre root, although the slope at the tip can be reduced by the presence of the shroud. All blades in the package move in phase (that is, the motion is symmetric) and with similar displacement amplitudes. The shrouding is thus forced to move with the blades and consequently this type of mode is sensitive to changes in the shroud mass.

The grouped, or batch, modes, which occur at frequencies considerably higher than their related detached

modes, can be divided into two types, symmetric and antisymmetric, although both exhibit deflection curves resembling the fundamental (or appropriate harmonic) of a beam simply supported at the tip and with an encastre root. Symmetrical modes show slight movement of the shroud and can thus be affected by changes in the shroud mass, but to a much lesser extent than the detached modes. Antisymmetric modes, where blades in corresponding positions each side of the package centre line have deflection curves with a 180^{o} phase shift, do not entail movement of the shroud and are thus least sensitive to changes in the shroud mass. With both types of batch modes considerable differences occur between the amplitudes of deflection of individual blades in the packet, although blades in corresponding positions about the centre line have the same amplitudes.

Examples of detached and related batch modes for a package vibrating in the tangential direction are shown in Figure 9.

The number of modal shapes within these bands is related to the number of blades (N) and also, according to Thomas and Belek (20) to the ratios

$$\frac{(EI)_s \; / \; (EI)_b}{(\rho A)_s \; / \; (\rho A)_b}$$

and L_s/L_b

where (EI) is the flexural rigidity

ρ is the mass density

A is the cross-sectional area

L is the length

and the suffices s and b refer to the shroud and blade respectively.

Thomas and Belek show that there are at least (N-1) batch frequencies in addition to the detached mode, but this can be increased if the flexural rigidity/weight ratio is low and the length ratio is high. Allen and others have shown that a total of N modal shapes can occur as a group (one detached, plus (N-1) batch frequencies), but these workers do not assess the effect of the above ratios. Shiga found that the introduction of uncoupled torsional vibration gave rise to N flexural vibrations and N torsional vibrations.

The large number of close frequencies which can occur with blade packages if the number of blades is high can give rise to multiple roots and subsequent ill-conditioning of the calculation. Both Prohl (8) and Stuwing (28) referred to the problem of ill-conditioned arrays due to loss of accuracy in the computation. Allen (1) minimised the effect by solving for the symmetric and antisymmetric modes independently and thus was able to reduce the apparent number of blades from N to $\frac{1}{2}(N + 1)$ or less. However, it may be noted that this technique relies on the matrix of the coefficients relating the blade tip and root reactions possessing either symmetrical or skew-symmetrical properties. While this was true for the case of untwisted blades moving in the tangential direction, considered by

Allen, it cannot be held to be generally true when considering pretwisted blades and vibration in all three planes. Thus, this improvement to the simple solution has not been adopted in the current work.

In fact, the central nominal values of frequencies in the groups can be found accurately by solving for packages with a reduced number of blades and it is shown by Smith (9) who compared packages of six and twenty blades and Shiga (27) who analysed packages of from four to seven blades that the bandwidth of the group remains constant, so that the frequencies become closer with increase in the number of blades. Allen, however, concluded that the frequency bandwidth increased with the number of blades and that the increase could not be estimated reliably by extrapolation. In either case it is probable that the variation in the frequencies of similar packages, due to manufacturing tolerances, will offset any errors due to analysing a package of blades with the correct proportions but reduced in number. In addition, since the method requires the solution of an array of size (6xN by 6xN), when considering movement in all three planes, a reduction in the number of blades (N) considerably reduces the computation time and the likelihood of the calculation becoming ill-conditioned.

For the purpose of this investigation the number of blades considered has generally been reduced to three, the minimum required to demonstrate the coupling effects

referred to above, although additional packages of five and seven blades have been analysed theoretically to assess the affect of this increase.

2.3.3 The Blade Package Model

Use of the Myklestad analysis for the solution of a package of shrouded blades is a direct extension of the technique for a single blade. Each blade, with its related shroud bands is treated separately and in turn, the root reactions of all other blades in the package being taken as zero and thus the ends of the bands remote from the blade under consideration are, effectively, clamped.

A typical blade as described above, with the variables defining the end conditions, is shown in Figure 10. Two further assumptions follow from this diagram. It can be seen that the reactions and movements are shown to act at the points J, A, B, C and D. However, although this is only strictly valid for thin beams, the degree of approximation is reduced by the introduction of shear flexibility and rotary inertia and despite the further supposition that plane, transverse unstrained sections remain plane during the vibration it is considered that an improvement on thin beam theory is obtained. Secondly, in the analysis of pretwisted blades the shroud bands are assumed to be rectangular in plan, whereas the true shape is that of a lozenge. Although without justification, this may be considered as an extension of the previous assumption and considerably simplifies the shroud model,

enabling the same basic Myklestad calculation to be used for blades and shrouds, with only minor modifications to allow for the dimensional differences. In fact, an improvement could be made to the shroud model to allow for the true shape, but it was felt that the additional complications would not be justified.

It is obvious that the two end blades are not typical of the example shown in the diagram, since one shroud band is missing, but this affects only the detail and not the principle of the method.

The variables as shown in Figure 10 are consistent with the Myklestad analysis for the individual beams, but are inconsistent when considering the package as a whole. It is convenient, therefore, to define a local co-ordinate system relating to the individual beams (Figure 10) and a global co-ordinate system relating to the package as a whole (Figure 11). The Myklestad method is applied to the beams which comprise the package as described in detail below.

In section 2.2.1 it was shown that reactions and movements at the tip of a beam could be calculated from a set of linearly independent end conditions at the root and the frequency parameter V. This is retained when dealing with the blade packages, although the value of V requires to be altered when dealing with "stiff" (y) blade motion and the shroud since it is based on the "flexible" (I_x) second moment of area of the blade. In addition

further calculations are required to establish the longitudinal and torsional effects necessary for the complete analysis. Thus, four linearly independent conditions are needed for the Myklestad calculations (two pairs for each plane), one being set to unity and the other to zero in turn. With the longitudinal and torsional calculations this enables the tip conditions to be expressed by the four matrix transformations:

$$\begin{bmatrix} X \\ X' \\ M_X \\ F_X \end{bmatrix}_{tip} = \left[A_1\right]_X \begin{bmatrix} M_X \\ F_X \end{bmatrix}_{root} \tag{2.52}$$

$$\begin{bmatrix} Y \\ Y' \\ M_Y \\ F_Y \end{bmatrix}_{tip} = \left[A_1\right]_Y \begin{bmatrix} M_Y \\ F_Y \end{bmatrix}_{root} \tag{2.53}$$

$$\begin{bmatrix} Z \\ F \end{bmatrix}_{tip} = \left[A_2\right] \left[P\right]_{root} \tag{2.54}$$

$$\begin{bmatrix} \theta \\ T \end{bmatrix}_{tip} = \left[A_3\right] \left[T\right]_{root} \tag{2.55}$$

remembering that slopes and displacements at the built-in root are zero.

$[A_1]$ is a (4 x 2) array of the coefficients calculated from the step by step integration for each value of the relevant frequency term V and $[A_2]$ and $[A_3]$ are the longitudinal and torsional coefficient arrays, which may be developed as follows.

If the beam is non-uniform the tabulation method due to Holzer (5), which was used as the basis of the Myklestad technique, may be applied to calculate the coefficients. However, in the case of a beam with constant cross section the simpler, exact solutions may be used.

a) Longitudinal Vibration

Consider an element of length dz at a distance z from the blade root, undergoing a steady state vibration at a circular frequency of ω. If the displacement and tensile force are defined as Z and P respectively then the elemental inertia force (-dP) is given by

$$\left(\frac{m}{L}\right) dz\omega^2 Z$$

and the strain $\left(\frac{dZ}{dz}\right)$ by

$$\frac{P}{EA}$$

Then, $\frac{dP}{dz} = -\left(\frac{m}{L}\right) \omega^2 Z$

and thus $\frac{d^2P}{dz^2} = -\left(\frac{m}{L}\right) \omega^2 \frac{dZ}{dz}$

Therefore $\frac{d^2P}{dz^2} + \left(\frac{m\omega^2}{EAL}\right) P = 0$ (2.56)

This is the characteristic equation, with a solution of the form:

$$P = C_1 \cos \Lambda \frac{z}{L} + C_2 \sin \Lambda \frac{z}{L} \qquad (2.57)$$

where $\Lambda^2 = \frac{m\omega^2 L}{EA}$

Since the blade root is encastre Z = 0 at z = 0,

from which $C_2 = 0$

and by substitution $C_1 = P_{root}$

The longitudinal reactions and movements at the tip are thus given by the matrix equation

$$\begin{bmatrix} Z \\ P \end{bmatrix}_{tip} = \begin{bmatrix} \frac{L}{EA} \cdot \frac{\sin \Lambda}{\Lambda} \\ \cos \Lambda \end{bmatrix} \cdot P_{root} \qquad (2.58)$$

b) Torsional Vibration

In this case also a single exact calculation similar in principle to that used for longitudinal vibration may be used for the uniform beam.

Consider the angular displacement θ of an element of length dz at a distance z from the root of the blade, undergoing a steady state vibration at a circular frequency of ω. Let the torque acting on the element be T.

Then the elemental inertia moment (-dT) is given by

$$Ip \, \rho \, dz \, \omega^2 \, \theta$$

and thus $\frac{dT}{dz} = - Ip \, \rho \, \omega^2 \, \theta$

where Ip = polar moment of inertia

ρ = density

Therefore $\frac{d^2T}{dz^2} = - Ip\ \rho\ \omega^2\ \frac{d\theta}{dz}$

But $\frac{d\theta}{dz} = \frac{T}{GJ}$

where J = torsional constant

G = modulus of rigidity

thus $\frac{d^2T}{dz^2} + (\frac{Ip\rho}{GJ})\ \omega^2\ T = 0$ (2.59)

The general solution of equation (2.59) is of the form

$$T = C_1 \cos \Psi \frac{z}{L} + C_2 \sin \Psi \frac{z}{L} \quad (2.60)$$

where $\Psi^2 = (\frac{Ip\rho}{GJ})\ L^2\ \omega^2$

By consideration of the boundary conditions:

$$C_2 = 0 \text{ and } C_1 = T_{root}$$

Thus $T_{tip} = T_{root} \cos \Psi$

and $\theta_{tip} = \frac{T_{root}\ L}{GJ} \cdot \frac{\sin \Psi}{\Psi}$

which can be expressed in the form

$$\begin{bmatrix} \theta \\ T \end{bmatrix}_{tip} = \begin{bmatrix} \frac{L}{GJ} \cdot \frac{\sin \Psi}{\Psi} \\ \cos \Psi \end{bmatrix} T_{root} \quad (2.61)$$

St. Venant has shown that the torsional constant for a rectangular section can be calculated approximately from the equation of an ellipse, by

replacing the given cross-section by an elliptic cross-section having the same polar second moment of area and area as the actual section.

That is, $J = \frac{\pi a^3 b^3}{a^2+b^2} \simeq \frac{A^4}{4\pi^2 Ip} \simeq \frac{A^4}{40Ip}$

Thus $\psi^2 = (\frac{\omega^2 \rho}{GJ}) L^2 \omega^2 \simeq (\frac{\omega^2 \rho}{G} \frac{4\pi^2 Ip^2}{A^4}) L^2$

Now, the modulus of rigidity and Young's modulus are, as previously assumed, related by the expression

$$E = \frac{8}{3} G$$

and the circular vibration frequency is related to the dimensionless frequency parameter by

$$\omega^2 = V^4 . \frac{EI}{A\rho L^4}$$

Therefore $\psi^2 \simeq (\frac{8\rho}{3E} . \frac{V^4 EI}{A\rho L^4} . \frac{4\pi^2 Ip^2}{A^4}) L^2$ (2.62)

Remembering that, for a rectangular section

$$I = \frac{AT^2}{12}$$

equation (2.62) can be simplified to

$$\psi \simeq \frac{\sqrt{8}}{3} . \pi . \frac{TIp}{LA^2} . V^2 \quad (2.63)$$

Having thus established all the reactions and movements at a typical blade tip, referred to the local blade axes the corresponding movements at the shroud tips (A and C in Figure 10) are required. Obviously, if the blade is staggered, each of the variables (with the exception of longitudinal and torsional variables, which are independent of the blade angle) needs to be resolved into the local shroud co-ordinate system before transference. If the zone JAC at a typical blade/shroud junction, such as that shown in Figure 12, is considered as being rigid then the combination of resolved lateral and longitudinal movements will give rise to corresponding movements of the shroud, as shown by the fine outlines. Torsional motion of the blade will not give rise to displacement of the shroud provided that the angular displacement, θ, is small, since the movement of the points A and C will be functions of $(1 - \cos\theta)$ in the tangential direction and $(\sin\theta)$ in the axial direction. From geometrical considerations it can be deduced that the shroud movements are suitably represented by the matrix equation:-

$$\begin{bmatrix} X_A \\ X_B \\ X'_A \\ X'_B \\ Y_A \\ Y_B \\ \theta A \\ \theta B \\ Z_A \\ Z_B \end{bmatrix} = \begin{bmatrix} 1 & 0 & -(^{T}1/2) & 0 & 0 \\ -1 & 0 & -(^{T}1/2) & 0 & 0 \\ 0 & 0 & 1 & 0 & 0 \\ 0 & 0 & 1 & 0 & 0 \\ 0 & 0 & 0 & 1 & -(^{T}2/2) \\ 0 & 0 & 0 & 1 & -(^{T}2/2) \\ 0 & 0 & 0 & 0 & 1 \\ 0 & 0 & 0 & 0 & 1 \\ 0 & -1 & (^{T}2/2) & 0 & 0 \\ 0 & 1 & -(^{T}2/2) & 0 & 0 \end{bmatrix} \begin{bmatrix} Z_J \\ X_J \\ X'_J \\ Y_J \\ Y'_J \end{bmatrix} \qquad (2.64)$$

Substitution of these movements into equations (2.52) to (2.55) with the coefficients of the upper halves of the $[A]$ arrays allows the resultant root reactions for the shroud bands to be calculated. Corresponding tip reactions, resulting from the tip movements, are then available from the equations (2.52) to (2.55) by solving for the lower halves of the $[A]$ arrays and the root reactions.

Consider, for example, equation (2.52), applied to the shroud.

The array $[A_1]_x$ has been computed for two linearly independent inputs at the root, the first having the shear force set equal to 1 and bending moment zero, the second being the reverse. The array may be considered as two sub arrays relating movements and reactions, that is

$$\left[A_1\right]_x = \left[\begin{bmatrix}[A_{11}]\\ [A_{12}]\end{bmatrix}\right]_x = \left[\begin{bmatrix}X_S & X_B\\ X'_S & X'_B\end{bmatrix}\cdot\begin{bmatrix}M_S & M_B\\ F_S & F_B\end{bmatrix}\right]_x$$

where the suffices S and B indicate the input variable set to unity.

The known tip movements and array $[A_{11}]$ are used to establish the reactions at the root due to these displacements, a convenient method being the sequence of calculations below.

By transposing and rearranging (2.52) the equation

$$\left[X\ X'\right]_{tip} = \left[M_x\ F_x\right]_{root}\begin{bmatrix}X_S & X'_S\\ X_B & X'_B\end{bmatrix} \qquad (2.65)$$

is obtained.

Multiplying both sides of (2.65) by $\begin{bmatrix}-X'_S\\ X_S\end{bmatrix}$ yields

$$\left[X\ X'\right]_{tip}\begin{bmatrix}-X'_S\\ X_S\end{bmatrix} = \left[M_x\ F_x\right]_{root}\begin{bmatrix}0\\ X'_B\ X_S - X_B\ X'_S\end{bmatrix} \qquad (2.66)$$

If $X'_B\ X_S - X_B\ X'_S = \Delta$

then (2.66) becomes, on simplification

$$X'X_S - X_B X'_S = F_{x_{root}} \cdot \Delta$$

Thus
$$F_{x_{root}} = \frac{1}{\Delta}\left(X'X_S - XX'_S\right) \qquad (2.67)$$

Multiplying (2.65) by $\begin{bmatrix} -X'_B \\ X_B \end{bmatrix}$ and solving yields

$$M_{x_{root}} = \frac{1}{\Delta} (XX'_B - X'X_B) \qquad (2.68)$$

Having evaluated the root reactions $F_{x_{root}}$ and $M_{x_{root}}$ from equations (2.67) and (2.68) the tip reactions are easily obtained using the sub array $[A_{12}]$ in equation (2.52), thus,

$$\begin{bmatrix} M_x \\ F_x \end{bmatrix}_{tip} = [A_{12}] \begin{bmatrix} M_x \\ F_x \end{bmatrix}_{root} \qquad (2.69)$$

However, analysis of the equations (2.52) to (2.55) will show that care must be exercised when automatic computation is being used for their solution. If the trial value of the frequency parameter corresponds to a transverse, clamped-clamped natural vibration of the bands the array $[A_{11}]$ will be singular and equation (2.65) cannot be formed. For finite values of the shroud root reactions the tip movements must then also be zero, which condition corresponds to the clamped-clamped longitudinal natural vibration of the blade. Although this combination is possible it is considered to be inapplicable to this analysis of the blade package and thus if $[A_{11}]$ is found to be singular the frequency value is recorded for separate investigation and the analysis is repeated with V

increased by an amount less than the normal interval. A similar situation also occurs when considering the longitudinal and torsional vibration of the shroud. If, for example equation (2.58) is taken in two stages, to calculate first the shroud root reaction from the tip movement, then the corresponding tip reaction, the relationships

$$P_{root} = \left(\frac{L}{EA} \sin \Lambda\right)^{-1} Z_{tip} \qquad (2.70)$$

$$\text{and } P_{tip} = (\cos \Lambda)\, P_{root} \qquad (2.71)$$

are obtained.

A clamped-clamped longitudinal natural frequency for the band will give $(\sin \Lambda) = 0$ in equation (2.70), thus no solution will be available and the frequency value is again recorded and the particular trial abandoned.

It may be pertinent to record that no cases of such coincident vibrations were, in fact, found to occur in the current analysis.

However, in a typical case, reactions at the shroud ends A, B, C, and D, as shown in Figure 10 are obtained for a given value of the frequency parameter and independent initial conditions at the blade root. The reactions at A and C can now be transferred such that resultant reactions (from the blade and shroud bands) are considered to act at the point J. Since the shroud and blades are considered

to have finite thickness the forces at A and C act as J in conjunction with additional moments.

It is convenient to consider the resultant reactions expressed in terms of the global (package) co-ordinate axes, as defined in Figure 11, therefore component reactions, calculated in the blade and shroud local (Myklestad) axes are converted to the global system prior to forming the resultants. A comparison of Figures 10 and 11 enables this relationship to be deduced.

If the pth blade is being considered (where $1<p<N$) the resultant forces and moments in global co-ordinates are given by:

$$FJV_P = P_J+S_{XA}+S_{XC} \tag{2.72}$$

$$FJH_P = -S_{XJ}\cos\alpha+S_{YJ}\sin\alpha+P_A-P_C \tag{2.73}$$

$$FJR_P = -S_{XJ}\sin\alpha-S_{YJ}\cos\alpha-S_{YA}-S_{YC} \tag{2.74}$$

$$MJV_P = T_Y-B_{YA}-B_{YC} \tag{2.75}$$

$$MJH_P = B_{XJ}\cos\alpha+B_{YJ}\sin\alpha T_A-T_X+\frac{T_2}{2}(S_{YA}+S_{YC}) \tag{2.76}$$

$$MJR_P = B_{XJ}\sin\alpha+B_{YJ}\cos\alpha-B_{YA}+B_{YC}-\frac{T_1}{2}(S_{XA}-S_{XC}) + \frac{T_2}{2}(P_A-P_C) \tag{2.77}$$

If the extreme left hand blade is being considered (p=1) then there is no shroud to the left and the terms with suffix C are suppressed. Similarly if the extreme right hand blade is being considered (p=N) the terms with suffix A are suppressed.

The reactions computed at the remote ends of the shrouds (suffices B and D) are related to the tips of the adjacent blades (J_{p-1} and J_{p+1}). Thus, the forces and moments calculated for the previous blade and to be calculated for the next blade are modified by the expressions:

$$FJV_{p-1} = - S_{XB} \tag{2.78}$$

$$FJH_{p-1} = - P_B \tag{2.79}$$

$$FJR_{p-1} = S_{YB} \tag{2.80}$$

$$MJV_{p-1} = B_{XB} - S_{YB}\left(\frac{T_1}{2}\right) \tag{2.81}$$

$$MJH_{p-1} = - T_B - S_{YB}\left(\frac{T_2}{2}\right) \tag{2.82}$$

$$MJR_{p-1} = B_{YB} - S_{XB}\left(\frac{T_1}{2}\right) \tag{2.83}$$

$$FJV_{p+1} = - S_{XD} \tag{2.84}$$

$$FJH_{p+1} = P_D \tag{2.85}$$

$$FJR_{p+1} = S_{YD} \tag{2.86}$$

$$MJV_{p+1} = - B_{XD} + S_{YD}\left(\frac{T_1}{2}\right) \tag{2.87}$$

$$MJH_{p+1} = T_D + S_{YD}\left(\frac{T_2}{2}\right) \tag{2.88}$$

$$MJR_{p+1} = - B_{YD} + S_{XD}\left(\frac{T_1}{2}\right) \tag{2.89}$$

Again, if p=1 equations (2.78) to (2.83) have no meaning and are suppressed and if p=N equations (2.84) to (2.89) are suppressed.

To summarise, for each trial value of the frequency parameter, V, coefficients relating 6N resultant reactions at the blade tips to the 6N independent reactions at the blades are obtained. For a free vibration of the blade package the tip resultants must all be zero. As with the single cantilever this is true only if the determinant of coefficients which relates the reactions is zero. In matrix form this relationship is expressed by the equation:

$$\begin{bmatrix} FJV_1 \\ FJH_1 \\ FJR_1 \\ MJV_1 \\ MJH_1 \\ MJR_1 \\ \cdot \\ \cdot \\ \cdot \\ FJV_N \\ FJH_N \\ FJR_N \\ MJV_N \\ MJH_N \\ MJR_N \end{bmatrix}_{tip} = [C] \begin{bmatrix} P_1 \\ S_{X1}\sin\alpha+S_{Y1}\sin\alpha \\ -S_{X1}\sin\alpha+S_{Y1}\cos\alpha \\ T_1 \\ B_{Y1}\sin\alpha+B_{X1}\cos\alpha \\ B_{Y1}\cos\alpha-B_{X1}\sin\alpha \\ \cdot \\ \cdot \\ \cdot \\ P_N \\ S_{XN}\cos\alpha+S_{YN}\sin\alpha \\ -S_{XN}\sin\alpha+S_{YN}\cos\alpha \\ T_1 \\ B_{YN}\sin\alpha+B_{XN}\cos\alpha \\ B_{YN}\cos\alpha-B_{XN}\sin\alpha \end{bmatrix}_{root} \qquad (2.90)$$

Again, the requirement for a zero left hand side to equation (2.90) and thus a natural frequency of vibration of the package, is that $\det|C| = 0$ and, therefore, once the (6N x 6N) determinant is evaluated a similar routine to that described in section 2.2.2 may be used to search for a solution.

2.4 Evaluation of the Determinant of Coefficients

It has been shown in previous sections that the Myklestad method requires the terminal variables calculated from the step-by-step integration along the beam to be zero for the estimated frequency to coincide with a natural frequency of vibration. In the simple case of the single beam vibrating in one plane the terminal variables consist of a (2 x 2) determinant of the reactions calculated from two linearly independent input variables, the solution of which is straightforward. When the beam is considered to vibrate in two planes, as with the introduction of pretwist, the determinant size is increased to (4 x 4), whilst a package of N blades, permitted to vibrate in all three planes requires the solution of a (6N x 6N) array.

In order to evaluate the determinants from the latter two cases, without undue loss of accuracy, the arrays need to be reduced by a method of pivotal condensation. The technique used in this study is similar to the standard reduction method due to Gauss, but has been modified to prevent a zero element in the leading diagonal causing a breakdown of the process.

The first column of the array is scanned to locate the non-zero element of greatest modulus, which is used as the "pivot" for that column. Multiples of this row are then subtracted from all other rows such that their elements in column one are reduced to zero. The process is then repeated with column two and so on, with the proviso that the pivotal element is not in a row previously used as a pivot row, so that no row contains more than one pivot. The result is a square array in which each

column and row possesses only one non-zero element and which can be readily evaluated to provide the residual parameter required for the search routine. Should a non-zero pivot be unavailable then the value of the determinant is zero, but each column is still traversed to find the total number of columns without pivots, since this is a measure of the number of independent modes of vibration which can occur at that trial frequency. If the modal shapes are required in addition to the resonant frequency it is necessary to find the column(s) which become null when premultiplied by the original array. For this reason the original array must be stored and the pivotal condensation performed on a duplicate. The appropriate columns required for the modal shapes are then extracted by a routine also based on pivotal condensation.

2.5 Conclusion of the Theoretical Analysis

The lumped parameter method of Myklestad has been developed from the anlaysis of single beams, vibrating in one plane, to that of a package of thick, shrouded blades free to vibrate in all three planes. The effects of taper and pretwist have also been assessed. In the analysis of blade packages flexural, longitudinal and torsional vibration are permitted to occur, with full allowance for coupling of modes. Although this results in an increase in the size of the problem as a whole no increase in the number of elements comprising the model itself is required for a given accuracy.

It is proposed that an analysis of a blade package with a limited number of blades will give adequate information to enable both detached, symmetrical vibration frequencies and the bandwidth of grouped modes to be established economically. Should a more thorough investigation, with, perhaps an increase in the number of blades, be required in certain areas then the accuracy of the model can be improved and a more detailed search of this particular range of interest can be initiated.

Whilst it has been shown that a Myklestad solution is amenable to the introduction of centrifugal effects due to rotation of the blade package, these have not been included in the current investigation because it was considered that the experimental confirmation of this aspect would necessitate a disproportionate demand on the available resources.

A comparison of the exact solution for exponentially tapered beams has been compared with the results from lumped parameter models to demonstrate the validity of the approximate

method. In addition results from a Myklestad analysis of a series of blade package models have been compared with data obtained by experimentation and a detailed appraisal of this is given in Chapter 4.

3. EXPERIMENTAL CONFIRMATION OF ANALYTICAL TECHNIQUE

3.1 Introduction and Choice of Experimental Technique

There are several methods available for the experimental analysis of vibration, varying in their sensitivity, ease of application and interpretation of results. Broadly, such methods may be divided into two groups, those using transducers and those relying on optical effects.

The use of transducers, such as strain gauges, accelerometers, or position sensing devices is generally simple in application and interpretation of the data obtained. However, measurement is restricted to discrete points on the object and with the former two techniques the transducer must be in contact with the object, which may affect the vibration being measured. Allen (1) minimised this by the use of gramophone pick-ups, which reduce the area of contact virtually to a point, yet retain sufficient sensitivity and discrimination to enable vibrations to be measured over a wide frequency range. Even so, use of these methods becomes restricted when considering complex objects or motion in more than one plane, since it becomes difficult to interpolate between the measuring stations. Allen used five transducers in a group and investigated ten positions of this group for each frequency under observation. This necessitated repeating every test under control conditions.

Optical techniques overcome the latter problem and also have the advantage of being non-contacting, but are still often restricted in application.

Ligtenberg (29) showed that Moiré fringes are formed when the reflections of a diffraction grating in the polished surface of an object are compared using a double-exposed photograph of the object when stationary and then when vibrating. The fringes are shown to thicken in the area of the antinode, but the method is insensitive, difficult to interpret and is restricted to polished, flat surfaces. Tolansky and Wood (30) devised an accurate method in which the vibrating object, which again must be a flat plate, is compared with an optical flat to form Fizeau fringes, which show the surface nodes. Inclination of the surfaces, combined with illumination with monochromatic light gives rise to a series of sharp, parallel fringes, which broaden in the antinodal region.

Photoelastic materials, either in the form of a coating (which may affect the vibration being studied) or as the model itself may also be used. These materials become doubly refracting when strained, the effect being proportional to the magnitude of the strain. When polarized monochromatic light is passed through, or reflected from, the material it is split into two orthogonally polarized components, each being parallel to a principal stress direction and with a propagation velocity proportional to the stress magnitude. If the light is then viewed through a polarizer crossed with the original polarizer such that only the horizontal components of these rays are seen, then, when the components are in phase, a dark fringe is formed for points on the object having similar principal stress differences. Although this technique can be used with complex shapes it is complicated both to use and

interpret, is insensitive and requires the use of special materials. Similar disadvantages occur with Schlieren techniques.

The advent of the Laser (a powerful source of coherent light) in 1960, its application to Gabor's system of holography (31), by Leith and Upatnieks (32) and the subsequent use of holography to observe vibration modes by Powell and Stetson (33) and Archbold and Ennos (34), inter alia, has enabled considerable advances to be made in the study of vibrating systems. Laser holography offers several advantages over the methods discussed above, in that it is non-contacting, comparatively simple to use and interpret, is sensitive and accurate and can give a complete picture of the complex vibrations of an intricate opaque object. Although in some cases special surface coatings can improve the technique they are not, generally, necessary. Measurements may be carried out in real time or remotely by the use of photographs, or the time-averaged technique of Powell and Stetson. Measurements may even be carried out in adverse environments (35) by the use of pulse lasers.

Another simple and sensitive method which utilises the high power and coherence of the Laser is the Laser speckle interferometry technique due to Mottier and Eliasson (36), Stetson (37) et al. Although only the nodal pattern can be observed (in a form similar in appearance to Chladni sand patterns) the technique is valuable for assessment of modal shapes in real time.

The advantages of Laser holography and speckle interferometry

show them to be ideally suited for the confirmation of the results derived from the theoretical analysis of blade packages vibrating in three planes and the particular techniques adopted will be discussed in further detail.

3.3 Principles of Laser Holography and Interometry Applied to Vibration Analysis

3.3.1 Time Averaged Holography

It is well known that a photographic plate is capable of recording only the intensity of the light incident upon it and thus phase information (relating to line of sight distance) is lost. Gabor (31) demonstrated that if the plate was illuminated by two beams of coherent light, one, the object beam, reflected from the object, the other, the reference beam, directed at the plate, then the two beams would interfere. The fringe pattern recorded acts as a diffraction grating that, when illuminated by one beam, will diffract it such that a reconstruction of the other beam is formed. Hence, on illumination of the photographic plate (or hologram) with the reference beam a diffracted beam is formed which is a replica of the original object beam and thus an observer will see a fully three-dimensional image of the object. This may be expressed mathematically as below:

In general the intensity I, of a light source is given by the product of the amplitude, a, and its complex conjugate a*. If we use the suffices r and o to represent the reference and object beams then the intensity at the hologram plate is given by :

$$I_p = (a_r + a_o)\ (a_r^* + a_o^*)$$

$$= a_r\, a_r^* + a_o\, a_o^* + a_r\, a_o^* + a_o\, a_r^* \qquad (3.1)$$

The first two terms of this expression are obviously the intensities of the reference and object beams and the

expression can be further simplified by writing

$$a_r = a_r e^{i\phi r} = a_r (\cos \phi_r + i \sin \phi_r)$$

$$a_r^* = a_r e^{-i\phi r} = a_r (\cos \phi_r - i \sin \phi_r)$$

Similarly for a_o and a_o^*

Equation (3.1) thus becomes

$$I_p = I_r + I_o + 2a_r a_o \cos (\phi_o - \phi_r) \qquad (3.2)$$

the final term of this expression giving rise to the fringe pattern, which is recorded on the photographic plate.

To reconstruct the image the hologram is illuminated with the reference beam and the transmitted intensity, which is the product of the original intensity at the plate, I_p, and the reference beam amplitude, a_r, is given by the modified form of (3.1):

$$a_r I_p = a_r I_r + a_r I_o + a_r a_r a_o^* + a_r a_r^* a_o$$

$$= a_r I_r + a_r I_o + a_r a_r a_o^* + I_r a_o \qquad (3.3)$$

It is the final term in equation (3.3), the reference beam intensity, modulated by the object beam amplitude, which is identical to the original wavefront and gives rise to the virtual image at the object position. The term $a_r a_r a_o^*$ gives rise to a real, focussed conjugate image behind the hologram, when a collimated reference beam is used to illuminate the plate.

Before forming the equations pertaining to an object in motion it is relevant to consider the sequential recording, on a single photographic plate, of an object which is slightly

displaced between exposures. If the same reference beam is used for each exposure and the amplitudes of the object beams for the two object positions are a_{o1} and a_{o2}, then equation (3.1) becomes, for each case

$$I_{p1} = I_r + I_{o1} + a_{o1}a_r^* + a_{o1}^*a_r$$
$$I_{p2} = I_r + I_{o1} + a_{o2}a_r^* + a_{o2}^*a_r$$

The hologram superimposes these two intensities to give a total intensity of

$$I_{pt} = I_{p1} + I_{p2}$$
$$= 2I_r + I_{o1} + I_{o2} + a_r\,(a_{o1}^* + a_{o2}^*) + a_r^*\,(a_{o1} + a_{o2})$$

It can be seen by comparison with equation (3.3) that on reconstruction with the reference beam (of amplitude a_r) the virtual image is given by the final term

$$a_r a_r^*\,(a_{o1} + a_{o2}) = I_r\,(a_{o1} + a_{o2})$$

Now, since the intensity of a light source is given by the products of its amplitudes (aa^*), the intensity of the image is given by

$$I_i = (a_{o1} + a_{o2})(a_{o1}^* + a_{o2}^*) \qquad (3.4)$$

if the reference intensity, I_r, onto which this is modulated, is ignored.

Additionally, if the object displacement is small with respect to its distance from the hologram then,

$$|a_{o1}| = |a_{o2}|$$

and thus

$$a_{o1} = a_o \; e^{i\phi_1}$$

$$a_{o2} = a_o \; e^{i\phi_2}$$

Equation (3.4) can now be simplified to;

$$I_i = 2 \; a_o^{\;2} \{1 + \cos (\phi_1 - \phi_2)\} \qquad (3.5)$$

The phase change $(\phi_1 - \phi_2)$ is a direct result of the object displacement, d, which gives rise to a difference of 2d in the path lengths of the light reflected from the object. Considering the simple case where the hologram is illuminated and viewed normally, with the object motion perpendicular to the surface, the phase change and displacement are related by the expression:

$$(\phi_2 - \phi_1) = (\frac{2\pi}{\lambda}) \; 2d \qquad (3.6)$$

where λ = wavelength of the light

and thus it can be seen that whenever the phase changes by $(\phi_2 - \phi_1) = 2\pi$ the image intensity, I_i in equation (3.5), becomes zero and a dark fringe is formed. In the same more general case, where the angle of object illumination, measured from the perpendicular to the object surface, is α and the angle of observation, measured from the same perpendicular is β then the equation (3.5), deriving the image intensity, is modified to give:

$$I_i = 2 \; a_o^{\;2} \{1 + \cos \; (\phi_i - \phi_2)(\cos \alpha + \cos \beta) \}$$

and since $(1 + \cos x)/2 = \cos^2 \frac{1}{2} x$

$$I_i = 4 \; a_o^{\;2} \cos^2 \tfrac{1}{2} \; (\phi_1 - \phi_2)(\cos \alpha + \cos \beta)$$

It can be seen then that the reconstructed image from such a double exposed hologram will display a series of fringes which are a function of object displacement. This effect is exploited in the study of statically deflected objects or the stroboscopic illumination of vibrating objects, where the motion is "frozen", usually once per cycle by "chopping" or pulsing the Laser beam.

However, Powell and Stetson (33) have demonstrated that a fringe pattern can be recorded from a vibrating object, using the basic hologram recording apparatus, but without the complications necessary to "freeze" the object stroboscopically. In the preceding paragraphs it has been shown that two images may be superimposed on a single emulsion such that they appear to have occurred simultaneously. For the case of an object which is vibrating with simple harmonic motion the recorded image consists of an infinite number of "sub-images", each of which represents a particular position of the object in its cycle and the intensity of which is proportional to the time spent in that position. Considering the position probability density function for simple harmonic motion (Figure 13) it can readily be seen that the object spends most of its time at, or near, the two extreme amplitude positions and the intensity of these two images is sufficient to suppress the others. The result is that a fringe pattern, similar to that occurring with an object which has merely been displaced, is seen when the exposure is made over a large number of cycles.

The following analysis gives the form of these "time-averaged" fringes.

Let the amplitude of the object beam be considered as a function of the object position, p, and time, t, and expressed as $\bar{a}_o\ (p,t)$, then if the object remains at a given position for a time $(\Delta t/T)$ of the exposure time the image amplitude is given by

$$\bar{a}_i\ (p_1) = \bar{a}_o\ (p,t)\ \frac{\Delta t}{T}$$

For the complete exposure the total amplitude of the image is, therefore

$$\bar{a}_o\ (p) = \frac{1}{T}\int_o^T \bar{a}_o\ (p,t)\ dt$$

But, for small object displacements

$$\bar{a}_o\ (p,t) = |\ a_o\ |\ e^{i\phi(p,t)}$$

Thus

$$\bar{a}_i\ (p) = |\ a_o\ |\ \frac{1}{T}\int_o^T e^{i\phi(p,t)}\ dt$$

Reconstruction with the reference beam gives rise to a virtual image of intensity

$$\bar{I}\ (p) = |\ a_o\ |^2\ |\ \{\frac{1}{T}\int_o^T e^{i\phi(p,t)}\ dt\}\ |^2 \qquad (3.7)$$

$\phi(p,t)$ is the phase difference due to the object displacement, which, for a sinusoidal motion illuminated and viewed normally, can be expressed as

$$\phi(p,t) = (\frac{2\pi}{\lambda})\ 2d = (\frac{2\pi}{\lambda})\ 2d.\sin\ \omega t$$

where ω is the circular frequency of vibration. It is convenient to write

$$\phi(p) = (\frac{2\pi}{\lambda})\ 2d_o$$

(This expression will obviously be more complicated if the angles of illumination and observation are not normal.)

Equation (3.7) can now be written

$$\bar{I}(p) = |a_o|^2 \left| \{\frac{I}{T}\int_o^T e^{i\Phi(p)\sin\omega t}\, dt\} \right|^2 \qquad (3.8)$$

Now, it can be shown that

$$e^{i\Phi(p)\sin\omega t} = J_o\{\Phi(p)\} + \sum_{n=1}^{\infty} J_{2n}\{\Phi(p)\cos 2n\omega t\} + \sum_{n=o}^{\infty} J_{2n+1}\{\Phi(p)\sin(2n+1)\omega t\}$$

where the function $J_n(x)$ is known as the Bessel function, defined, for a non negative value of n, by the expression

$$J_n(x) = \frac{x^n}{1.3.5....(2n-1)}\,\pi\int_{-1}^{+1}(\cos xt)(1-t^2)^{n-\frac{1}{2}}dt$$

But if the exposure time, T, is much greater than the periodic time of the motion then T can be regarded as tending to infinity and all the Bessel functions under the integral will tend to zero except for the zero order function. For this case equation (3.8) is simplified to

$$\bar{I}(p) = |a_o|^2 \left| J_o\{\Phi(p)\} \right|^2 \quad \text{as } T \to \infty \qquad (3.9)$$

For illumination and viewing at angles of α and β as defined previously the intensity given by equation (3.9) becomes:

$$\bar{I}(p) = |a_o|^2 \left| J_o\{\Phi(p)\}(\cos\alpha+\cos\beta) \right|^2 \qquad (3.10)$$

It can be seen, therefore, that the image is now of an intensity which varies as the square of a zero-order Bessel function (Figure 14) and whenever the vibration amplitude term, Φ, has

values corresponding to 2.4, 5.52, 8.634 etc. a dark fringe will occur. When it takes the value zero, that is, at the nodes, the fringes will be significantly brighter and thus can be readily identified on reconstruction. However, it is also obvious from Figure 14 that fringe brightness decreases rapidly with amplitude.

3.3.2 Real Time Holography

The advantages of a technique by which a series of object displacements or vibrational modes can be investigated concomitantly are obvious. In holography this can be achieved by recording a hologram of the object in its original, or static condition. If, after processing, the photographic plate is returned to its original position and viewed, with the reference beam, while the object also remains illuminated, the image and object are seen to be superimposed. Any subsequent static or dynamic deformation results in a series of fringes which are an interferometric comparison of the object in its original state (represented by the reconstructed image) and the object in its new state. Thus, any number of deformations may be investigated from the single recording, limited only by the stability of the combined optical and mechanical system (since rigid body motions of any element in the system will introduce spurious fringe patterns unrelated to, but affecting, the fringe pattern under investigation).

Fringe patterns obtained in this way are referred to as "real time" and the form of these real time fringes is obtained from the following analysis:

The instantaneous disturbance at the object can be considered as the vector sum of the reconstructed image wavefront (representing the object in its original state) and the new wavefront being radiated by the deformed object. This gives rise to an instantaneous intensity of:

$$\bar{I}_r\,(p,t) = \left|a_o\right|^2 \{2 + e^{i\phi(p,t)} + e^{-i\phi(p,t)}\}$$

In this case the intensity is averaged over an integration time defined by the speed of response of the human eye, yielding, after manipulation

$$\bar{I}\,(p) = 2\left|a_o\right|^2 \{1 + J_o\phi(p)\} \qquad (3.11)$$

or,

$$\bar{I}\,(p) = 2\left|a_o\right|^2 \{1 + J_o\phi(p)(\cos\alpha+\cos\beta)\} \qquad (3.12)$$

where the illumination and viewing angles are α and β respectively. A comparison of these equations with (3.9) and (3.10) shows that, not only is there an additional unity term, but the Bessel function is of the first power not the second. These factors cause a substantial reduction in fringe contrast and in the latter case also reduce the number of fringes observed for a given vibration amplitude to half that of a time averaged hologram.

3.4 Phase Determination

In preceding paragraphs it was stated that time-averaged holographic analysis does not usually retain information about the relative phase of movement between various points on the object. It has been shown, however, that such information may be ascertained in real time by temporal modulation of the reference beam (38,39). It can be seen from the equations 3.9, 3.10, 3.11 and 3.12, that the argument of the Bessel function is a function of the magnitude of the object wave phase change. If the reference beam is modulated at a frequency equal to that of the object vibration, but of variable phase, the Bessel argument becomes a function of the object wave phase and the required object phase relationships may be derived from the resultant fringe pattern.

This effect is achieved in practice by causing one of the reference beam mirrors to vibrate at the same frequency as the object on an axis parallel with the beam path. At a certain magnitude this modulation will cause the nodal fringe to move from its true position. Alteration of the phase of the reference mirror signal, at this magnitude,moves the apparent node in one direction until the relative phase between the object and reference waves is zero, at which point the node movement stops and reverses. A comparison of the values of the relative phases of the excitation signal at which this occurs allows the relative phases between various points on the object to be determined.

In the simple case, where only two object phases exist (0^{o} and 180^{o}) regions of the same phase can be determined easily.

A phase shift is added to the reference beam as described, which causes movement of the nodes towards some antinodes, but away from others. By denoting the areas to which the nodes have moved as positive and those from which they have moved as negative the object phases are verified. Real time observation of these nodal movements is facilitated by the use of the Laser Image Speckle Interferometer, as described in the following section.

3.5 Laser Speckle Interferometry

The final technique of use in vibration analysis, is that of Laser image-speckle interferometry. Although this is not strictly a holographic method, since no hologram is recorded, it does utilise the coherent light from the Laser. The technique exploits the fact that any surface illuminated by Laser light exhibits a speckled appearance due to the mutual interference of the elementary light waves reflected from it. The phases of these waves are distributed randomly, with the result that the interference pattern appears as a random distribution of bright and dark spots which vary in size and shape. Since this speckle pattern contains information about the incident wave front, the position of the object relative to both the source and the observer and the scattering properties of the object,a variation in any of the parameters will give rise to a change in the observed pattern which can be measured by comparison with the original pattern.

Various techniques have been developed to exploit this effect for vibration analysis particularly Mottier and Eliasson (36), Archbold et al (40) and Hughes (41). The method due to Hughes requires particularly sophisticated equipment, but is capable of producing recordings of vibrating objects showing detailed, equal contrast fringe patterns. Archbold et al have developed a system which, although capable of showing only nodal positions in real time, gives greater contrast than live-fringe holography, with relatively simple apparatus. The basis of this method is that if the object is made to vibrate at amplitudes of more than a few wavelengths of the light the speckle pattern observed on a static

object become blurred, except at nodal positions. Sensitivity is increased by adding a reference beam, of similar intensity to the speckle pattern, at the viewing aperture. If the two fields are coherent then interference will occur and displacements of a quarter wavelength will cause reversal of the speckle pattern due to reversal of the relative phases of the two fields. Slow, continuous motion of the object will cause the pattern to twinkle, whilst rapid vibration will cause the speckle pattern to blur out except at the nodes, where a high contrast pattern will remain. The similarity with Chladni sand patterns is obvious. The Laser Image Speckle Interferometer due to Stetson (37) and based on the principles of Archbold et al (40) is shown in Figures 15 and 16.

3.6 Application of Laser Techniques to the Confirmation of the Analytical Method

An outline of the basis of Laser holographic and interferometric techniques relevant to the analysis of vibrations has been given. There has been much development and many methods, of varying degrees of sophistication, are now available. A comparative survey was therefore made from which conclusions on the type of rig required for this study could be reached.

As may be adjudged from the previous discussions (3.3) stroboscopic holography offers certain advantages in the study of vibrating objects. High, equal contrast fringes are obtainable and even in the case of live fringe techniques fringes of a clarity similar to those from a static deformation can be obtained. However, this factor does mean that nodal and antinodal positions are not obvious, though they can be deduced. In addition the apparatus required is complicated. High power output, suitable for illuminating large, vibrating objects, is obtainable from "Q-switched" pulse Lasers (such as Ruby or Neodymium-Glass) fitted with a Kerr or a Pockels cell. If the oscillator driving the object is also used to provide a synchronous pulse to this cell a high power, short duration pulse of light is caused to be emitted at a suitable moment in the vibration cycle. Continuous wave Lasers may also have the beam "chopped" or interrupted using a Pockels cell (Fryer (42) after Von Winkle), a drilled disc, or by passing it through a drilled spindle driven by a small high speed turbine (Archbold and Ennos (43)). However, it is essential to ensure that the chopping frequency remains stable and equal to the object driving frequency, which requires complex additional equipment. Also the use of a continuous wave

Laser necessitates long exposure times, as only a fraction of the light output is used to illuminate the object, which increases the stability requirement for the system.

Since the available Laser, a continuous wave, Helium-Neon type, was of low power output (15 mW) it was considered that the disadvantages of stroboscopic methods made it inappropriate for the current investigation when compared with the simplicity of the normal time averaged method. In addition, although amplitude information is not easily obtained and generally phase information is lost the extreme brightness of the nodes expedites a qualitative analysis. It is, however, possible to derive phase information in real-time, which offsets this disadvantage of the "frozen-fringe" technique.

Thus, since for the purposes of this investigation confirmation of the theoretical analysis only was required it was decided to develop a basic system from which satisfactory real-time analyses and time-averaged recordings could be made.

3.7 The Experimental Rig

All experimental work was carried out in the Holography Laboratory, School of Mechanical, Aeronautical and Production Engineering, Kingston Polytechnic.

3.7.1 Optical Equipment

The basis of the system was a Spectra Physics Model 124A 15 mW Helium-Neon Laser mounted remotely from the main equipment on a vibration isolated wall fixture. All optical equipment and the model were arranged on a vibration isolated cast iron surface table measuring 6 ft x 3 ft. The initial layout is shown diagrammatically in Figure (17), the final arrangement in Figures (18) and (19).

For stability all optical components were mounted on heavy bases supported on three pointed feet. Initially the beam splitter (BS1) was of the variable type, the glass substrate being coated in six discrete segments capable of reflecting from 5% to 50% of the incident beam. This enabled the optimum ratio of reference beam intensity to object beam intensity to be determined for the model. In general it may be stated that, for maximum diffraction efficiency and thus optimum image brightness, this ratio should be 1:1 at the film plane. Now, this is obviously a function not only of the beam splitter, but also related to the reflection characteristics of the object. However, particularly with low power Lasers, if the reference beam intensity is reduced to that of the object beam the exposure time is increased to a value

outside the linear portion of the Amplitude Transmittance - Exposure curve for the photographic emulsion, which reduces the fidelity of the image. In practice ratios of 5:1 are not uncommon. To a certain extent the beam ratio may also be controlled with the beam expanders. Although the main function of these is to expand the Laser beam, using a microscope objective focussed on a pinhole, from an approximation to a point source to illuminate the object and photographic plate it can be seen that its magnification value and distance from the object or plate determines the intensity. However, illuminating a larger area than necessary in order to reduce the intensity wastes light which would be better utilised in the other beam.

For the models used in this work tests showed that approximately 95% of the original beam was required to illuminate the object to give a suitable ratio at the film plane. Problems were experienced in using the variable beam splitter to give this ratio since, in spite of an anti-reflection coating the reflection from the back surface of the glass substrate interfered with the front surface reflection, causing interference fringes across the reference beam. The variable splitter was, therefore, replaced with a plain glass wedge prism, of angle 5^{o}, which gave rise to twin diverging reflected beams, each approximately 4% of the incident beam. This factor was exploited in the final layout by using one beam as the hologram recording reference beam, the other as the speckle interferometer reference beam.

Recordings were made on Agfa Gevaert 10E75 film and glass plates. This emulsion has a high resolution capability (in excess of 2000 lines/mm) and is thus very insensitive to light, having an equivalent ASA rating of 0.6, which does, however compare favourably with Kodak 649F emulsion which has a similar resolution but an equivalent ASA rating of 0.03. For reasons of economy and convenience 35mm film was used for most time-averaged recordings. The film carrier was a modified Shackman Oscilloscope Camera, shown in Figure (20). The lens, lens hood and shutter were removed, which then necessitated covering the front interior of the camera with black paper to avoid stray light affecting adjacent film during the exposure of a frame. A flap of black paper fitted to the camera top cover ensured that the camera was light tight except when the cover was lifted for exposure. Glass plates were held in the "gallows" mount shown in Figure (21). The plate is inserted into a slot in the arm and clamped in position between two perspex jaws using three screws. This arrangement allows for in-situ processing of the plate by immersion in the containers of chemicals when recording for real time holography.

Exposures were made using the Synchro-Compur shutter from the Shackman Camera, which was mounted on the wall above the table. Exposure times were calculated using a Gossen Lunasix CdS exposure meter. A reflected light exposure value was recorded from the object and reference

beams striking a white card placed at the film plane. The exposure value and an empirically determined ASA value of 10 allowed the exposure time to be read off against an arbitrarily chosen "f-number" of 1. Since the object is not being imaged through a lens and aperture the f-number, expressed as the ratio of focal length/aperture diameter, is actually meaningless and the value was adopted purely for convenience and the ASA rating determined from this.

Although successful real time holograms were made the low fringe contrast (see 3.3.2) made interpretation difficult and permanent recording by photographing the image impractical. Ultimately location and analysis in real-time were carried out using the Laser Image-Speckle Interferometer due to Stetson (37) and shown in Figures (15) and (16), which has the advantages of reducing the stability requirement and not requiring a chemical processing stage. The instrument is arranged as a telescope so that the achromatic doublet objectives (L1 and L2) image the entrance aperture, A, onto the pupil of the eye. The aperture is adjustable by the observer to give a suitable compromise between speckle size and contrast and image brightness against the reference field. The reference field is introduced into the system by the prism, P, and is imaged by lens L2. The second reflection from the prism is stopped by the exit aperture. The cylindrical lens C is to correct astigmatism introduced by the presence of the prism and the polarizing filter, F, removes

any light polarized in quadrature to the reference field. It is particularly important with this instrument that the path lengths of the object and reference beams are equal, or differ by a multiple of twice the Laser cavity length, ensuring that the temporal coherence between the two fields is a maximum. In addition, as the object is viewed through a very small aperture (typically 1mm in diameter) the reflected light observed from the object is of very low intensity and in order that it is not obliterated the reference beam must also be of low intensity. In the arrangement shown (Figure 18) the second reflected beam from the wedge prism (BS1) was directed on to another beam splitter, BS2, which reflected approximately 20% through a 20X beam expander onto the interferometer prism to give object and reference fields of similar intensity.

In addition to the location and identification of vibrational modes prior to recording the detailed pattern by time averaged holography the speckle interferometer was used to investigate relative phases of the motion of the model blades using the method of Neumann et al as described in (3.4), where the reference beam is temporally modulated by a vibrating mirror. For these tests the second beam splitter was replaced with a small, 10mm diameter mirror cemented to a ring piezo-electric excitation gauge, constrained to vibrate axially and driven by the same oscillator as the object.

3.8.2 Models

Initially, in order to assess such variables in the

optical system as stability, beam ratios and exposure times, a simple cantilever model measuring 6 in x 1.5 in x 0.5 in was used. Having resolved these parameters the model was subsequently machined to a tapered beam to check the theoretical analysis of the cantilever described in section 2.2.3.

The cantilever was subsequently replaced by the series of blade package models denoted A1, A2, A3, B1, B2 and B3 and shown in Figures (22) and (23). The blade dimensions were based on those used by Allen (1), which had an effective thickness and radius of gyration typical of current turbine blades, with allowance made for camber. The models were scaled down to half size, with the exception of the shroud thickness, initially taken as 6.3mm (A1 and B1) and subsequently reduced to 4.5mm (A2 and B2) and 2.5mm (A3 and B3) to assess the effect of this parameter on the vibration characteristics.

To avoid fabrication problems and estimations of the joint efficiency the basic models A1 and B1 were machined from the solid in normalised mild steel, subsequent models being obtained by machining the shroud down to the specified dimension. The clamping faces were ground to match the clamp.

Initial experiments with the cantilever had shown that increased image brightness and fringe and speckle contrast were obtained if the models were coated with a retro-reflective material, which reflects most of the light back in the incident beam direction instead of the

scattering obtained with an untreated surface. The models were, therefore, painted with "Codit" Reflective Material which consists of highly reflective glass beads suspended in a diffuse, low reflectivity, white pigment. The light reflected from the glass beads retains its polarization, while the pigment reflection is highly depolarized, and the difference in reflectivity of the two materials enhances the speckle effect utilised in the speckle interferometer. Tests before and after coating the models showed this finish did not affect their response.

The method of model excitation was chosen to minimise any influence on the vibration characteristics from the driving source. The small size, low mass and wide dynamic and frequency ranges of piezo-electric excitation gauges made them most suitable for this investigation. Adverse effects due to adding an excitation source such as an electro-mechanical shaker tend to be minimised if the source is fitted at a node, but piezo-electric gauges are most effective when positioned at the point of maximum strain. Initial tests compared the displacements and modal shapes due to gauges placed at the base of a blade (that is, at a node) and at the tip (an antinode for the detached flexural modes), but no differences were apparent. It should be noted, however, that to obtain maximum strain a 25.4mm long gauge was used which, being a third of the length of the blade, extended well beyond the nodal and antinodal regions. For subsequent tests the gauge was cemented centrally at the base of the outer face of the left hand blade.

In order to ascertain that the resonant frequency excited by a given input frequency was equal to that frequency and not a harmonic of it a piezo-electric strain gauge of the same size as the excitation gauge was fitted to the inside face of the right hand blade. A comparison of the input signal to the excitation gauge and the output from the strain gauge on a twin beam oscilloscope enabled not only the frequencies to be compared but also the precise resonant frequency to be verified when recording a time averaged hologram by adjusting the frequency to given maximum output from the strain gauge. This coincided with the point at which the nodes observed in real time with the speckle interferometer decreased to a minimum width. Additionally, a comparison of the phase of these two signals enabled the relative phase of the vibration of the outer blades to be verified. A similar strain gauge fitted in a corresponding position on the centre blade enabled the relative phases of adjacent blades also to be confirmed.

Early work showed that it was essential to locate the models in a massive clamp which would damp out the object vibration and prevent transmission to the optical components. The clamp is shown in Figure 24 from which it can be seen that it is fabricated from two normalised steel billets ground together on the base and inside faces to enable the models to be an accurate sliding fit. The models and spacers were also ground flat and square together for this reason. The fixed spacer and billets

were drilled and bolted together with 1 in Whitworth studs and nuts, tightened sequentially. The clamp was assembled on a surface table to ensure that the base and inside faces were mutually perpendicular. The models were held in place by the free spacer and clamped with the end plate, the four socket screws being tightened sequentially. The effectiveness of this clamp in damping out the model vibration was verified by comparing resonant frequencies of a linearly tapered cantilever mounted in the clamp with values obtained from the analysis described in section (2.2.3), in which it was assumed that the assembly acted as a rigid body.

It was decided that observation of the shroud behaviour in conjunction with that of the blades would assist the analysis of modal shapes. Inclination of the clamp and model towards the hologram plane at an angle of 25^{o} enabled the shroud surface to be completely visible. The clamp was supported on the front lower edge and by a toolmaker's jack placed centrally at the back. The assembly was placed on a 1.6mm thick bonded rubber mat to prevent sliding between the clamp and surface table.

The models were aligned initially such that the maximum area of the three blade faces was visible. However, since the fringe pattern recorded shows motion in a direction perpendicular to the plane of the hologram only, movement parallel to and perpendicular to the blade faces would be difficult to establish. Further holograms were recorded for the two 2.5mm shroud models (A3 and B3) with the blade

faces parallel and subsequently perpendicular to the hologram plane.

3.7.3 Instrumentation

The driving signal for the excitation gauge was supplied by a Ling Dynamic Systems TPO 25 25 watt power oscillator via a 1:40 step-up transformer to obtain the voltage required to achieve suitable vibration amplitudes. The gauge input voltage and frequency were monitored using an Advance Digital Voltmeter and Timer Counter. In addition a twin beam oscilloscope was used to compare the input excitation signal and the strain gauge outputs to confirm frequency values and phases of vibration. When originally establishing input signal levels to give a suitable vibration amplitude the input signal trace was also used to monitor the maximum level obtainable without distortion, since clipping of the signal could give rise to harmonics generating spurious resonances.

To assess the relative phases of the object motion as described previously (3.4) a Feedback TWG 500 Variable Phase Function Generator supplied two signals, of the same frequency, but variable in phase, to two Ling Altec TPO 20 Oscillator Amplifiers. The amplified signals were then used to drive the model and mirror excitation gauges via 1:40 transformers.

3.7.4 Sequence of Operations

To obtain a series of recordings of the resonant frequencies and modal shapes for each model the following sequence of operations was adopted.

a) Recording

i) At the beginning of a series of tests a white card was placed at the hologram plane and an exposure reading light from the object and reference beams recorded to ascertain the exposure time required.

ii) The model was observed through the speckle interferometer and the excitation signal frequency gradually increased.

iii) At an observed resonant frequency, where the speckle pattern was visible only at the nodes the right hand blade strain gauge output was compared with the excitation signal to verify that the frequencies were equal and that the strain gauge output was at a maximum for a given excitation signal level.

iv) The camera was then moved into position, in front of the interferometer and the time averaged hologram of that frequency recorded.

In the initial tests a series of holograms was recorded to establish the excitation signal level required to give an adequate number of high contrast fringes. If the signal is too low the fringes are of high contrast but too broad and too few in number to give sufficient information about the modal shape. If the signal is too high, then pronounced fading of the image brightness occurs (as described in the analysis of section 3.3)

and the fringe contrast is reduced. In addition the fringe spacing tends to be too close for adequate interpretation.

Having ascertained a voltage which gave a suitable compromise between the two extremes described above, this value was retained for subsequent tests at the corresponding frequency for other models.

v) Steps (ii) to (iv) were repeated for each model to give the required number of modal shapes.

vi) The film was then processed using Agfa Gevaert G3P developer and G335 fixer.

b) Reconstruction

As discussed earlier (section 3.5) the reference beam used in the recording of a hologram was of low intensity, the power being of the order of 0.25mW before expansion. This did not give a reconstructed image of sufficient brightness to photograph easily and a separate reconstruction layout was adopted using a 2.5mW Helium-Neon Laser and (X10) expander arranged in a similar geometry to that of the original reference beam.

The holograms were held between two spring loaded glass plates in a film strip carrier, which ensured that the film remained flat. A 35mm single lens reflex camera with a 55mm focal length lens was positioned immediately behind the hologram and the image photographed on Ilford FP4 monochrome film,

rated at 200ASA. Exposure times were determined using an Asahi Pentax Spotmeter, which, since the light sensitive cell has an acceptance angle of only 1^{o}, could be used to give exposure readings for individual light fringes. Experience showed that a good negative was obtained by exposing for a fringe of average brightness, neglecting the extremely bright fringes occurring at the nodes.

The negatives were than enlarged and printed for subsequent analysis. Examples are shown in Figures (25) to (39).

c) Phase Determination

In order to assist in the analysis of the holograms recorded a further series of tests was made in real time to derive the relative phases of the blade movements. The simplified technique due to Neumann et al described in section 3.3 was used in conjunction with observation of the relative phase of the output signals from the strain gauges on the centre and right hand blades of the model, using the twin beam oscilloscope.

Since the grouped modes can be readily identified by a comparison of the phases of motion of $(\frac{N}{2})$ blades if N is even, or $(\frac{N}{2} + 0.5)$ blades if the number of blades (N) is odd, observation of the strain gauge signals gave sufficient information. The method using the vibrating mirror was found, in practice, to be less easy, both in operation and interpretation and

required additional instrumentation and thus the former method was used in preference. However, it should be noted that where more complete phase information is required reference beam modulation becomes the preferred technique.

3.8 Concluding the Experimental Analysis

It has been shown that the sensitivity and detail of Laser holographic and interferometric techniques provide the ideal tool for vibration analysis. The method is non contacting and, therefore, does not affect the vibration being measured. It does not require special models to be made and can yield complete information on modal shapes.

In this investigation these techniques have been used to enable a comparison to be made between the natural frequencies and modal shapes of a series of blade packages, derived experimentally and predicted by the lumped parameter Myklestad routine developed in Chapter 2. It is considered that conventional methods of vibration analysis using transducers would have been inadequate to supply the information required for the analysis of pretwisted blade packages, permitted to vibrate in three planes.

A detailed comparison of the experimental results and theoretical predictions is presented in the following chapter.

4. PRESENTATION OF RESULTS

4.1 Introduction

In Chapter 2 a method for the prediction of the natural vibration frequencies of packages of pretwisted turbine blades was established. In the following chapter experimental techniques utilising Laser holography and interferometry were discussed and proposed for the verification of the theoretical solution.

In this chapter data from the theoretical and experimental analyses are presented and the suitability of the Myklestad approximation as a design tool is discussed.

It should be noted that, because the experimental models investigated were neither subject to variations of cross section and pretwist, nor to centrifugal forces, these effects have been excluded from the computer program developed from the analysis given in Chapter 2. However, it has been shown in the preceding analysis that such effects may be included, with a negligible increase in complexity.

4.2 Presentation of Results

In the first chapter, Armstrong and Stevenson were quoted as having shown that, in general, the first and second flexural modes and the first edgewise and torsional modes are the dominant mechanisms causing vibration induced fatigue failure. It is thus of limited, or academic, interest to calculate higher order modes and consequently the data presented has been limited to the first, second and third "detached" flexural modes, the first and second sets of "grouped" flexural modes, the first edgewise mode and the first detached and grouped torsional modes.

A total of six package models has been considered both experimentally and theoretically. Three of the models had 0^{o} pretwist, the remaining three had a constant pretwist of 30^{o}. The three models in each set have been analysed to assess the effect of variation of shroud thickness on the natural frequencies. Drawings of the models are given in Figures 22 and 23.

Although the designer is primarily interested in frequencies and the modal shapes are of less importance, the latter have been included in this analysis to enable the modes to be positively identified for the purpose of comparison between the theoretical and experimental results.

Now, the modal shapes of pretwisted blade packages can become complex and, although the displacement of any point on a blade can be easily calculated once the frequency has been established, such data are somewhat imperspicuous, particularly when being compared with the displacement fringes obtained from the holographic analysis. It was decided, therefore, that a pictorial representation of the theoretical data would be more

appropriate for comparative purposes. Whilst simple line drawings are adequate for representing the flexural and edgewise modal shapes, the introduction of torsion or pretwist and thus coupled bending-torsion modes, requires an improved representation.

A program was developed, therefore, to normalise the displacement data and translate the information into single, symbolic characters representative of the displacement moduli. By maintaining a correlation between character density and magnitude of displacement it was possible to output, for example, the displacement perpendicular to the blade force in the form of a character pattern equivalent to the fringe pattern derived from the holographic analysis. Examples of the theoretical modal shapes, complementary to those obtained experimentally are shown in Figures 25 to 39. The advantage of this technique for correlating experimental and theoretical results, particularly for the more complex shapes, is clearly demonstrated in these examples.

Having identified corresponding theoretical and experimental modal shapes it is possible to compare the frequency values and these are tabulated in Tables 5 to 10.

4.3 *Discussion of Theoretical and Experimental Results*

In comparing the experimental and theoretical results presented in Tables 5 to 10 it is necessary to distinguish between errors due to the approximate nature of the analytical model and those inherent in the experimental technique. Whilst it is convenient to express the differences in the calculated frequency values as a percentage of the experimental values, since the complexity of the problem precludes an exact mathematical solution it must be remembered that the latter are not necessarily the true natural frequencies of the model defined for the analysis.

It has been shown by several workers and confirmed in the analysis of exponentially tapered beams undertaken in the study, that lumped parameter solutions converge asymptotically to the true solution with the error inversely proportional to the second, or the fourth power of the number of masses depending on the end conditions. The error also tends to increase with mode number. It may be concluded, therefore, that, provided the determinant of end-conditions is capable of accurate solution, calculated values will tend to be overestimated in proportion to the accuracy of the model and the mode number.

It can be seen from the tabulated values that, in general, the errors are positive, notable exceptions being the results obtained for the unstaggered model with a 6.3mm shroud (denoted A1) and the third, detached, flexural modes on all models, except the pretwisted model with a 2.5mm shroud (B3). It is interesting also to note that the introduction of pretwist tends to make more positive the errors evident with untwisted

blades. It is difficult to attribute this to some cause in the mathematical model and it is, therefore, necessary to question whether the experimental models fulfil the basic requirements of the mathematical model. In particular the mathematical solution assumes that the blade package is fully encastré with no movement at the base of the blades permitted. Although the design of the clamp and package is such that this condition is adequately met in the direction of the H-axis (as defined in Figure (11)) the same is not true for movement along the R-axis, since the clamping force is exerted in the H-direction. Intuitive analysis will show that the effect of this will be to increase the effective lengths of the blades and thus reduce the expected resonant frequencies. Further it may be deduced that this effect will be a maximum for movement solely in the R-direction and a minimum for movement only in the H-direction, whilst torsional motion and movement in both planes will have errors due to clamping lying between these limits. Indeed, it may be further postulated that the effect will be more noticeable in the detached modes, where all blades are moving in the same direction than in the symmetrical batch modes where the motion of a blade in one direction is counteracted by motion of the adjacent blade in the opposite direction.

It may be concluded, therefore, that the flexural modes of the untwisted blade package models will exhibit a minimum (probably zero) error due to the inefficiency of the clamp, whilst the edge modes for these models will be subject to the maximum clamping error. Thus the differences between experimental and calculated values for the flexural modes of the untwisted models (A1, A2 and A3) can be assumed to be due to the assumptions made in defining the mathematical model alone, whereas all other models will

exhibit differences due to a combination of the errors inherent in the mathematical and the experimental models.

4.3.1 Errors Due to Mathematical Modelling of the Blade/Shroud Junction

It can be seen from Tables 5 to 10 that the errors due to the approximate nature of the mathematical model vary with shroud thickness, being negative when the shroud/blade thickness ratio is 1, but becoming more positive as this ratio decreases. The values obtained from the Myklestad solution of the model investigated by Thomas and Belek, given in Table 1 also fit this trend. Since the error is a function of shroud thickness it may be deduced that the error arises from the simplifications made in modelling the blade/shroud junction. However, the true deformation of the material at this junction is extremely complex and it is considered that the assumption that the junction acts as a rigid body, with the forces and moments acting at and about the points A, B, C, D and J, as shown in Figure (10), remains valid. It was shown by Allen (1) and is further investigated in this study, that the inclusion of "junction factors", by which the effective thickness of the shroud and blade at the junction may be modified, can reduce the error due to this assumption. A series of junction factors was investigated for each model in order to arrive at empirical values suitable for reducing the error due to simplifying the mathematical modelling of the junction to a minimum. The effect of applying a junction factor varies not only with the ratio of the shroud/blade thickness but also with the

modal shape and the following points may be noted:

i) The first detached mode (the fundamental) is less sensitive to changes in the effective shroud thickness at the junction, but the frequency decreases with decreasing effective blade thickness at the junction.

ii) The first symmetric batch mode is sensitive mainly to changes in the effective shroud thickness at the junction, the frequency again decreasing with reduction in shroud thickness. A reduction in blade thickness, however, shows a slight increase in frequency.

iii) The first anti-symmetric batch mode is sensitive to both shroud and blade effective thickness, decreases in either causing a reduction in the resonant frequency.

iv) Higher modes become sensitive to changes in both junction factors in accordance with the trends described above.

These effects reflect the translational and/or rotational movement of the shroud at a resonant frequency and demonstrate that a single pair of junction factors for a given shroud/blade thickness ratio will be a compromise for all modal shapes.

Table 11 lists the first six resonant frequencies for the untwisted models derived from the use of those empirically determined junction factors shown to reduce to a minimum the differences between theoretical and experimental values.

4.3.2 Errors Due to Clamping

As has been discussed previously, whilst the untwisted package models fulfil the basic requirements of the mathematical model for the calculation of flexural modes in the direction of the H-axis, inefficient clamping in the R-direction may lead to lower values than predicted for the torsional and edge modes of these models and all modes of the pretwisted models.

The results obtained reinforce this argument, as can be seen from Tables 7 and 10, in which the largest difference between predicted and measured values occurs at the first flexural mode in the R-direction. It is difficult to assess quantitatively the effect of inefficient clamping except insofar as it will reduce the expected frequency values. A suitable model of a package with fully encastré blade roots may be obtained by manufacturing the model with a more massive base. However, although this would allow a more thorough assessment of the accuracy of the mathematical solution it may be considered somewhat academic since blade packages of this type would be unlikely in practice. Another approach would be to incorporate an allowance in the mathematical solution to enable the root conditions to be more accurately modelled. This may be achieved either by increasing the effective blade length, or by modifying the end-conditions assumed to assist at the blade root. For the built-in root the end-conditions are that the shear force and bending moment take finite values, whilst rotation and displacement

are zero. However, any suitable finite values for all end-conditions can be used to attain an improved approximation to the state existing at the blade root.

It must also be noted that, when considering blades attached to a turbine disc the axial modes will be influenced by the disc, as described in section 1.4. The assumption that the disc is infinitely stiff no longer holds and the blade/disc assembly requires to be investigated as a whole.

4.4 The Effect of Shrouding Turbine Blades

It has been shown in preceding discussions that the fitting of a shroud to a series of turbine blades has the effect of introducing frequencies in addition to the vibration characteristics of the individual blades.

In the mathematical solutions due to Prohl (8) and Smith (9), in which the shrouds were represented only by their centrelines, with the mass concentrated at the blade tips, the full effect of shrouding could not be established. In such models it can be seen that the effect of increasing shroud thickness (and thus mass) will merely cause the vibration frequencies to be reduced. The detached modes, in which all the blades move in phase with similar displacement amplitudes, will be most sensitive to this change in mass, whilst the symmetrical batch modes, involving only slight movement of the shroud will be less sensitive to the change. The anti-symmetric batch modes, in which blades in corresponding positions each side of the package centreline are 180^{o} out of phase, involve no longitudinal movement of the shroud and are, therefore insensitive to changes in shroud mass.

The current study has demonstrated the inadequacy of this representation and shown that the stiffness of the blade/shroud combination can become the dominant mechanism in controlling changes of frequency due to changes in shroud thickness, particularly with the batch modes, where a change in mass alone has a limited effect on frequency.

This is clearly shown, both experimentally and theoretically by the results tabulated in Tables 5 to 10.

Referring to the experimental values for the untwisted

models it can be seen that a reduction in shroud thickness from 6.3mm (equal to the blade thickness) to 4.5mm causes the fundamental frequency to increase, implying a "mass controlled" mechanism, whilst the batch mode frequencies are reduced, implying a "stiffness controlled" mechanism. The second and higher order detached modes show a slight decrease in frequency, demonstrating a tendency towards the stiffness controlled mechanism, but with mass remaining an important factor.

A further decrease in shroud thickness, from 4.5mm to 2.5mm causes the frequencies to be reduced in all cases, the extra stiffness induced by the addition of a shroud being of greater importance than the mass when this is small.

These observations are generally supported by the theoretical results although the errors assumed to be due to the simplification of the blade/shroud junction give rise to some variations. If the junction factors described in section 4.2 are applied then agreement is improved.

Similar trends to those described above are apparent for the pretwisted models.

It is clear, therefore, that the additional stiffness provided by the shroud is an important aspect in determining the natural frequencies of blade packages, particularly when the additional tip mass due to the shroud is low.

4.5 The Effect of the Number of Blades Comprising the Package

The simplified models investigated in this study were restricted to packages of three blades. This was considered sufficient to introduce coupling effects, whilst considerably reducing the computation time required by a larger number of blades. In section 2.3.2 Smith (9) and Shiga (27) were shown to have concluded that, although an increase in the number of blades gives rise to a concomitant increase in the number of batch modes, the frequency bandwidth remains constant. Allen (1), however, found that the bandwidth increased, but that an estimate of this increase could not be predicted reliably by extrapolation.

In the current study packages of three, five and seven unstaggered blades, joined by a 2.5mm shroud were analysed. The results are summarised in the graph of Frequency versus Number of Blades (Figure 40), which shows that a slight increase in the detached mode frequencies may be expected. The lower frequency limit of the first batch modes remains sensibly constant, while, within the range considered, the upper limit shows an increase with the number of blades which appears to reach a maximum. A trend for the bandwidth to remain constant for packages of more than six blades is indicated.

However, the second batch modes show a rapid decrease in the lower frequency limit, with no apparent tendency to become constant, whilst the upper limit increases with number of blades, though at a slower rate than the former.

These changes in frequency do not follow the same trends as those observed by Allen, but give added emphasis to the conclusion that changes in bandwidth due to an increase in the

number of blades cannot be reliably predicted by extrapolation.

Although this factor may initially appear to offset the considerable economical advantages of analysing a package with a reduced number of blades, a frequency selective method of analysis enables areas of interest to be located economically with a small number of blades. These areas may then be investigated over a limited frequency range with a more representative model.

It may be concluded, therefore, that the limitations imposed by analysing packages comprising a small number of blades can be offset by the use of a frequency selective method of the Myklestad type,retaining the advantages of economy of computer time and storage requirements.

5. CONCLUDING THE ANALYSIS OF BLADE PACKAGES

In Chapter 1 several methods for the determination of the resonant frequencies of beams were compared to assess their suitability for the investigation of the vibration characteristics of packages of thick, pretwisted turbine blades. It has been the intention of the study to provide a perspicuous and adaptable method to enable the designer to predict the frequencies at which vibration induced fatigue failure could arise in such components.

Since exact mathematical solutions to this problem are not generally possible recourse must be made to approximate solutions. Of the methods investigated two appeared suitable for extension from a two-dimensional analysis to the three dimensions required by pretwisted blade packages; the finite element method and a modified form of the lumped parameter model due to Myklestad. Because the emphasis in the study has been to develop a design tool, preference was given to the method which was shown to be capable of a frequency selective solution and more amenable to modification to cater for non-uniformity of the blades and the complexity of the blade/shroud junction without an undue increase in the size of the problem or complexity of the model.

These factors led to the adoption of the modified lumped parameter model due to Myklestad, rather than the more accurate, but less adaptable finite element technique.

The theoretical study was supported by an experimental programme using Laser holographic and interferometric techniques to confirm the validity of the numerical solutions.

It has been found that generally good agreement is obtainable between the experimental and theoretical results for the modes

most likely to give rise to vibration induced fatigue failure of the blade packages and similar structures. Major differences between the calculated and experimental results could be shown to be improved by introducing factors to improve the modelling of the blade/shroud junction and also the end conditions existing at the blade roots. Although for the purposes of this study the theoretical analysis was restricted to non-rotating blades of constant cross-section and pretwist it was shown in Chapter 2 that the lumped parameter solution can be modified to include these parameters without an undue increase in the complexity of the problem.

It is, therefore, concluded that the lumped parameter modelling of turbine blade packages and similar structures offers a tractable and economical method for the prediction of resonant vibration frequencies at the design stage.

REFERENCES

1. Allen, V. C.

   The Effect of Shear Flexibility and Rotary Inertia on the Vibration Characteristics of Some Turbine Blade Configurations.

   M.Phil. Thesis, 1972

2. Fleeting, R. and Coats, R.

   Blade Failures in the H.P. Turbines of R.M.S. Queen Elizabeth 2 and Their Rectification.

   Trans.I.Mar.E. 82, 49, 1970

3. Ewins, D. J.

   Vibration Characteristics of Bladed Disc Assemblies.

   J.Mech.Eng.Sci. 15, 3, 165-186, 1973

4. Myklestad, N. O.

   A New Method of Calculating Natural Modes of Uncoupled Vibration of Airplane Wings and Other Types of Beams.

   J.Aero.Sci. 153-162, April 1944

5. Holzer, H.

   Die Berechnung der Drehschwinggungen.

   1921

6. Leckie, F. A. and Lindberg, G. M.

   The Effect of Lumped Parameters on Beam Frequencies.

   Aero. Quarterly 224-240, Aug., 1963

7. Zienkiewicz, O. C.

The Finite Element Method in Structural and Continuum Mechanics.

McGraw-Hill, 1967

8. Prohl, M. A.

A Method for Calculating Vibration Frequency and Stress of a Banded Group of Turbine Buckets.

Trans. A.S.M.E. 80 (1), 1958

9. Smith, D. M.

Vibration of Turbine Blades in Packets.

Proc. 7th Int. Conf. for App. Mech. (3), 1949

10. Mahalingam, S.

An Improvement of the Myklestad Method for Flexural Vibration Problems.

J.Aero.Sci. 46-50, Jan., 1959

11. Huang, T. C. and Wu, N. C.

Approximate Analysis of Flexural Vibrations of Beams.

12. Carnegie, W. D.

Solution of the Equations of Motion for the Flexural Vibration of Cantilever Blades Under Rotation by the Extended Holzer Method.

Bull.Mech.Eng.Educ. 6, 1967

13. Carnegie, W. D.

Vibrations of Pre-Twisted Cantilever Blading Allowing for Rotary Inertia and Shear Deformation.

J.Mech.Eng.Sci. 6, 105-109, 1964

14. Fu, C. C.

Computer Analysis of a Rotating Axial Turbomachine Blade in Coupled Bending-Bending Torsion Vibrations.

Int.J.Num.Methods in Engg. 8, 569-88, 1974

15. McCalley, R. B.

Rotary Inertia Correction for Mass Matrices.

G.E.C. (New York) Report DIG/SA, 63-73, 1963

16. McCalley, R. B.

Mass Matrix for a Prismatic Beam Segment.

G.E.C. Report KAPL-M-6913, 1968

17. Carnegie, W. D., Thomas, J. and Dokumaci, E.

An Improved Method of Matrix Displacement Analysis in Vibration Problems.

Aero. Quarterly 20, 321-332, 1969

18. Thomas, J. and Abbas, B. A. H.

Finite Element Model for Dynamic Analysis of Timoshenko Beam.

J.Sound Vib. 41 (3) 291-299, 1975

19. Thomas, D. L.

Comments on "Finite Element Model for Dynamic Analysis of Timoshenko Beam".

Letters, J.Sound Vib. 46 (2), 285-290, 1976

20. Thomas, J. and Belek, H. T.

Free Vibration of Blade Packets.

J.Mech.Eng.Sci. 19 (1) 13-21, 1977

21. Gupta, K. K.

Eigenvalue Solution by Combined Sturm Sequence and Inverse Iteration Technique.

Int.J.Num.Methods in Engg. 7, 17-42, 1973

22. Henshell, R. D. and Warburton, G. B.

Transmission of Vibration in Beam Systems.

Int.J.Num.Methods in Engg. 1, 47-66, 1969

23. Armstrong, E. K. and Stevenson, R. E.

Some Practical Aspects of Compressor Blade Vibration.

J.R.Ae.S. 64 (591) Mar., 1960

24. Cottney, D. J. and Ewins, D. J.

Towards the Efficient Vibration Analysis of Shrouded Bladed Disc Assemblies.

Trans. A.S.M.E. 1054-59, Aug., 1974

25. Timoshenko, S.

On the Transverse Vibrations of Bars of Uniform Cross Section.

Phil.Mag.Ser. 6, Vol.43, 1922

26. Timoshenko, S.

Vibration Problems in Engineering.

4th Ed. Wiley (New York) 1974

27. Shiga, M.

Natural Frequencies of Axial Vibration of Turbine Buckets for High Pressure Stage.

Bull. J.S.M.E. 16 (101) 1667-74, 1973

28. Stuwing, D.

Zur Berechnung der Eigenfrequenzen von Schaufelpaketen Axialer Turbomaschinen.

Maschinenbautechnik, 17 (9), 1968

29. Ligtenberg, F. K.

The Moiré Method: A New Experimental Method for the Determination of Movements in Small Slab Models.

Exp. Stress Analysis 12, (2) 83-98, 1955

30. Tolansky, S. and Wood, A. F. B.

Multiple Beam Interferometric Studies on Oscillating Quartz Crystals.

Physica, 24, 508-518, 1958

31. Gabor, D.

A New Microscopic Principle.

Nature, London, 161, 777-778, 1948

32. Leith, E. N. and Upatnieks, J.

Photography by Laser.

Sci.Amer. 212 (6) 24-35, 1965

33. Powell, R. L. and Stetson, K. A.

Interferometric Vibration Analysis by Wavefront Reconstruction.

J.Opt.Soc.Amer. 55 (12) 1593-1598, 1965

34. Archbold, E. and Ennos, A. E.

Observation of Surface Vibration Modes by Stroboscopic Hologram Interferometry.

Nature 217 (5132) 942-943, 1968

35. Erf, R. K., Gagosz, R. M. and Waters, J. P.

Holography in a Factory Environment.

The Engineering Uses of Coherent Optics (ed. Robertson, E. R.) C.U.P. 1976

36. Mottier, F. M. and Eliasson, B.

Optical Analogue to Chladni Vibration Patterns Using Laser Produced Speckles.

J.Opt.Soc.Amer. 60, 739, 1970

37. Stetson, K. A.

New Design for Laser Image-Speckle Interferometer.

Optics and Laser Technology 2, 1979-181, 1970

38. Neumann, D. B., Jacobson, C. F. and Brown, G. M.

Holographic Technique for Determining the Phase of Vibrating Objects.

App.Optics 9 (6) 1357-62, June, 1970

39. Aleksoff, C. C.

Time Averaged Holography Extended.

Appl.Phys. Letters 14 (23), 1969

40. Archbold, E. and Ennos, A. E.

Applications of Holography and Speckle Photography to the Measurement of Displacement and Strain.

J.Strain Analysis 9 (1) 10-16, 1974

41. Hughes, R. G.

The Determination of Vibration Patterns Using a Pulsed Laser with Holographic and Electronic Speckle Pattern Interferometry Techniques.

The Engineering Uses of Coherent Optics (ed. Robertson, E. R.) C.U.P. 1976

42. Fryer, P. A.

Vibration Analysis by Holography.

Rep.Prog.Phys. 33, 489-521, 1970

43. Archbold, E. and Ennos, A. E.

Techniques of Hologram Interferometry for Engineering Inspection and Vibration Analysis.

Engineering Uses of Holography, C.U.P. 1968

TABLE 1 : Comparison of Frequency Predictions for a Blade Package From a Finite Element Model and Myklestad Model

	Finite Element Model (Ref.20) Hz	Error %	Experimental Model (Ref.20) Hz	Error %	Myklestad Model (40-Steps) Hz
First detached mode	213.4	0.7	212	3.4	219.3
First batch modes	833.6	0.7	828	3.7	858.6
	834.4	0.8	828	3.7	860.5
Second detached mode	1220.1	0.7	1212	2.3	1239.8
Second batch modes	2646	2.5	2581	4.1	2687.9
	2667	2.5	2602	4.1	2709.8

Package details:-

Number of blades	3
Blade length	5.625 in
Shroud length	1.000 in
Blade cross section	1 x 0.187 in
Shroud cross section	0.14 x 0.093 in

Flexural Mode	Exact Solution Hz	Myklestad Model (10-Steps) Hz	Error %	Taper* (p)
1	1.875	1.871	0.21	
2	4.694	4.657	0.79	
3	7.855	7.754	1.28	0.0
4	10.996	10.798	1.80	
5	14.137	13.805	2.35	
1	2.176	2.166	0.46	
2	4.920	4.871	0.99	
3	7.992	7.873	1.49	1.0
4	11.095	10.873	2.00	
5	14.215	13.852	2.55	
1	2.503	2.485	0.72	
2	5.156	5.092	1.24	
3	8.147	8.003	1.77	2.0
4	11.211	10.954	2.29	
5	14.307	13.900	2.84	
1	3.223	3.180	1.33	
2	5.671	5.559	1.97	
3	8.512	8.296	2.54	4.0
4	11.490	11.135	3.09	
5	14.533	13.997	3.67	
1	4.860	4.704	3.21	
2	6.888	6.605	4.11	
3	9.438	8.981	4.84	8.0
4	12.228	11.551	5.54	
5	15.140	14.192	6.26	

*Taper is defined as the power (p) describing the rate of change of the flexural coefficient (EI) and the mass/unit length (ρ) with length (x)

$$EI_x = (EI)_o \, e^{-px} \; ; \; \rho_x = \rho_o \, e^{-px}$$

TABLE 2 : Resonant Frequencies of an Exponentially Tapered Cantilever

Flexural Mode	Exact Solution Hz	Myklestad Model (40-Steps) Hz	Error %	Taper* (p)
1	1.875	1.875	0.00	
2	4.694	4.692	0.04	
3	7.855	7.848	0.09	0.0
4	10.996	10.983	0.12	
5	14.137	14.116	0.15	
1	2.176	2.175	0.05	
2	4.920	4.916	0.08	
3	7.992	7.984	0.10	1.0
4	11.095	11.081	0.13	
5	14.215	14.192	0.16	
1	2.503	2.501	0.08	
2	5.156	5.152	0.08	
3	8.147	8.138	0.11	2.0
4	11.211	11.195	0.14	
5	14.307	14.282	0.17	
1	3.223	3.220	0.09	
2	5.671	5.663	0.14	
3	8.512	8.498	0.16	4.0
4	11.490	11.468	0.19	
5	14.533	14.499	0.23	
1	4.860	4.850	0.21	
2	6.888	6.869	0.28	
3	9.438	9.409	0.31	8.0
4	12.228	12.184	0.36	
5	15.140	15.081	0.39	

*Taper is defined as the power (p) describing the rate of change of the flexural coefficient (EI) and the mass/unit length (ρ) with length (x)

$$EI_x = (EI)_o \, e^{-px} \; ; \; \rho_x = \rho_o \, e^{-px}$$

TABLE 3 : Resonant Frequencies of an Exponentially Tapered Cantilever

Flexural Mode	Experimental Model	Myklestad Model Without Clamp Fixed-Free	Myklestad Model With Clamp Fixed-Free	Myklestad Model With Clamp Free -Free
1	455	479.1	479.8	482.4
2	1968	2124.6	2140.5	2119.7
3	4887	5249.5	5231.3	5282.1
4	9055	9660.4	9624.7	9691.7
5	14270	15055.6	-	-

TABLE 4 : Resonant Frequencies of a Linearly Tapered Beam, with Varying End-Conditions and Allowance for the Clamp

Mode Type	Experimental Model kHz	Myklestad Model kHz	Error %
FLEXURAL			
Detached	1.05	1.03	-1.3
Batch (symmetric)	4.49	4.38	-2.3
Batch (antisymmetric)	4.35	4.29	-1.6
Detached	5.78	5.60	-3.2
Batch (symmetric)	12.03	11.74	-2.4
Batch (antisymmetric)	11.27	11.47	-1.8
Detached	(15.15)	13.09	(-13.6)
EDGE			
Detached	-	2.43	-
TORSIONAL			
Detached	-	3.25	-
Batch (symmetric)	-	8.72	-
Batch (antisymmetric)	-	8.64	-

Pretwist 0^{o}

Shroud Thickness 6.3mm

TABLE 5 : Resonant Frequencies of Blade Package Model A1

Mode Type	Experimental Model kHz	Myklestad Model kHz	Error %
FLEXURAL			
Detached	1.08	1.09	+1.0
Batch (symmetric)	4.17	4.26	+2.2
Batch (antisymmetric)	4.17	4.26	+2.2
Detached	5.78	5.83	+0.8
Batch (symmetric)	11.56	11.71	+1.3
Batch (antisymmetric)	11.18	11.56	+3.4
Detached	(14.92)	13.62	(-8.7)
EDGE			
Detached	-	2.62	-
TORSIONAL			
Detached	-	3.33	-
Batch (symmetric)	-	8.89	-
Batch (antisymmetric)	-	8.77	-

Pretwist 0°

Shroud Thickness 4.5mm

TABLE 6 : Resonant Frequencies of Blade Package Model A2

Mode Type	Experimental Model kHz	Myklestad Model kHz	Error %
FLEXURAL			
Detached	1.05	1.10	+4.9
Batch (symmetric)	3.77	3.90	+3.4
Batch (antisymmetric)	3.84	4.02	+4.8
Detached	5.51	5.80	+5.4
Batch (symmetric)	11.21	11.47	+2.3
Batch (antisymmetric)	11.07	11.51	+4.0
Detached	12.93	13.95	+7.9
EDGE			
Detached	2.26	2.83	+25.4
TORSIONAL			
Detached	3.07	3.48	+13.4
Batch (symmetric)	-	9.06	-
Batch (antisymmetric)	8.70	8.83	+1.5

Pretwist 0^{o}

Shroud Thickness 2.5mm

TABLE 7 : Resonant Frequencies of Blade Package Model A3

Mode Type	Experimental Model kHz	Myklestad Model kHz	Error %
FLEXURAL			
Detached	0.97	1.03	+6.3
Batch (symmetric)	4.35	4.37	+0.4
Batch (antisymmetric)	4.54	4.57	+0.8
Detached	5.43	5.58	+2.8
Batch (symmetric)	11.67	11.70	+0.2
Batch (antisymmetric)	10.70	11.33	+5.9
Detached	(14.45)	13.17	-8.8
EDGE			
Detached	-	2.91	-
TORSIONAL			
Detached	-	2.96	-
Batch (symmetric)	-	8.58	-
Batch (antisymmetric)	-	8.70	-

Pretwist 30°

Shroud Thickness 6.3mm

TABLE 8 : Resonant Frequencies of Blade Package Model B1

Model Type	Experimental Model kHz	Myklestad Model kHz	Error %
FLEXURAL			
Detached	1.03	1.09	+5.5
Batch (symmetric)	4.07	4.24	+4.3
Batch (antisymmetric)	4.38	4.55	+3.8
Detached	5.50	5.79	+5.2
Batch (symmetric)	11.22	11.67	+4.0
Batch (antisymmetric)	10.50	11.43	+8.8
Detached	14.33	13.70	-4.5
EDGE			
Detached	-	2.69	-
TORSIONAL			
Detached	-	3.03	-
Batch (symmetric)	-	8.87	-
Batch (antisymmetric)	-	8.69	-

Pretwist 30°

Shroud Thickness 4.5mm

TABLE 9 : Resonant Frequencies of Blade Package Model B2

Mode Type	Experimental Model kHz	Myklestad Model kHz	Error %
FLEXURAL			
Detached	1.02	1.08	+7.0
Batch (symmetric)	3.70	3.91	+5.9
Batch (antisymmetric)	4.14	4.38	+5.9
Detached	5.28	5.72	+8.4
Batch (symmetric)	10.91	11.47	+5.1
Batch (antisymmetric)	10.44	11.40	+9.2
Detached	12.79	14.00	+9.5
EDGE			
Detached	2.27	2.50	+10.3
TORSIONAL			
Detached	2.67	3.11	+16.4
Batch (symmetric)	(9.54)	9.01	-5.6
Batch (antisymmetric)	8.43	8.68	+2.9

Pretwist 30^{o}

Shroud Thickness 2.5mm

TABLE 10 : Resonant Frequencies of Blade Package Model B3

Model	Junction Factors	Flexural Mode Type	Experimental Model kHz	Myklestad Model kHz	Error %
A1	2.0,1.5	Detached	1.05	1.04	-0.6
		Batch (symm)	4.49	4.43	-1.2
		Batch (antisymm)	4.36	4.42	+1.6
		Detached	5.78	5.69	-1.6
		Batch (symm)	12.03	11.88	-1.2
		Batch (antisymm)	11.27	11.71	+3.9
A2	0.75,0.5	Detached	1.08	1.09	+0.3
		Batch (symm)	4.17	4.20	+0.6
		Batch (antisymm)	4.17	4.16	-0.3
		Detached	5.78	5.77	-0.1
		Batch (symm)	11.56	11.52	-0.3
		Batch (antisymm)	11.18	11.32	+1.3
A3	0.25,0.0	Detached	1.05	1.05	0.0
		Batch (symm)	3.77	3.80	+0.6
		Batch (antisymm)	3.84	3.81	-0.7
		Detached	5.51	5.51	0.0
		Batch (symm)	11.21	11.22	0.1
		Batch (antisymm)	11.07	11.15	0.7

TABLE 11 : Resonant Frequencies of Blade Package Models A1, A2 and A3 Incorporating Junction Correction Factors

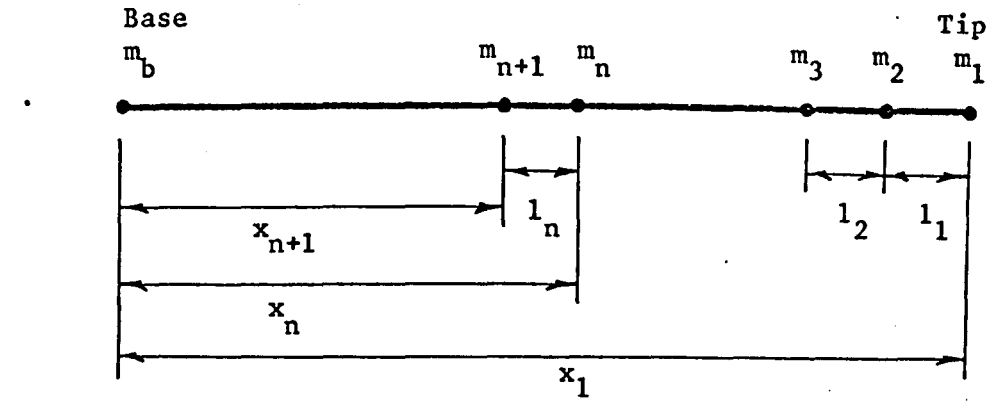

(a) Lumped parameter beam model due to Myklestad

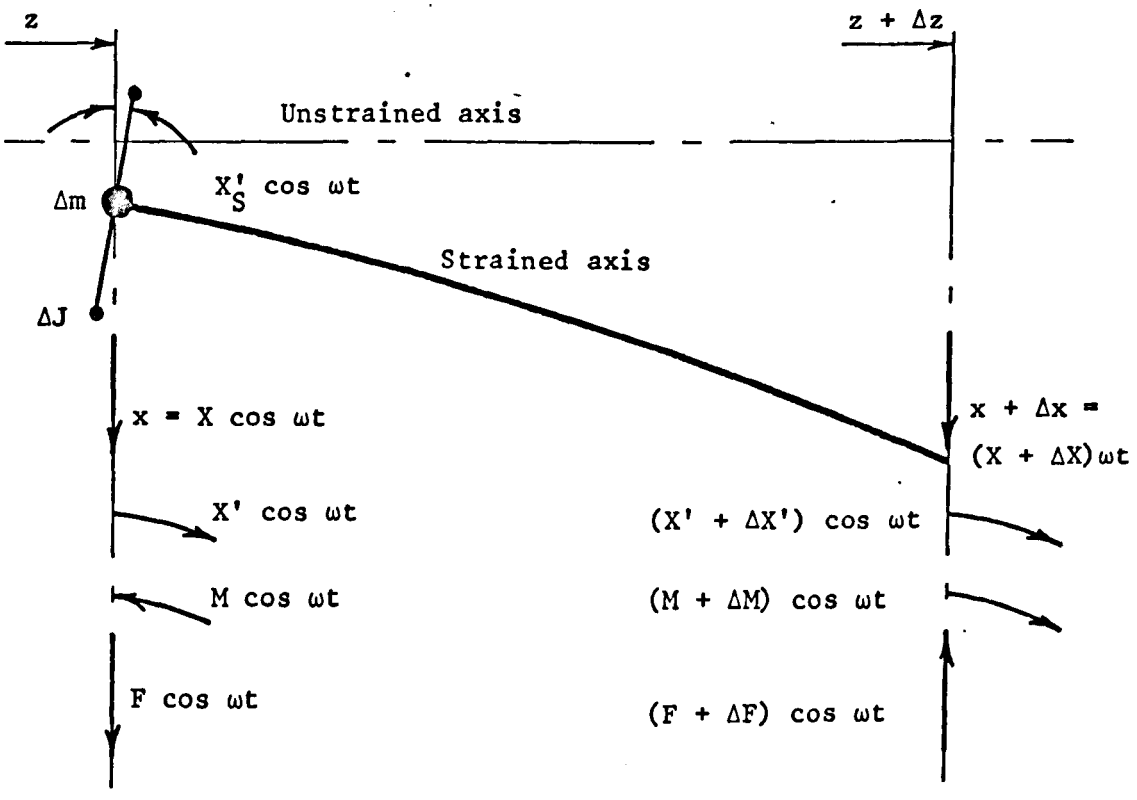

(b) Element of lumped parameter beam model

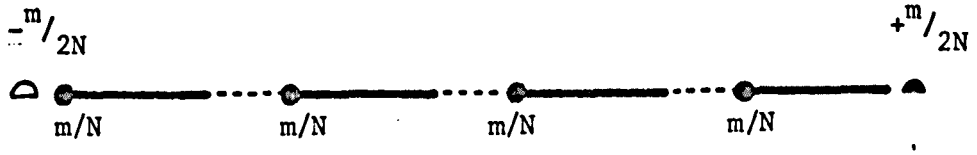

(c) Lumped parameter beam model modified to include "dummy" masses

FIGURE 1 : Lumped Parameter Models

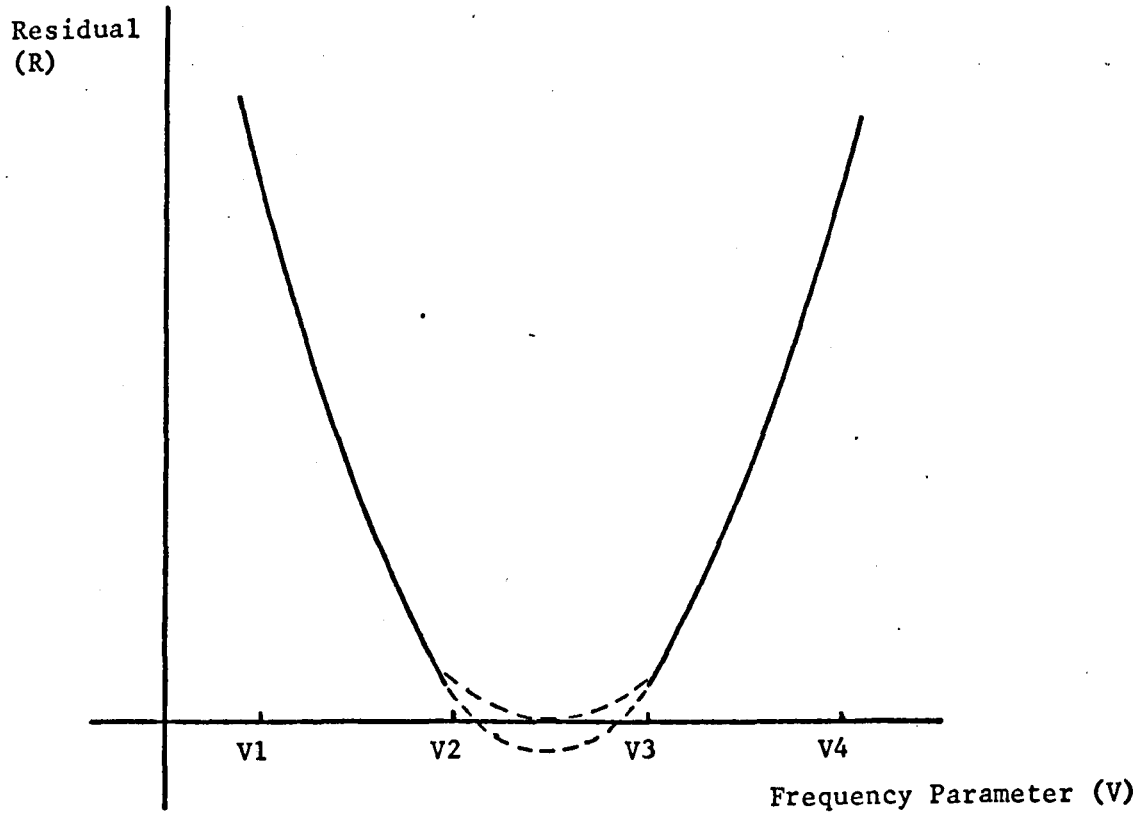

FIGURE 2 : Detection of Roots

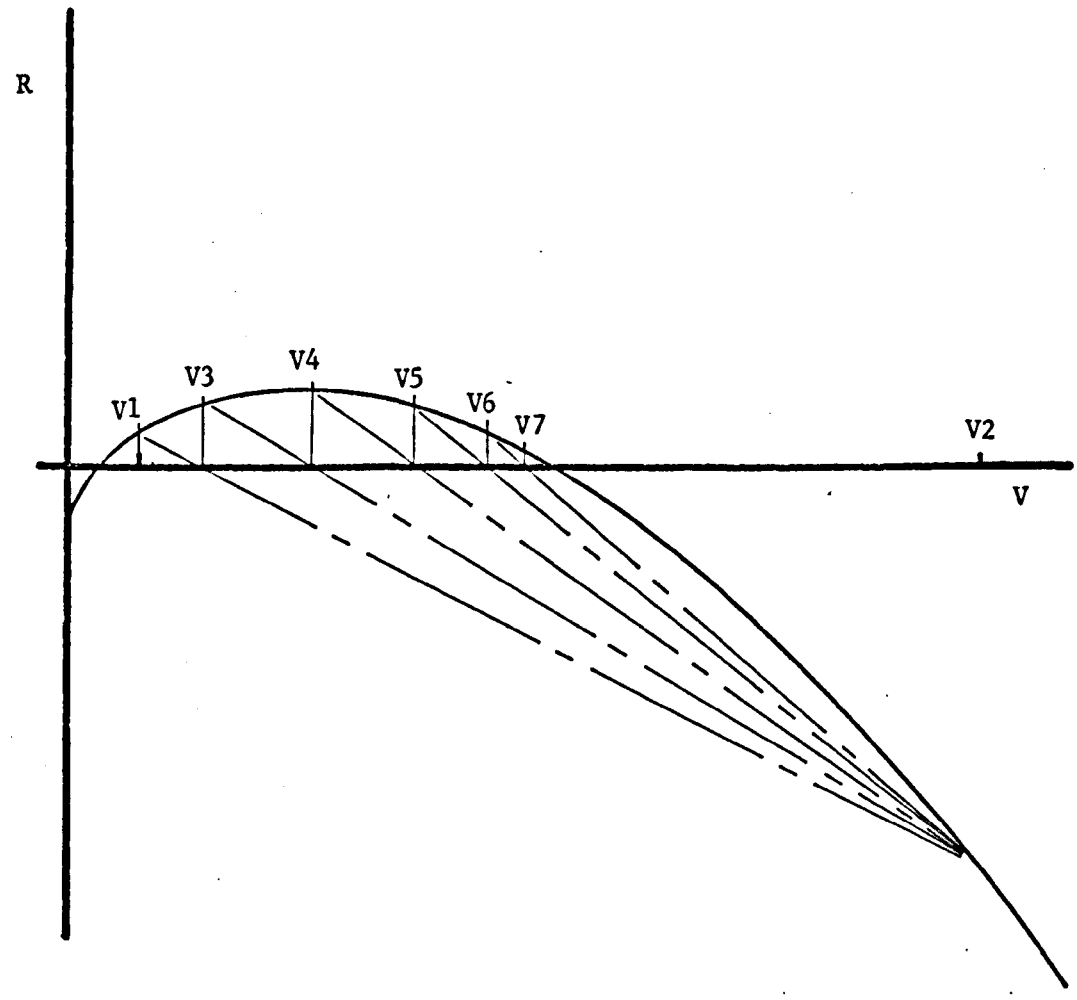

FIGURE 3 : Plot of Residual (R) vs. Frequency Parameter (V) Showing Slow Convergence to Root by Linear Interpolation

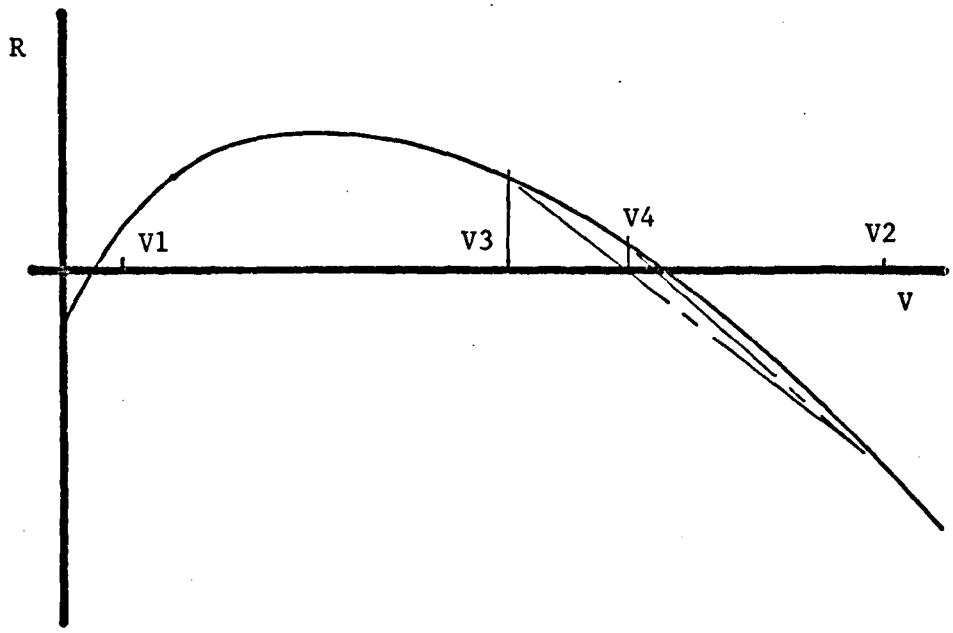

a) Turning Point Between First Trial and Subdivision

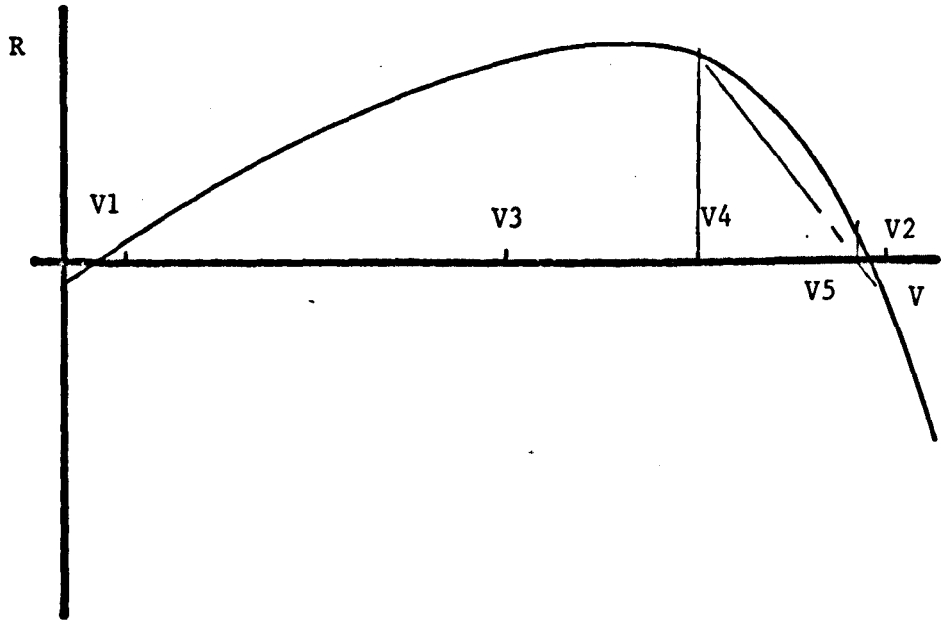

b) Turning Point Between Second Trial and Subdivision

FIGURE 4 : Plot of Residual (R) vs. Frequency Parameter (V) Showing Improved Convergence to Root Using Subdivision of Search Interval

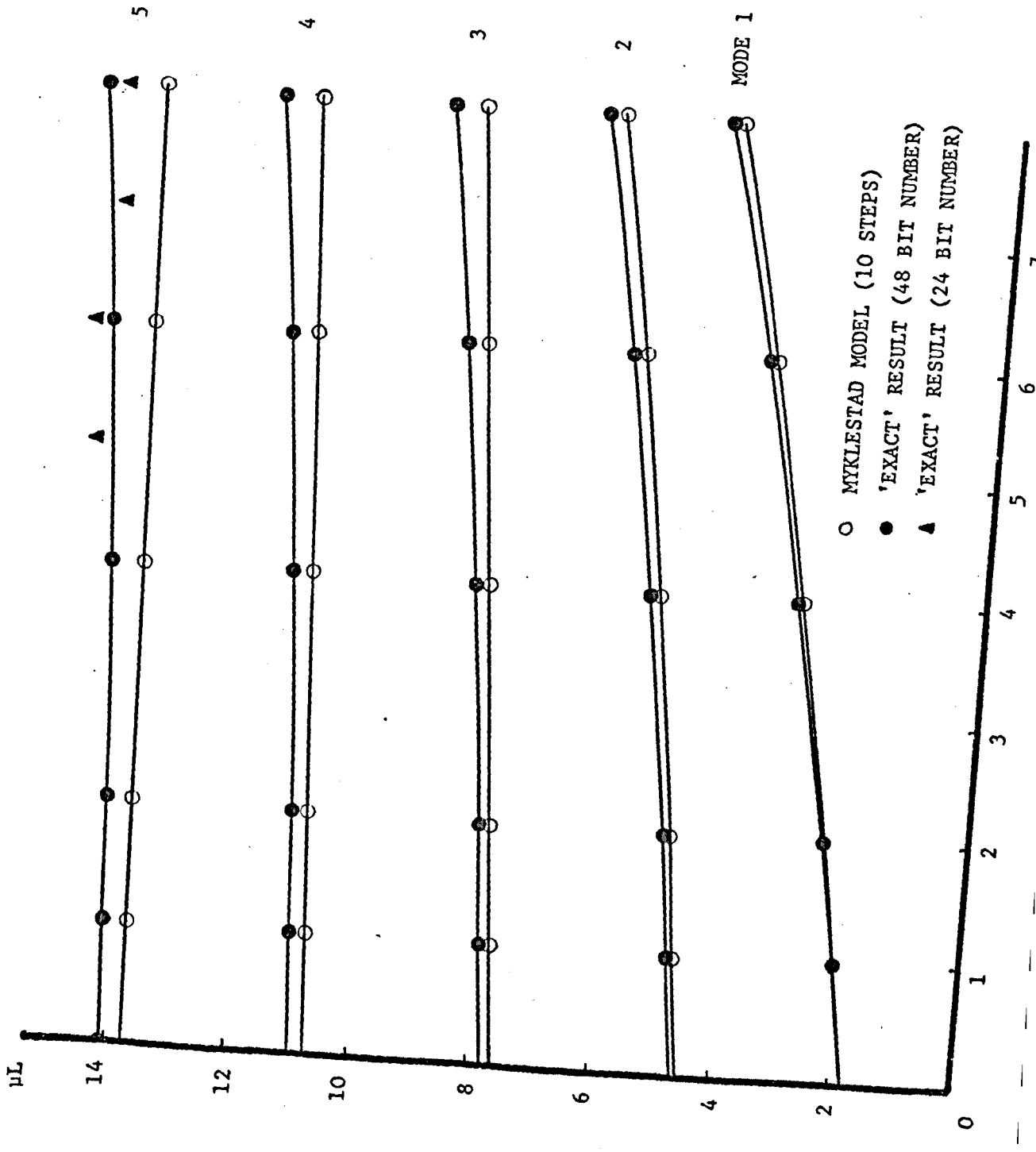

FIGURE 5 : Frequency Parameter (μL) vs. Taper (p) for Exponentially Tapered Cantilevers

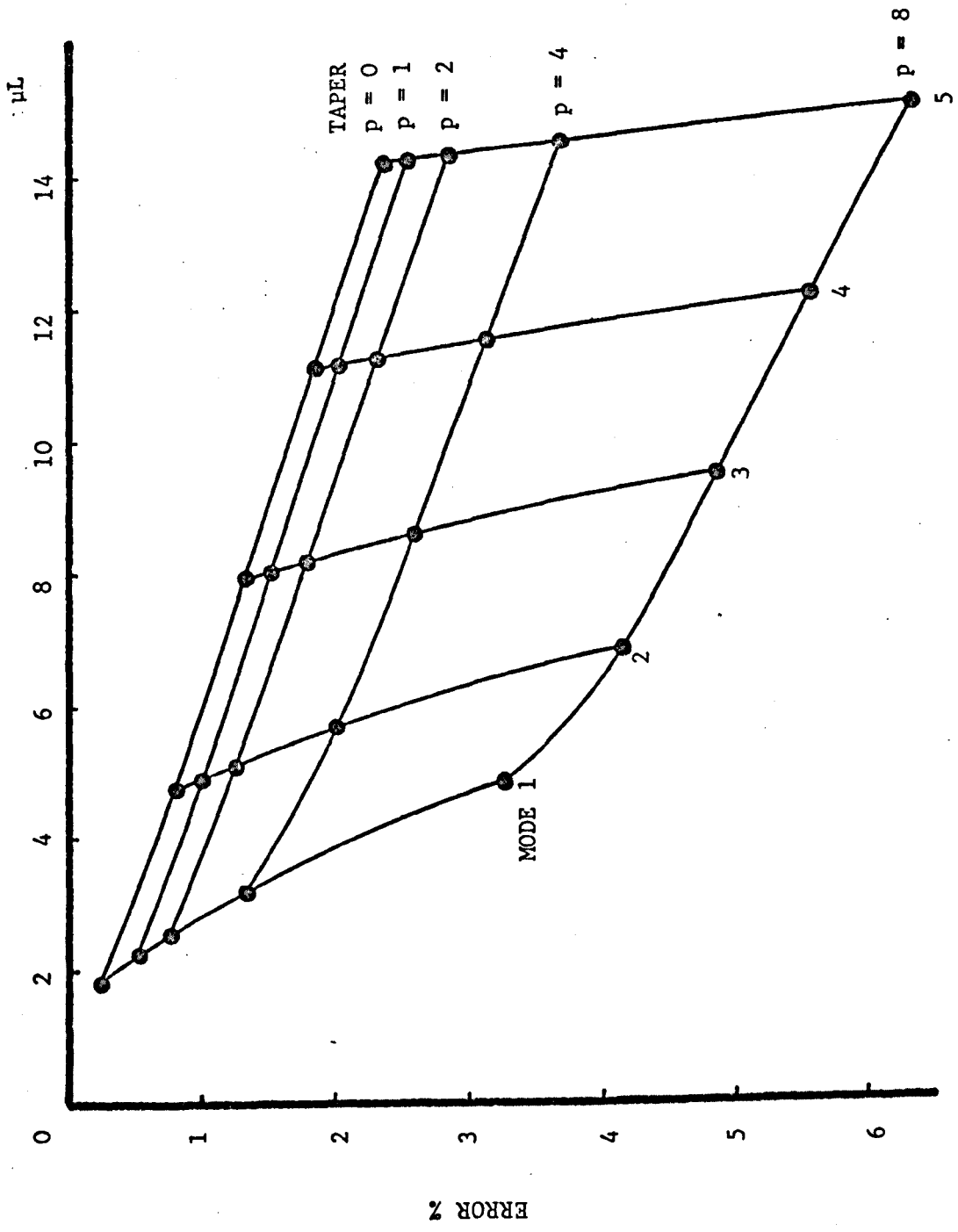

FIGURE 6 : Frequency Parameter (μL) vs. Error and Taper (p) for Exponentially Tapered Cantilevers

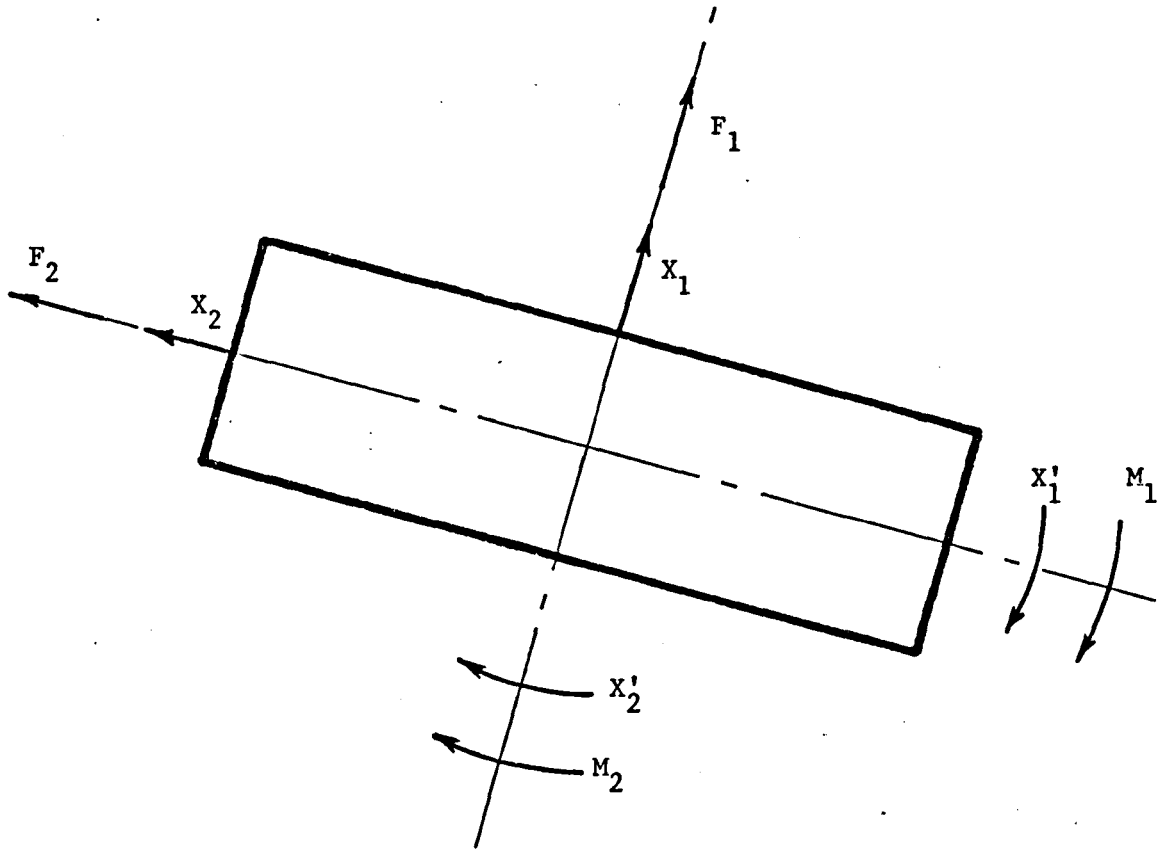

(a) Cross-sectional view along z-axis, defining variables

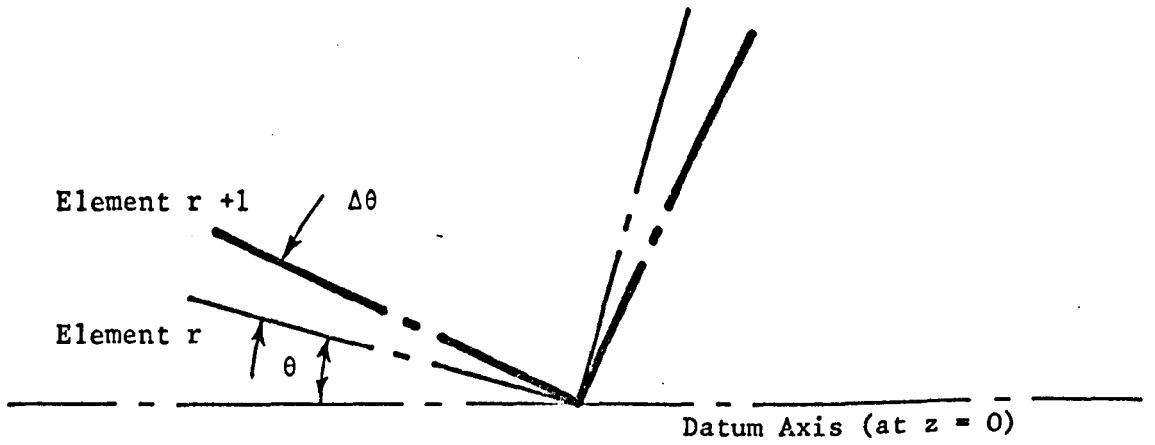

(b) Axes, showing angular relationship between successive elements along z-axis

FIGURE 7 : Pretwisted Element for Lumped Parameter Modelling

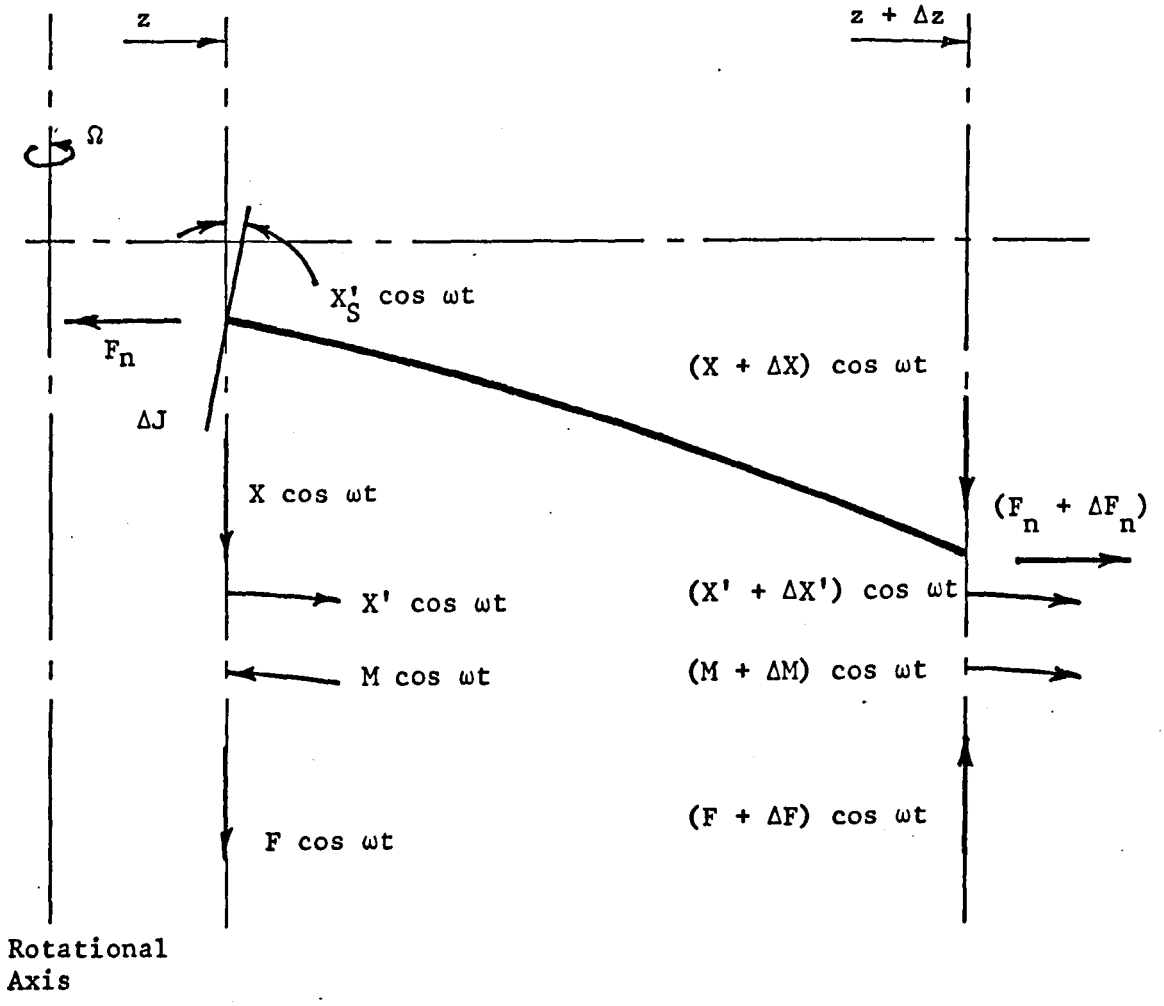

FIGURE 8 : Myklestad Element Showing Forces due to Rotation of the Blade

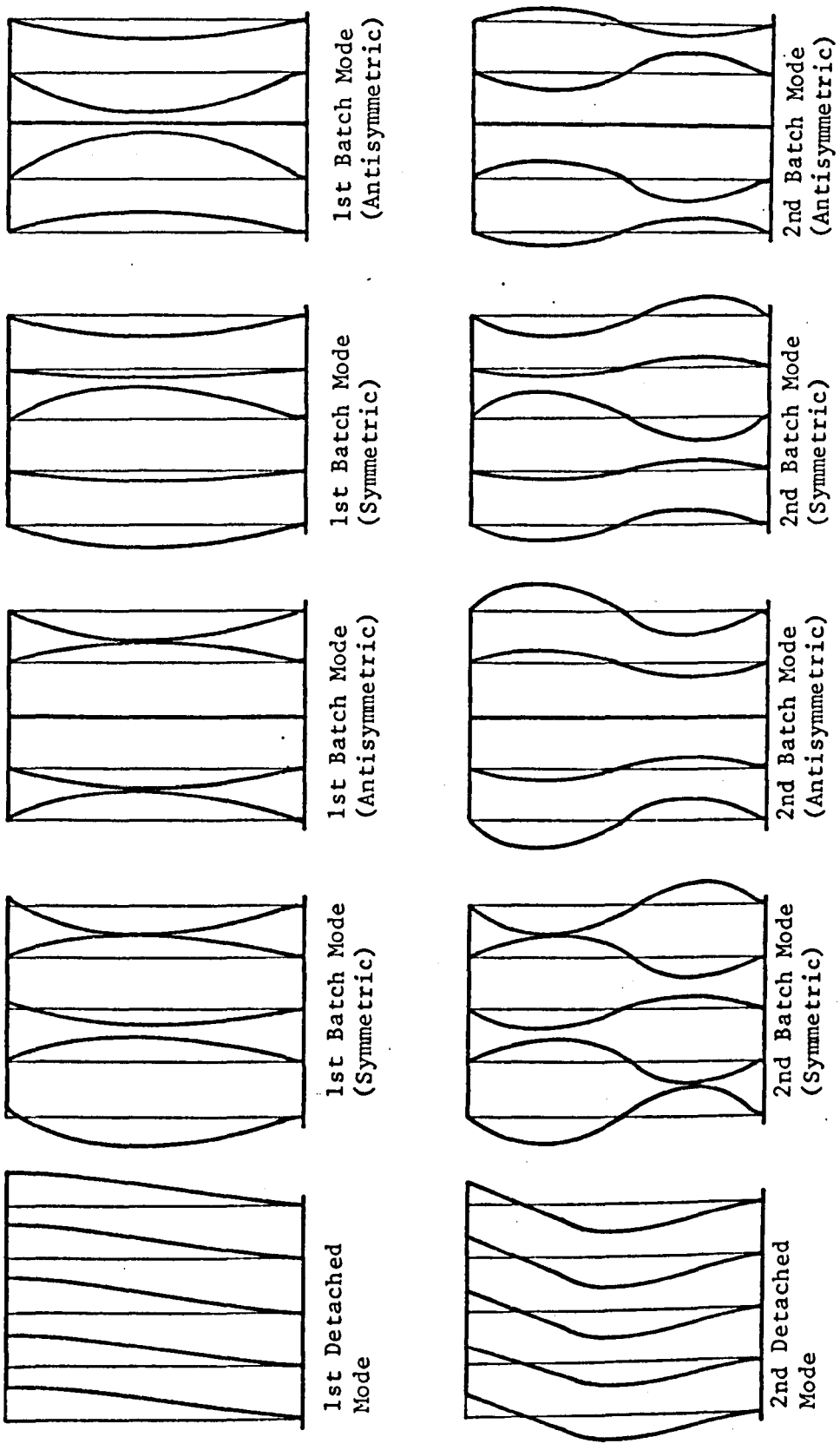

FIGURE 9 : Example Batch Modes (Five-Blade Package)

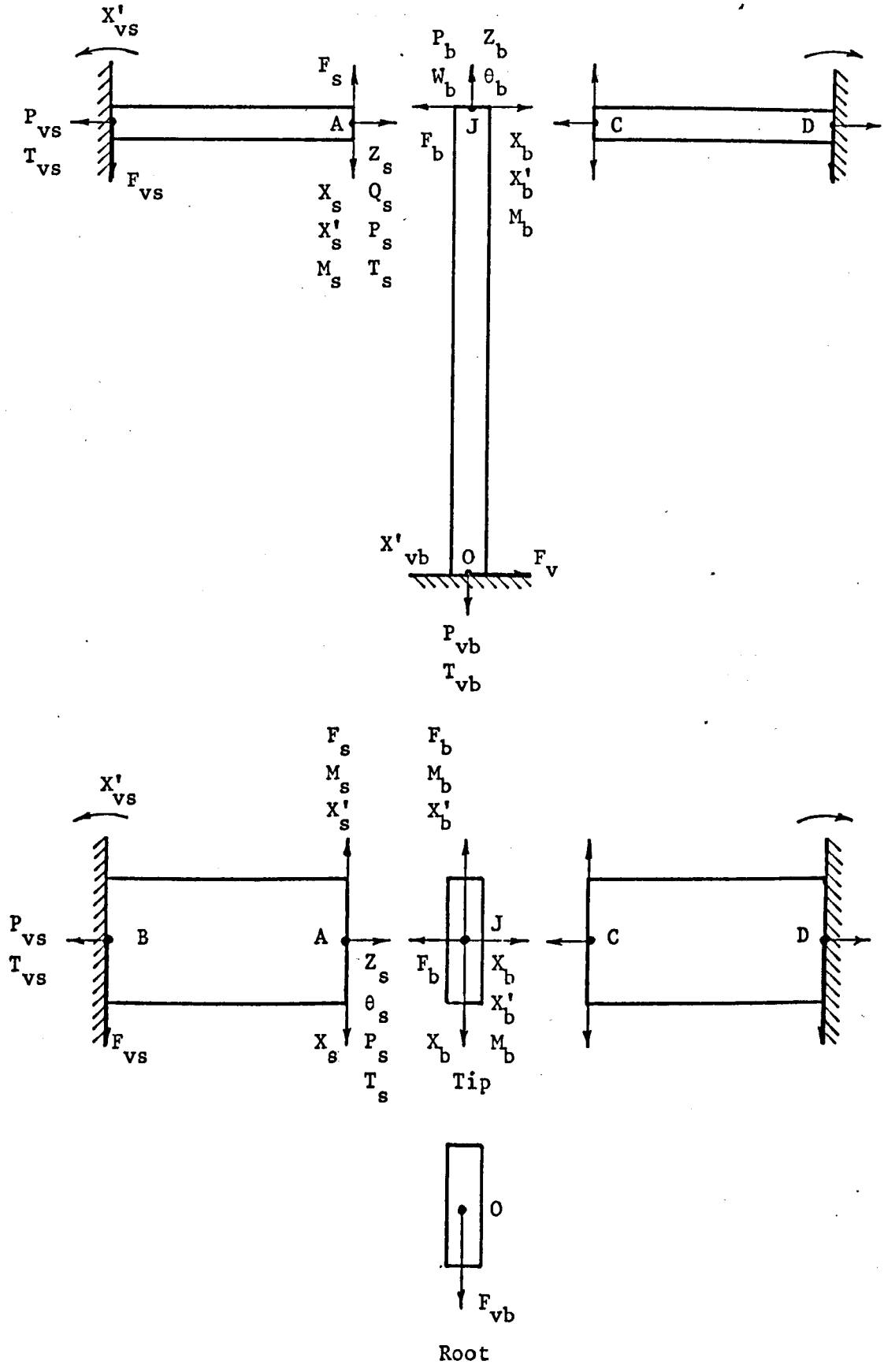

FIGURE 10 : Blade and Shroud Variables due to Inputs at the Blade Root and Remote Tips of the Shroud Bands

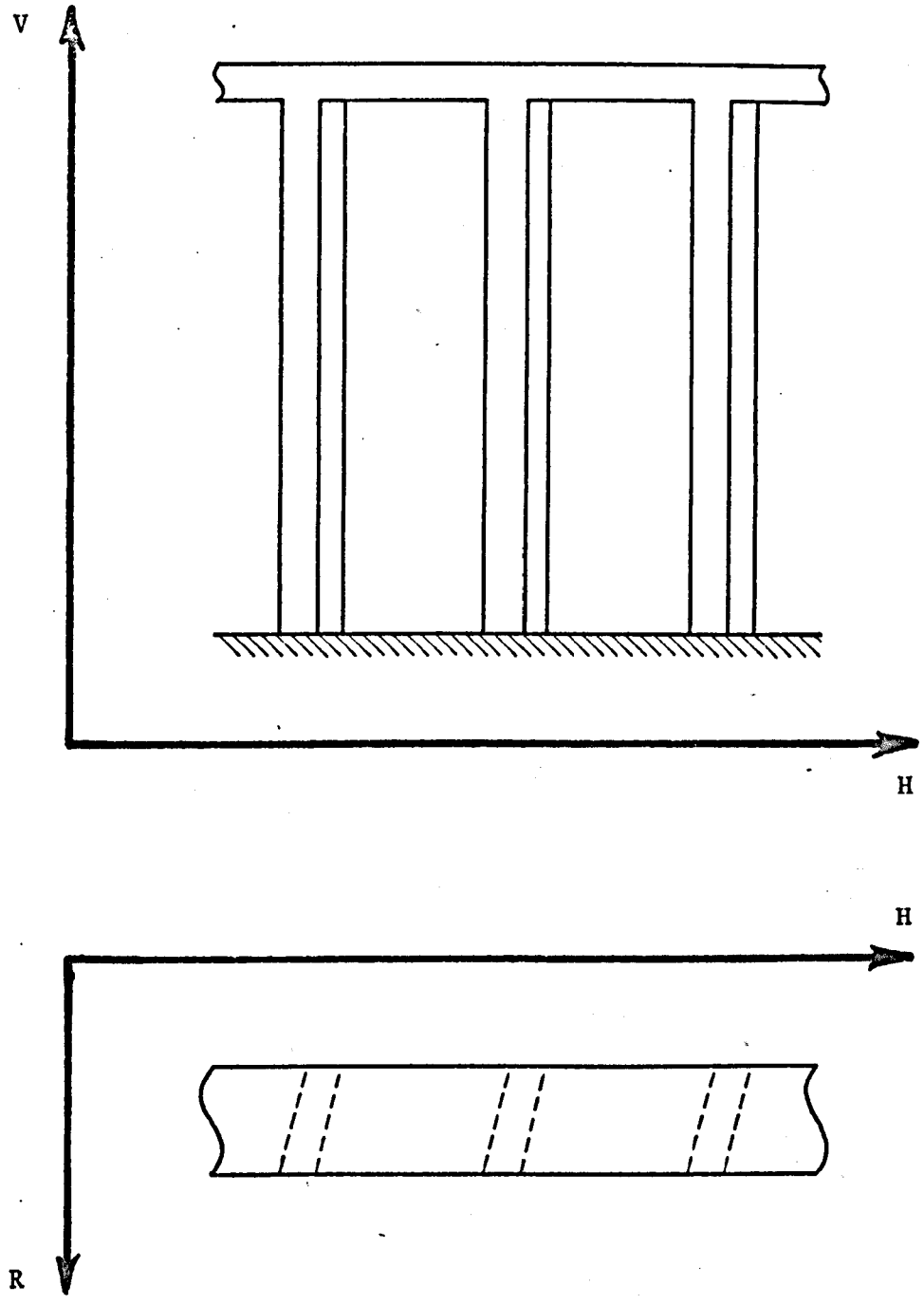

FIGURE 11 : Blade Package Axes

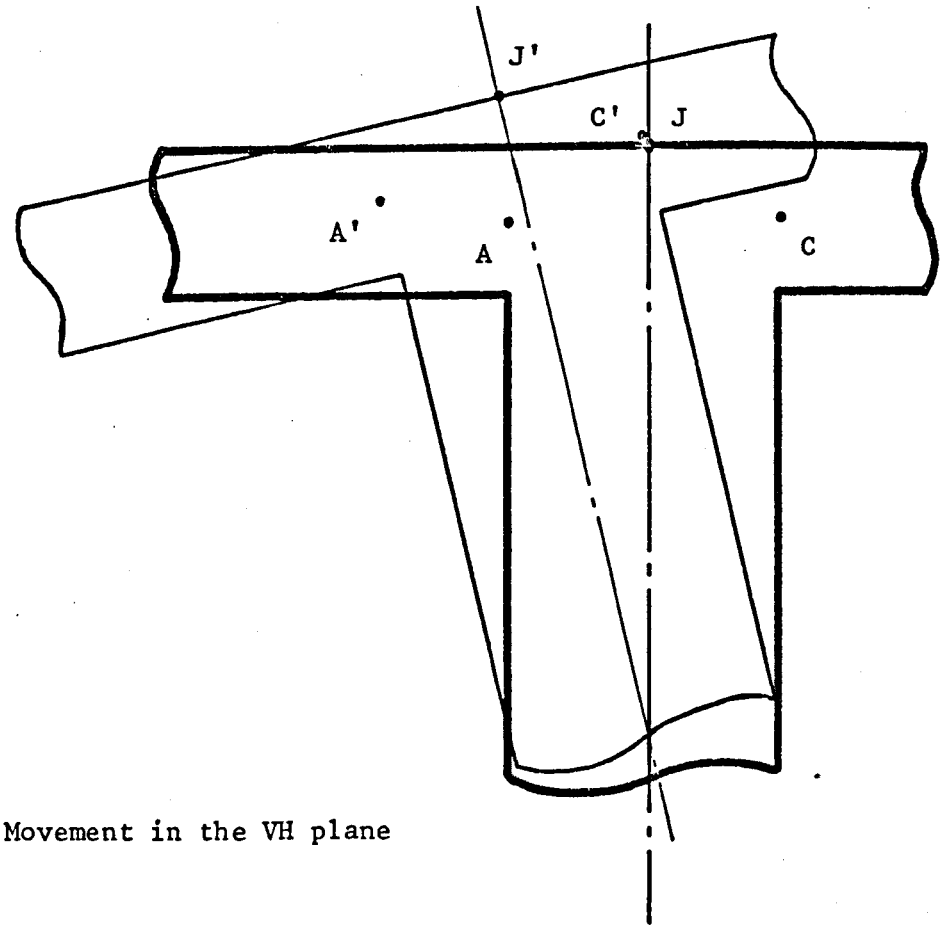

(a) Movement in the VH plane

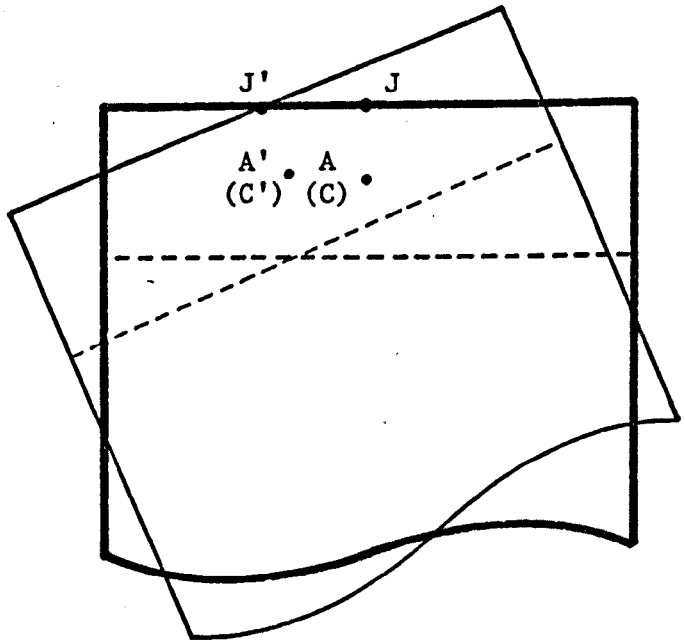

(b) Movement in the RH plane

FIGURE 12 : Movement of Blade/Shroud Junction

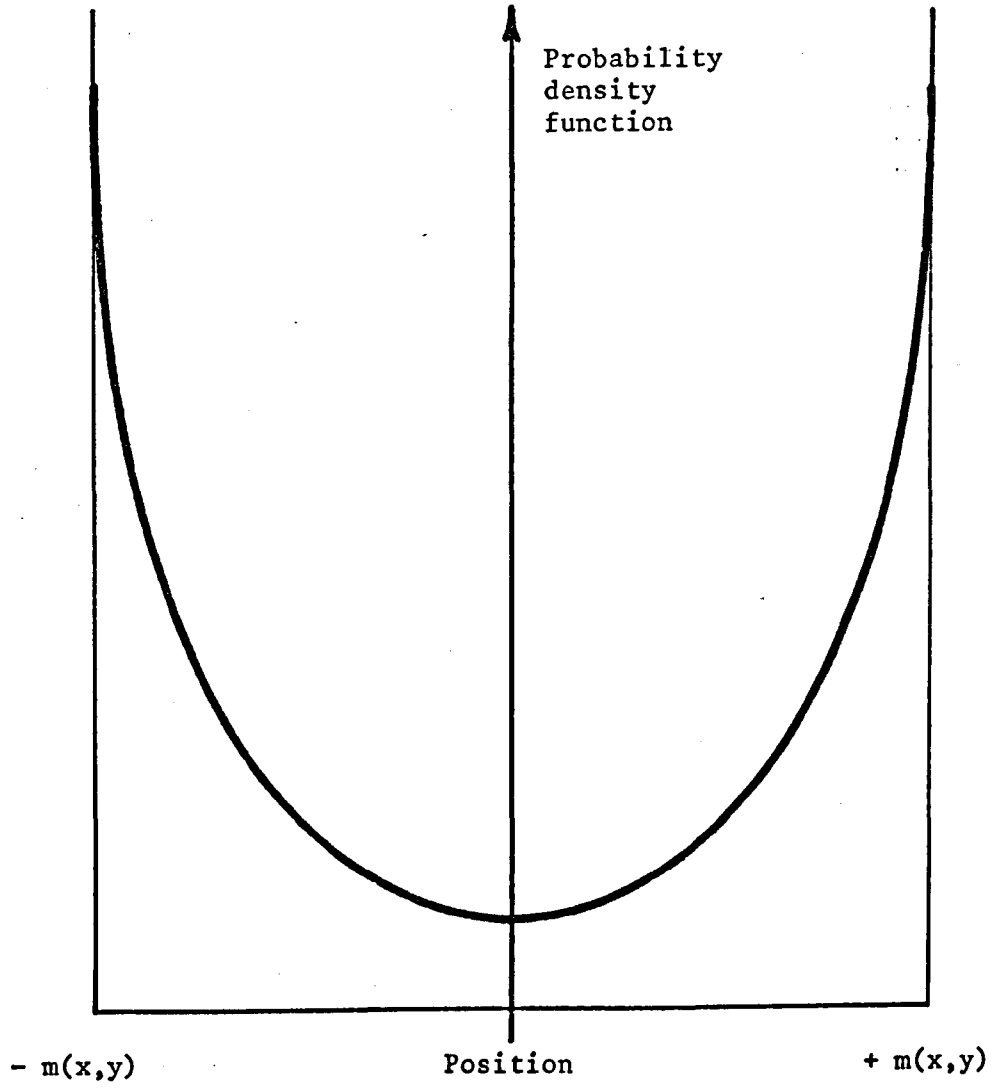

FIGURE 13 : Position Probability Density Function for Simple Harmonic Motion

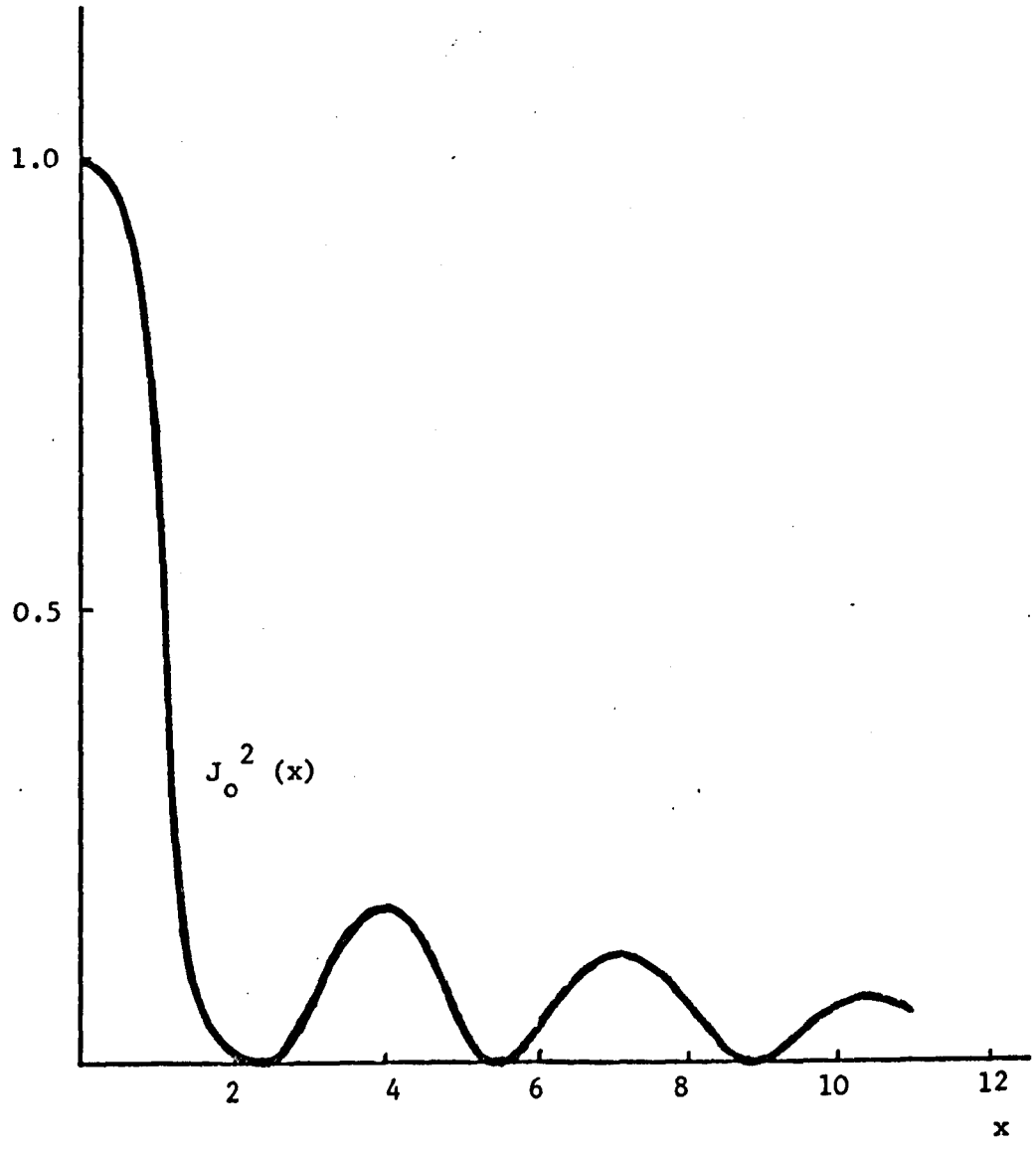

FIGURE 14 : Zero Order (Bessel Function)^2 Plot

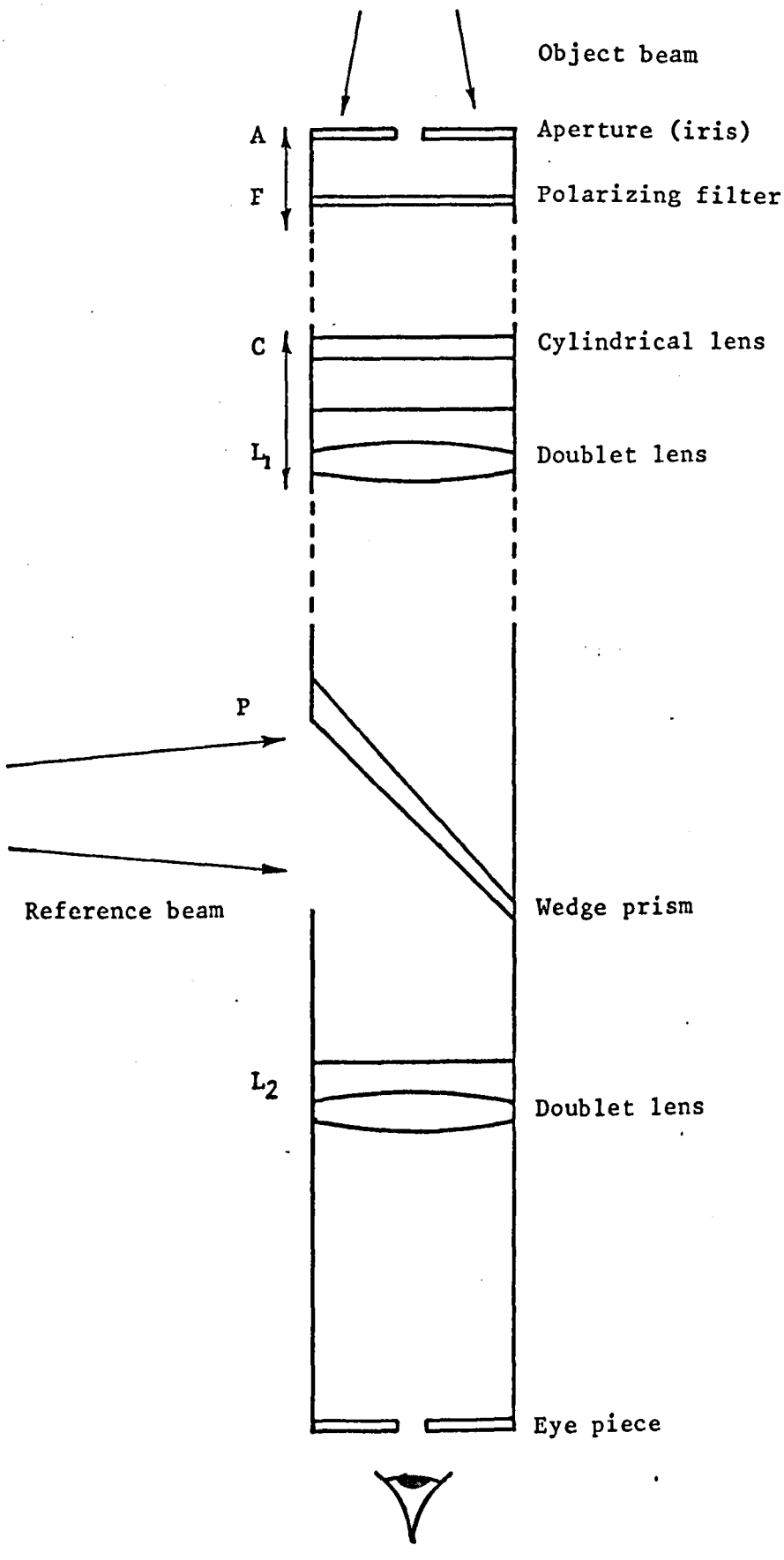

FIGURE 15 : Laser Image-Speckle Interferometer

FIGURE 16 : Laser Image-Speckle Interferometer

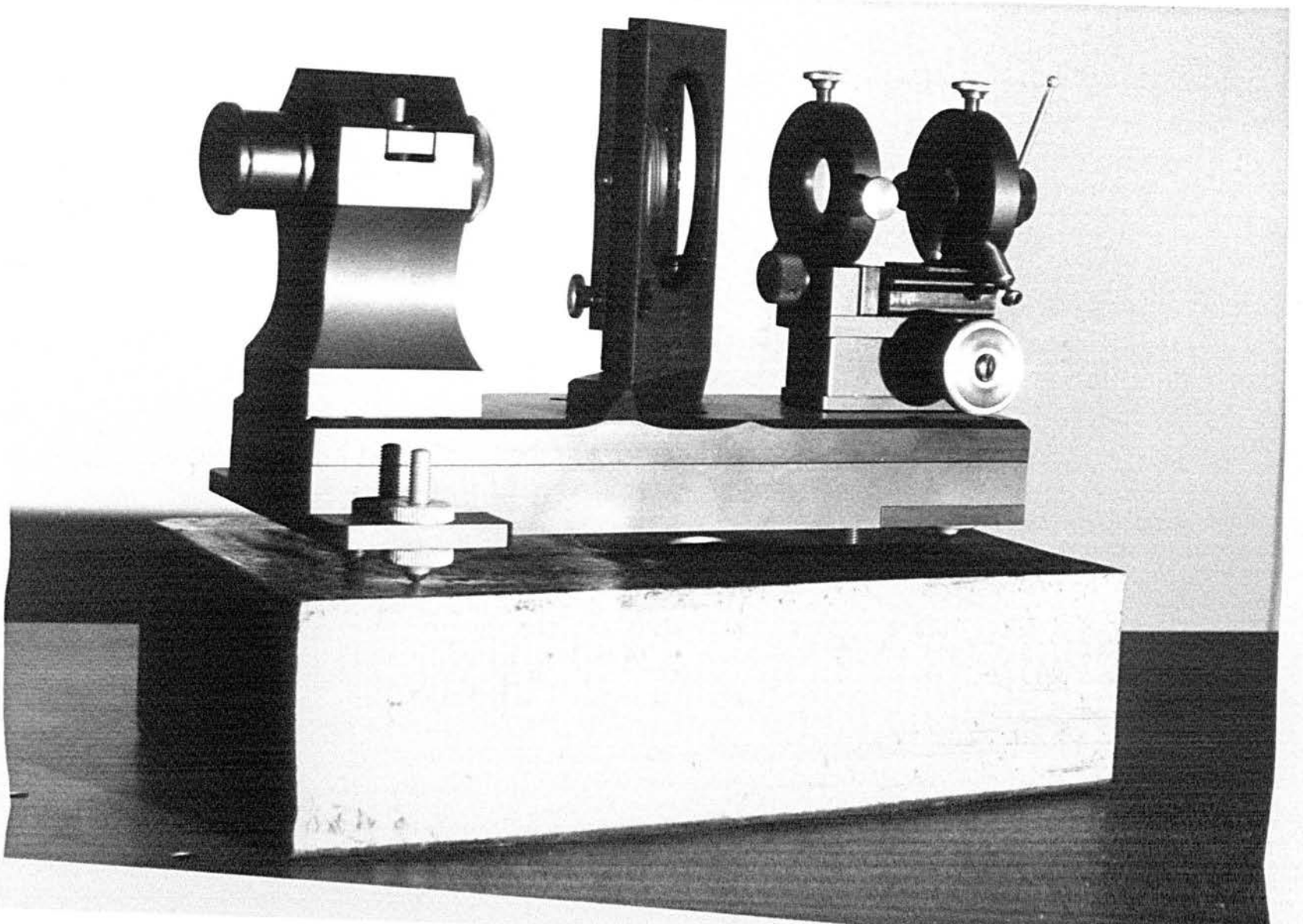

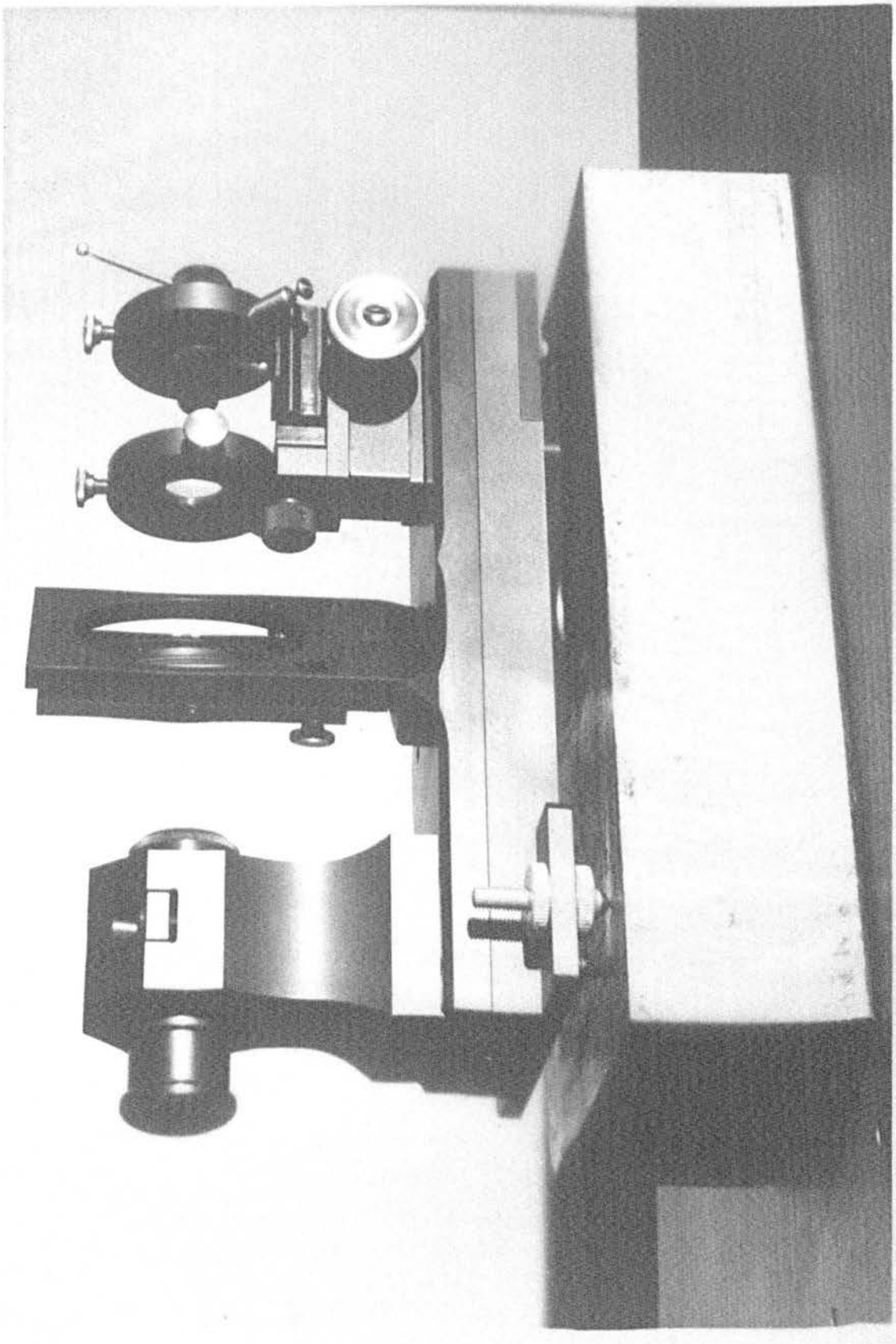

FIGURE 16 : Laser Image-Speckle Interferometer

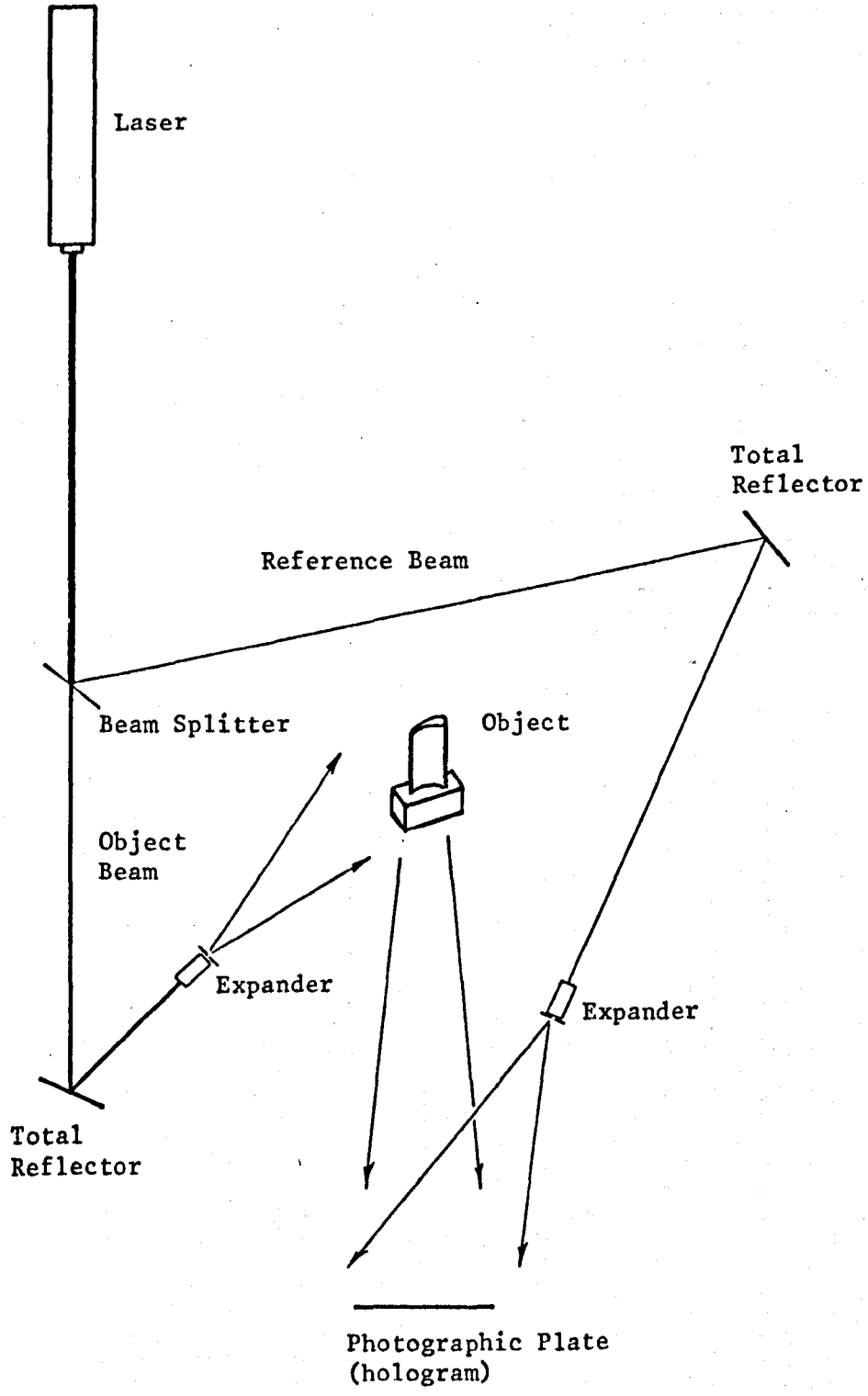

FICURE 17 : Basic Hologram Recording System

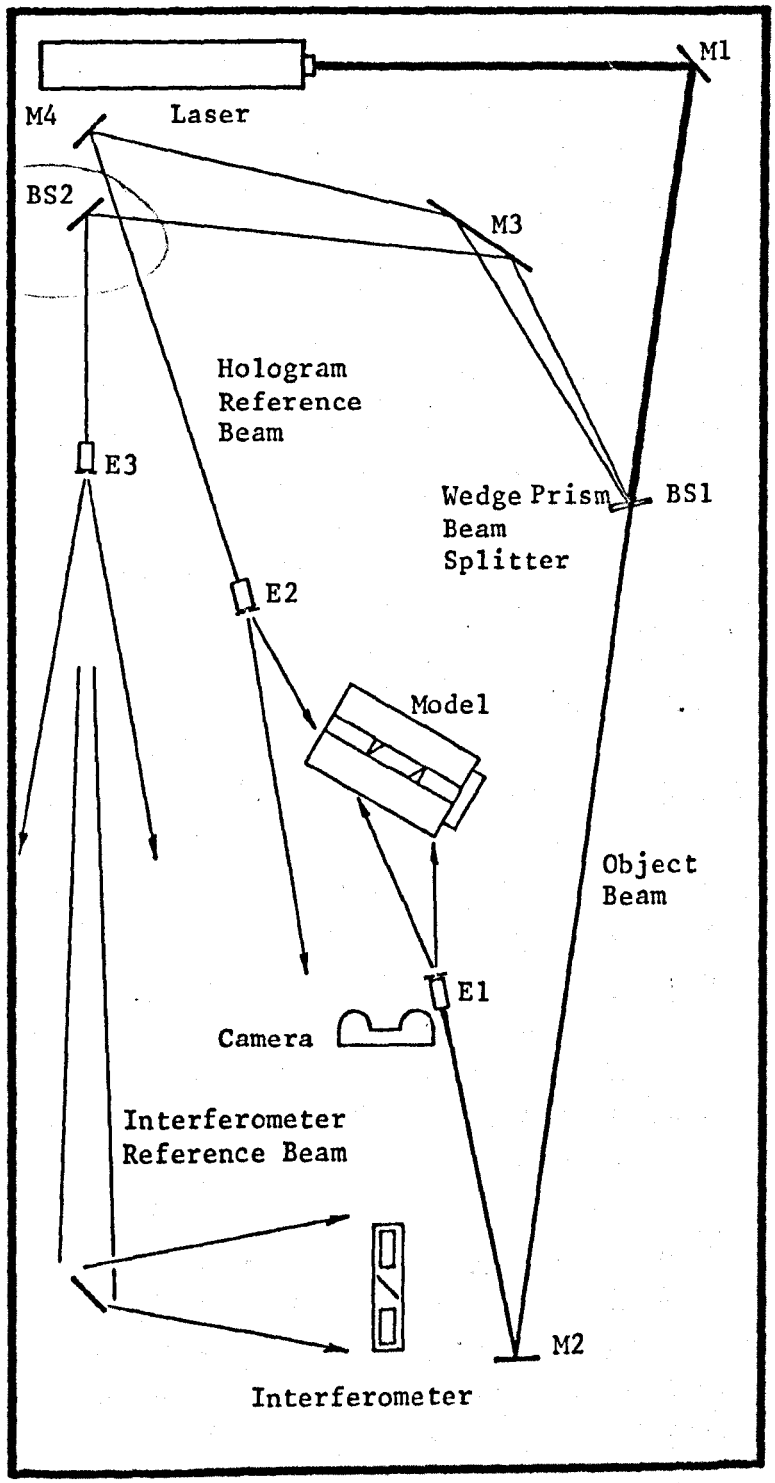

Key: Mn Total Reflector

BSn Beam Splitter

En Beam Expander

FIGURE 18 : Layout of Optical Table

FIGURE 19 : Layout of Optical Table

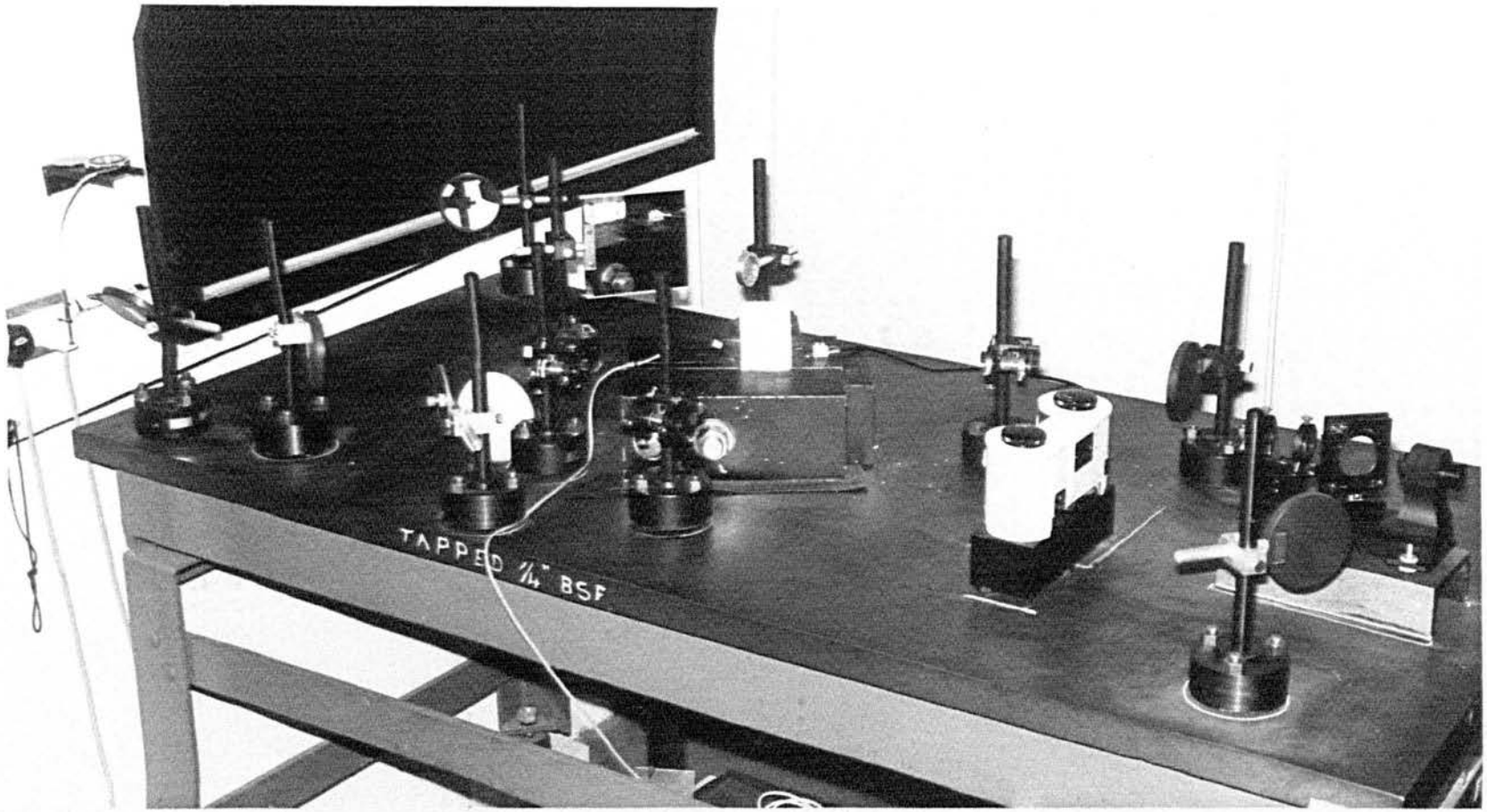
TAPPED ¼" BSF

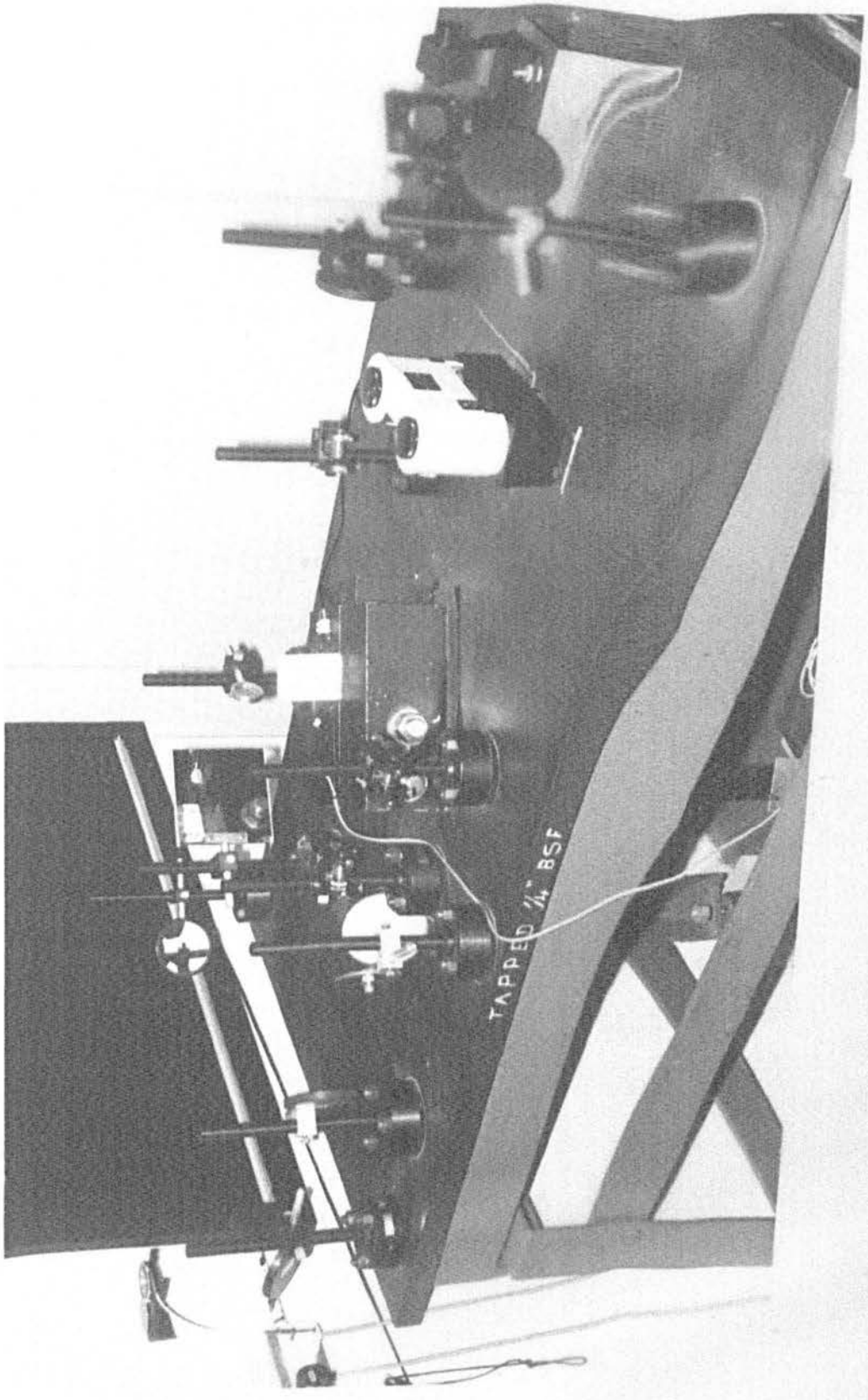

FIGURE 19 : Layout of Optical Table

FIGURE 20 : Modified Oscilloscope Camera

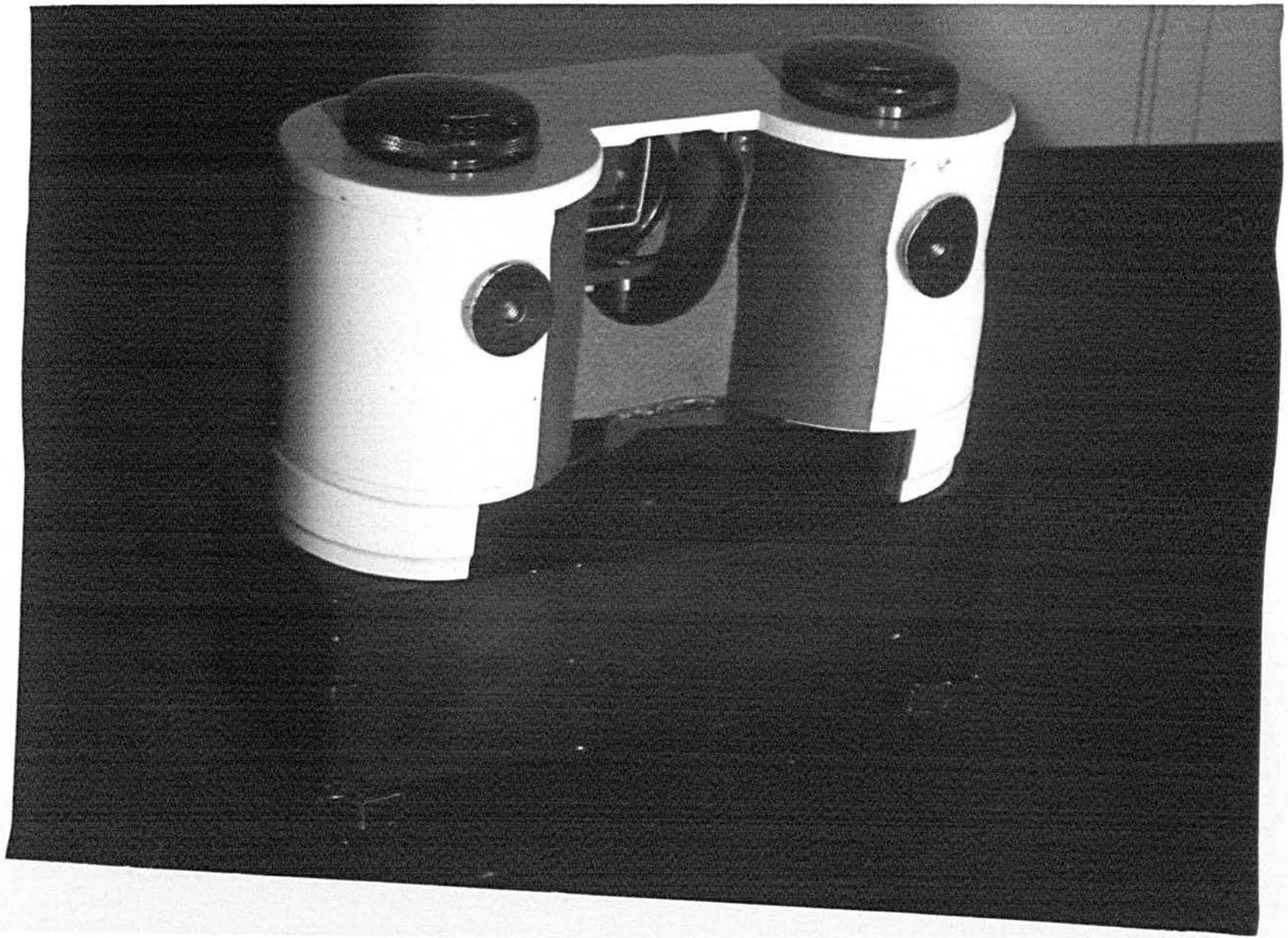

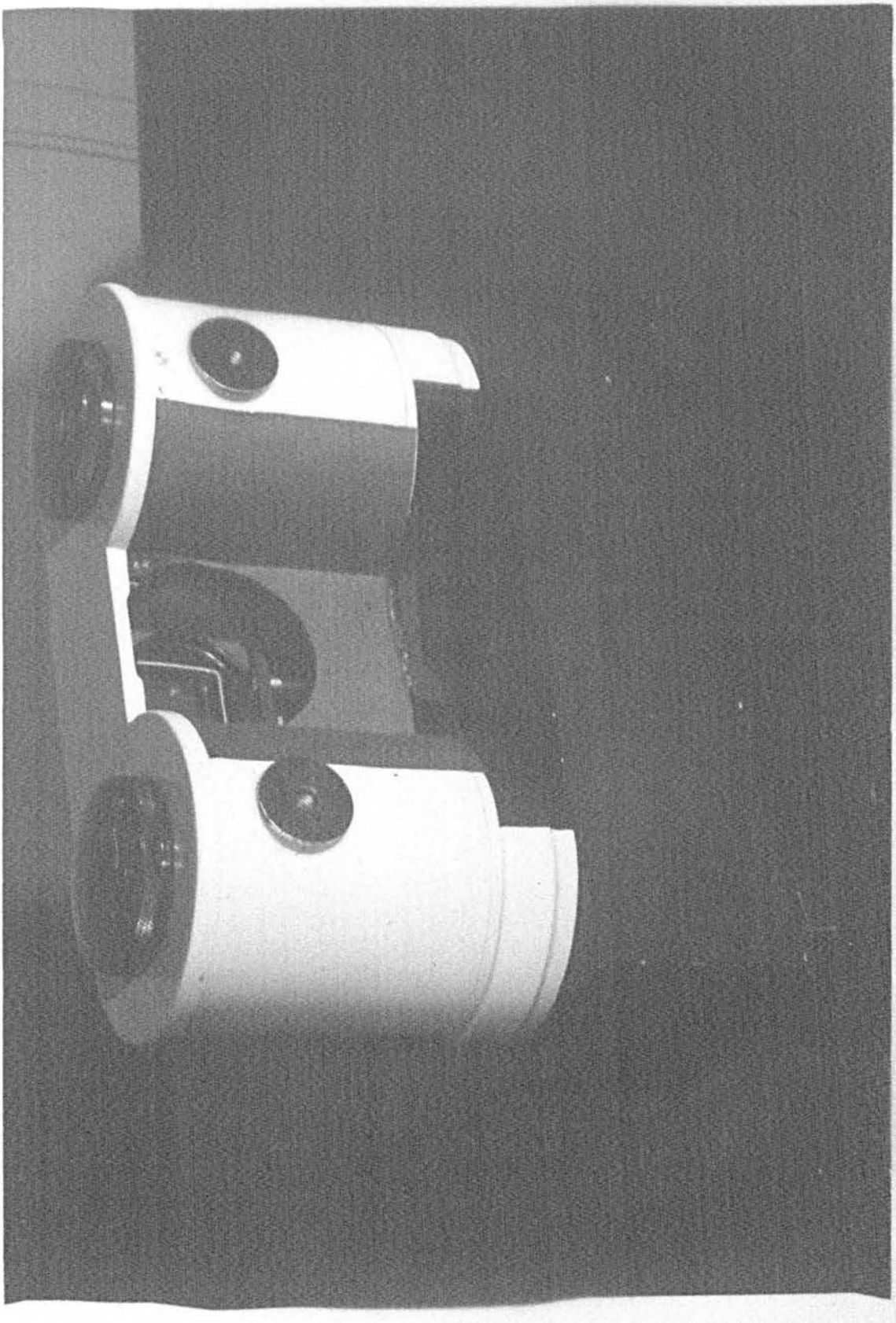

FIGURE 20 : Modified Oscilloscope Camera

FIGURE 21 : Photographic Plateholder for In-Situ Development of Real Time Holograms

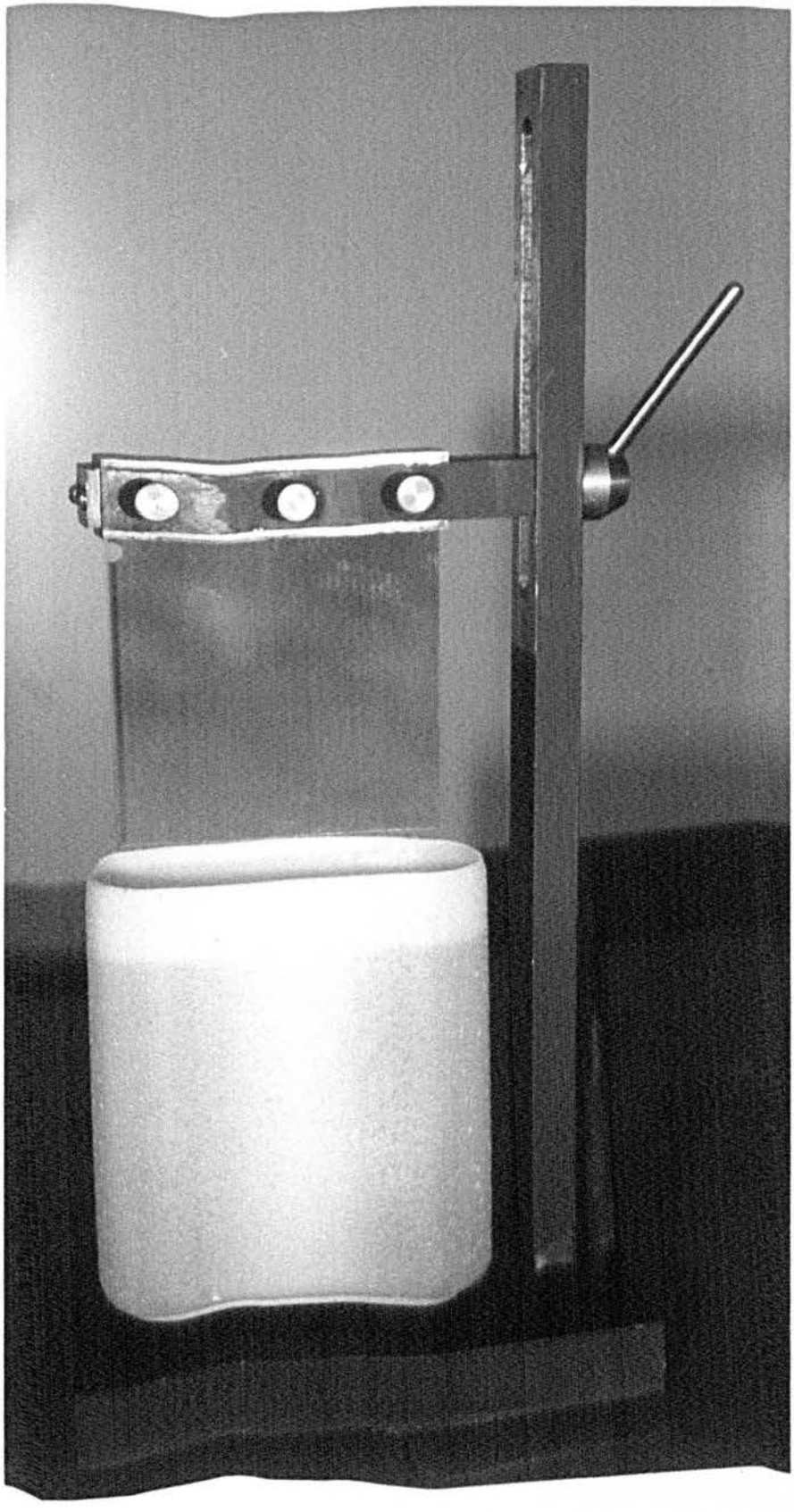

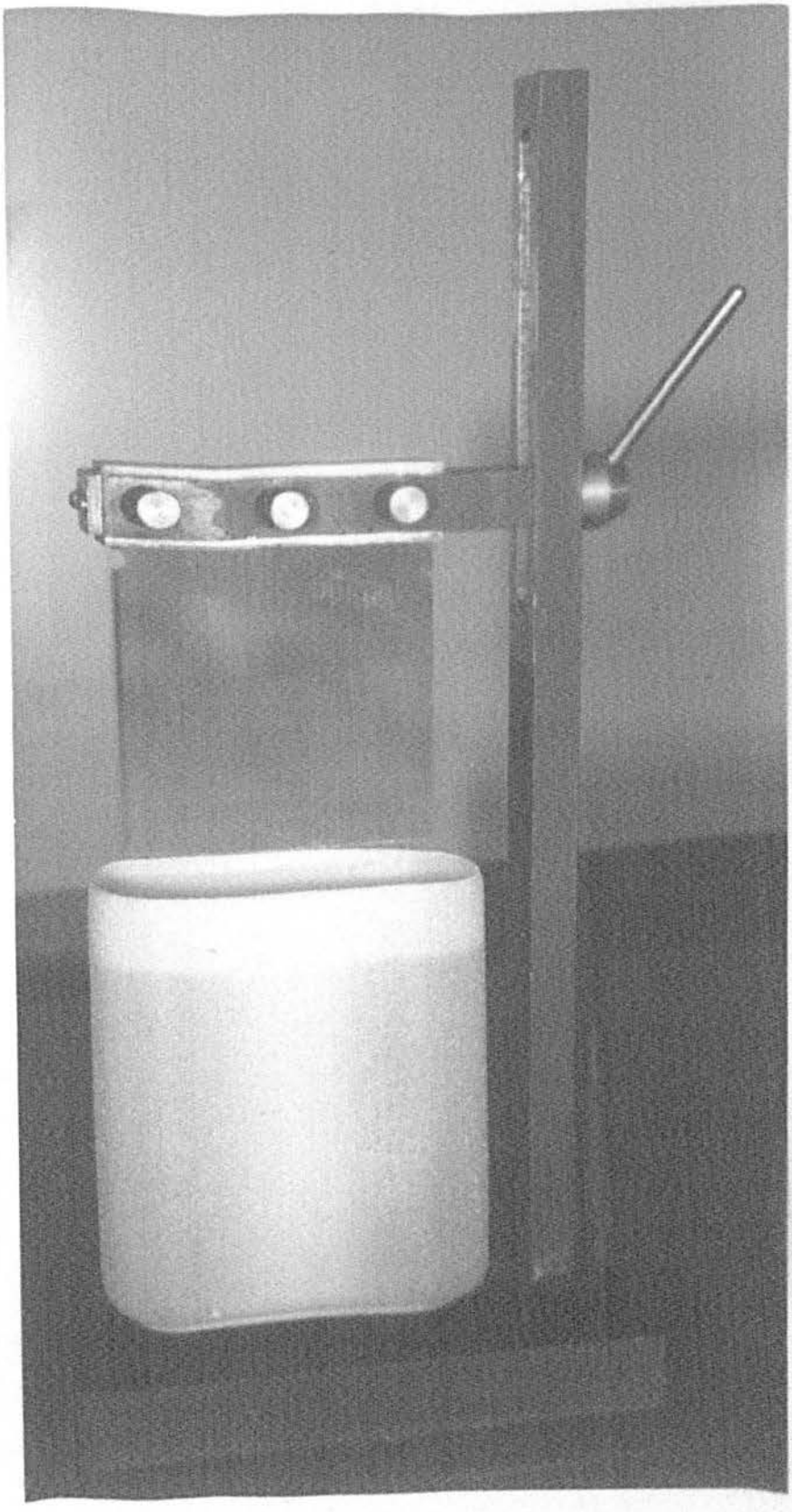

FIGURE 21 : Photographic Plateholder for In-Situ Development of Real Time Holograms

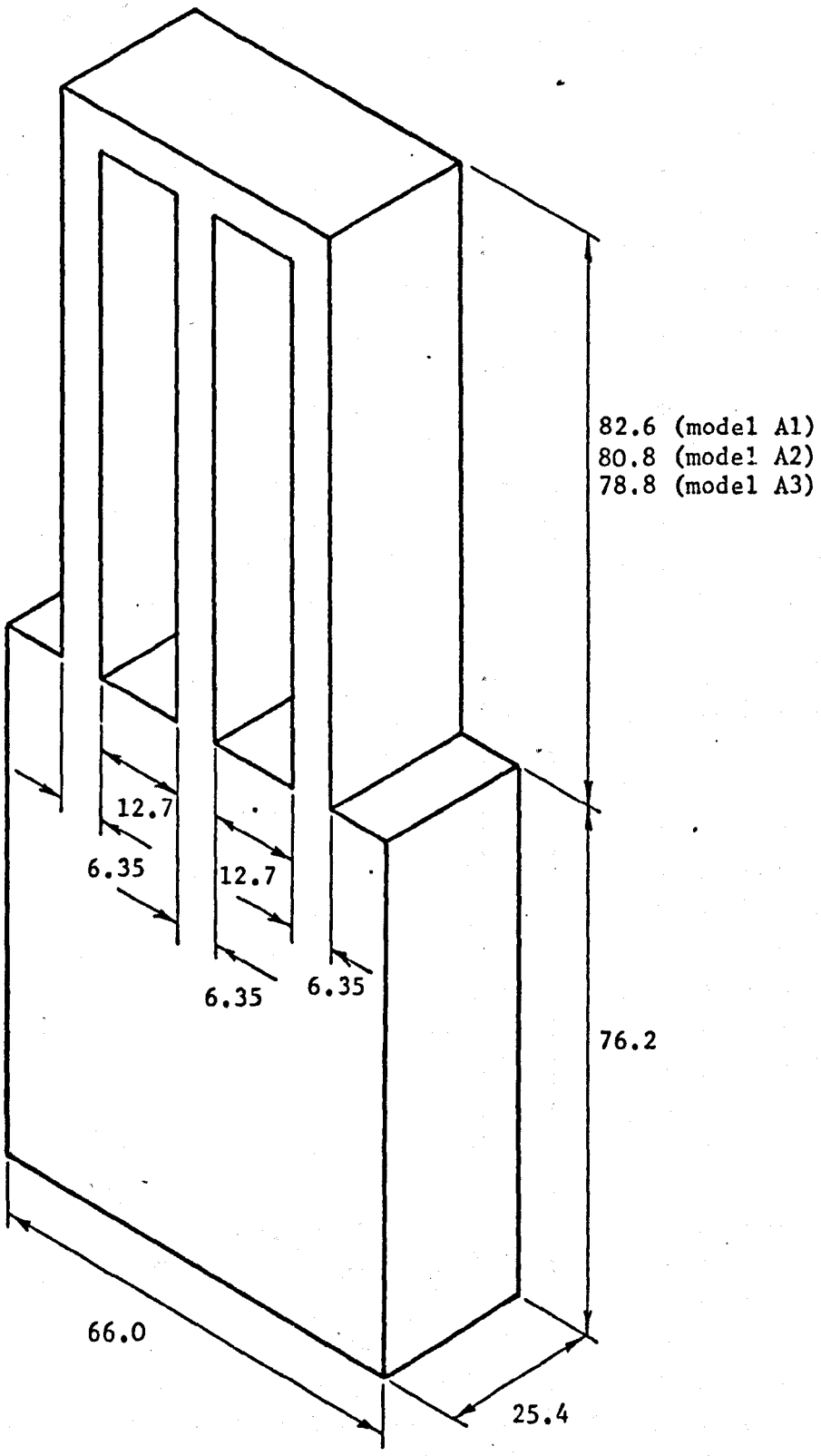

All dimensions in millimetres (tolerance ± 0.02)

Material: normalised bright mild steel

FIGURE 22 : Blade Package Model

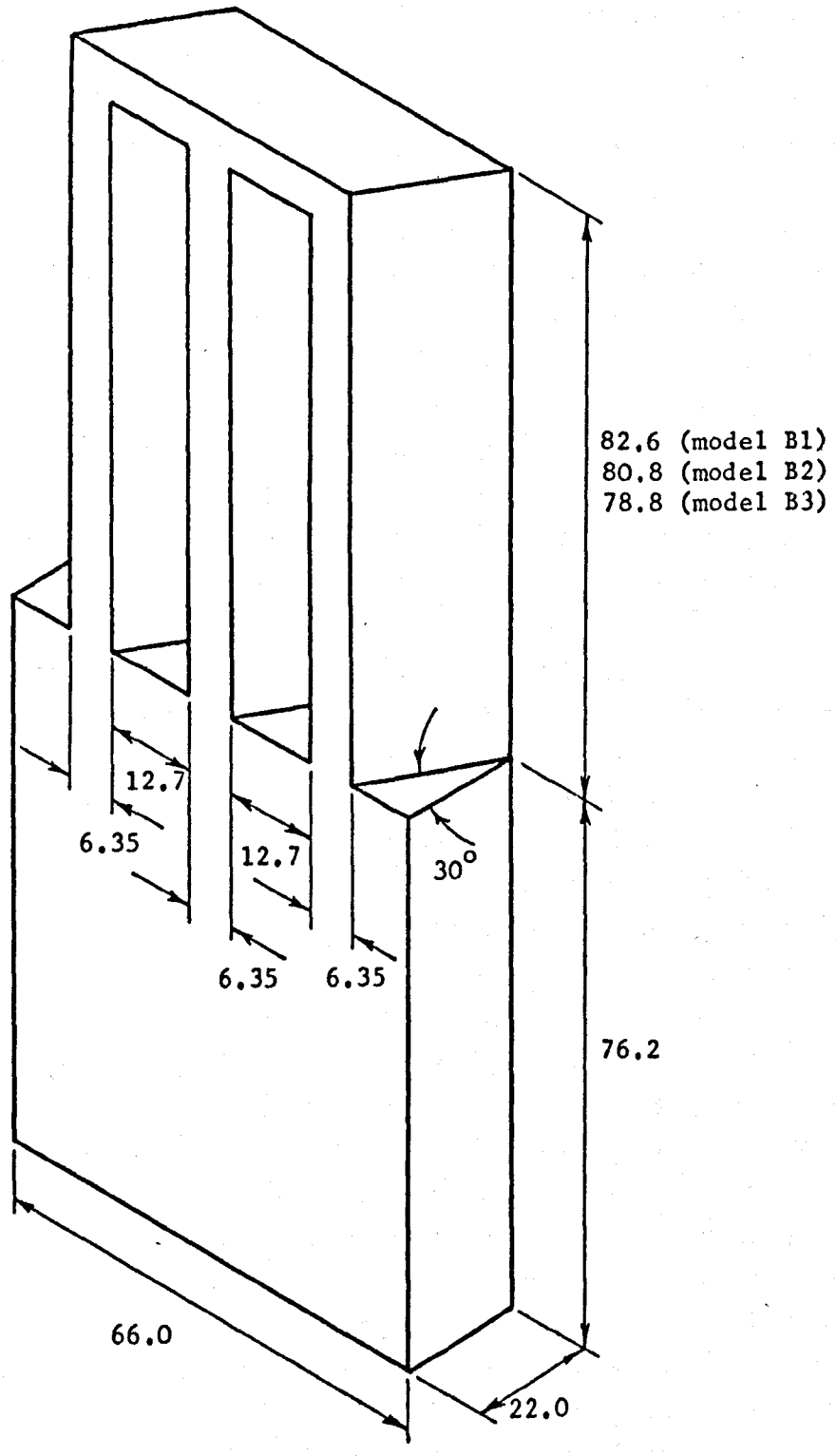

All dimensions in millimetres (tolerance ± 0.02)
Material: normalised bright mild steel

FIGURE 23 : Pretwisted Blade Package Model

FIGURE 24 : Clamp and Blade Package Model

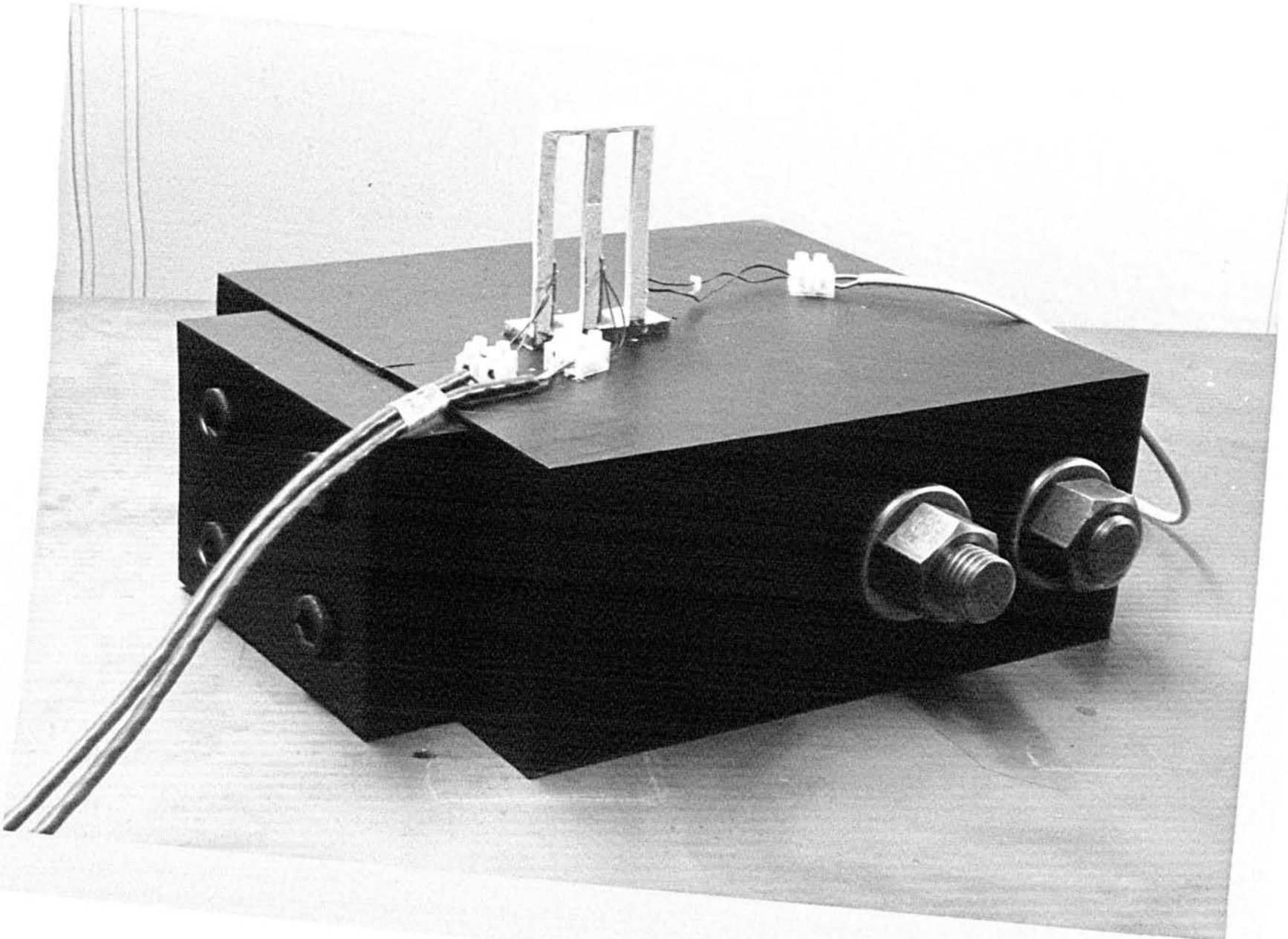

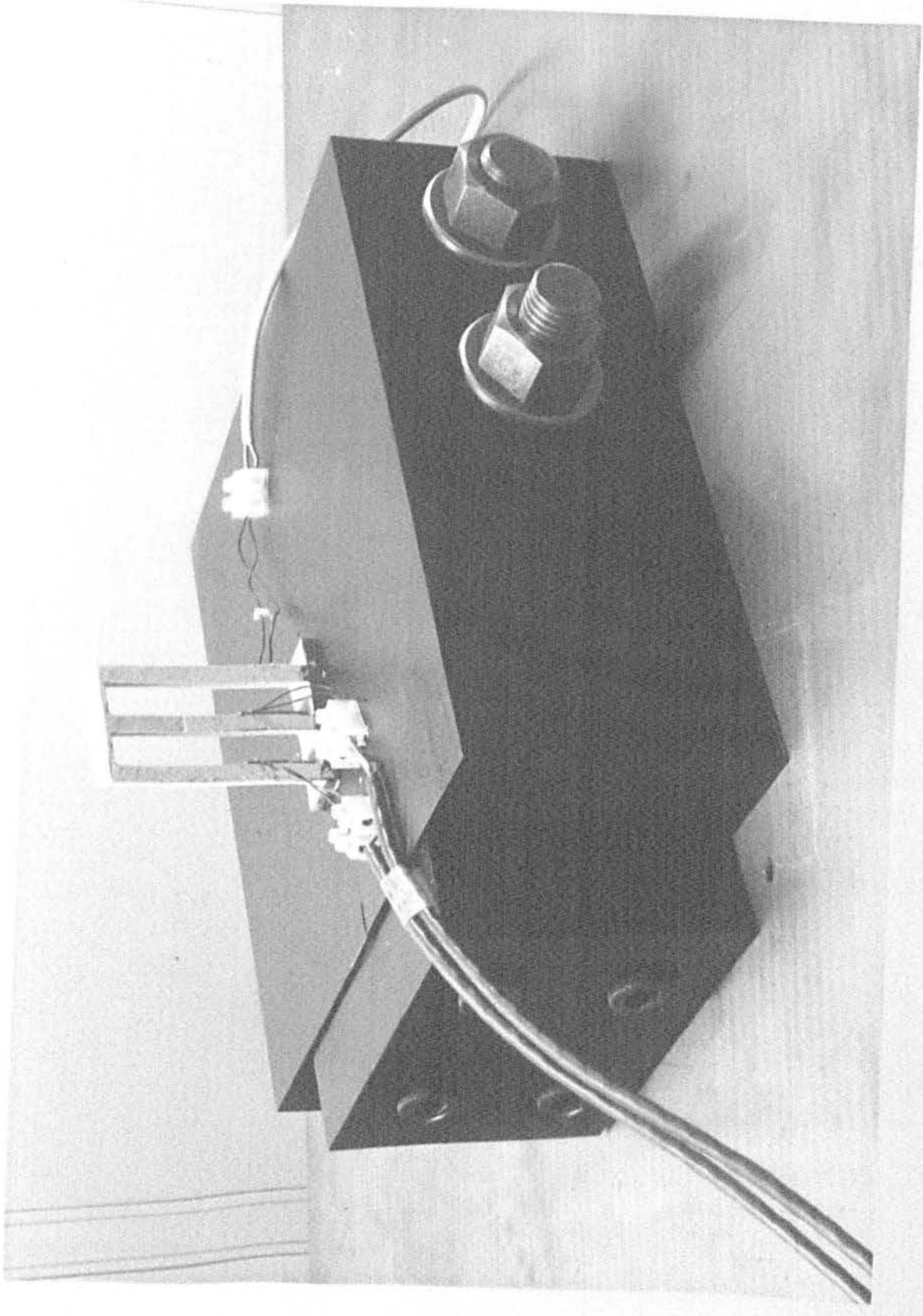

FIGURE 24 : Clamp and Blade Package Model

Predicted

1.104 kHz

First Detached Mode

Experimental

1.052 kHz

FIGURE 25 : Experimental and Predicted Modes

Model A3

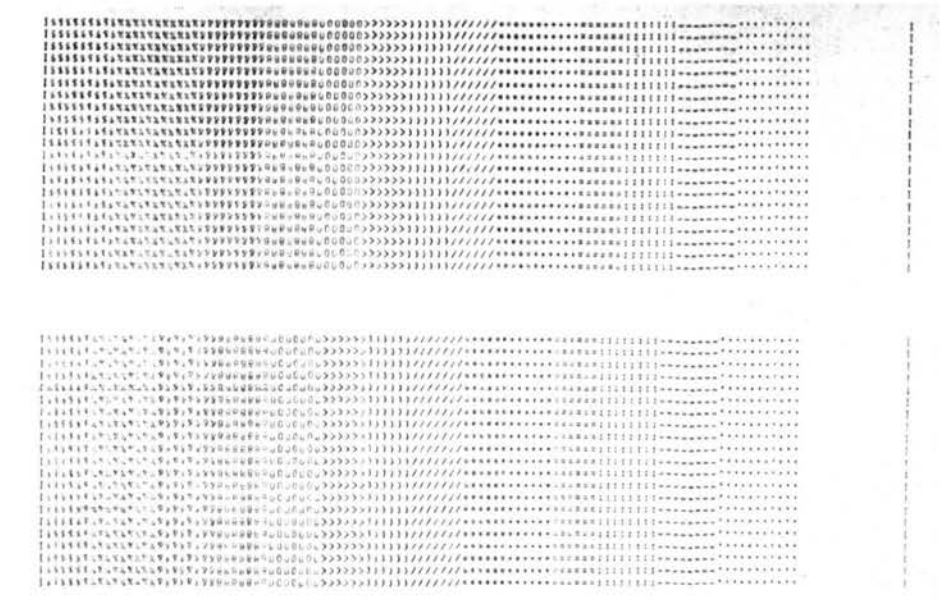

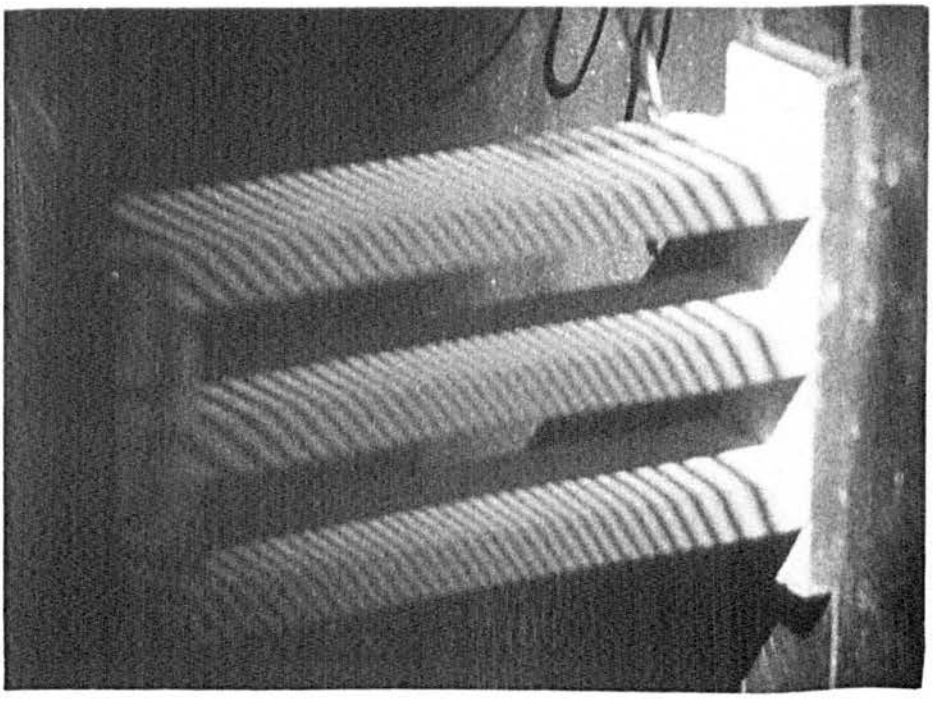

FIGURE 25 : Experimental and Predicted Modes

Model A3

Predicted

3.901 kHz

First Symmetric Batch Mode

Experimental

3.774 kHz

FIGURE 26 : Experimental and Predicted Modes

Model A3

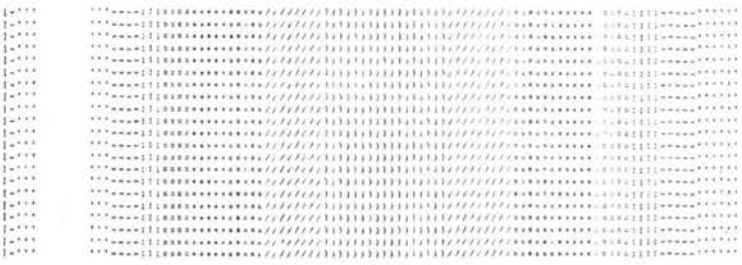

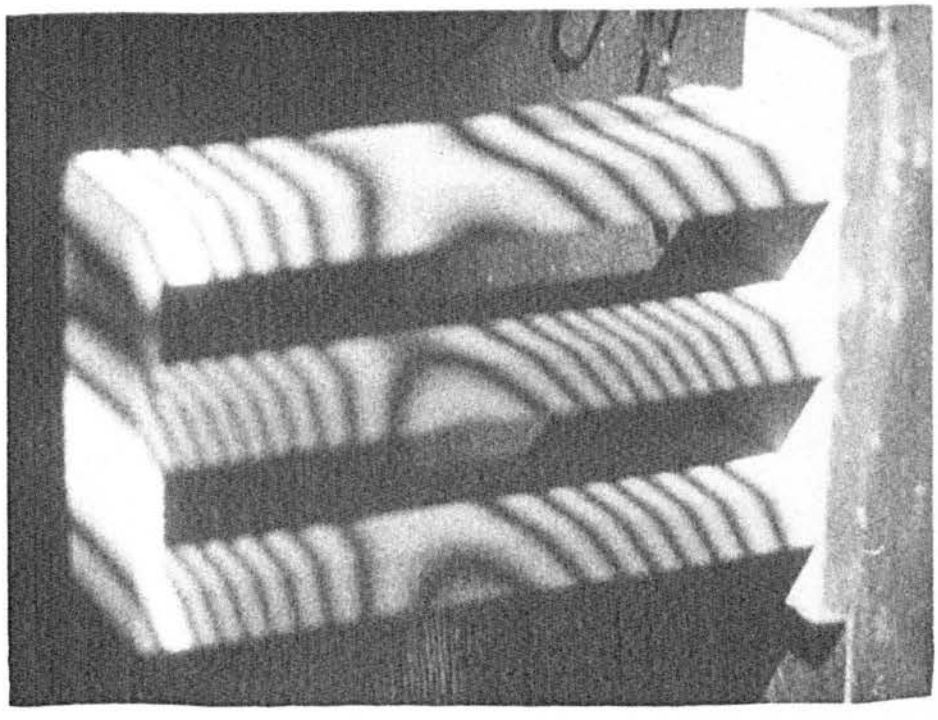

3.774 kHz Experimental 3.901 kHz Predicted

First Symmetric Batch Mode

FIGURE 26 : Experimental and Predicted Modes

Model A3

Predicted

4.024 kHz

First Antisymmetric Batch Mode

Experimental

3.838 kHz

FIGURE 27 : Experimental and Predicted Modes

Model A3

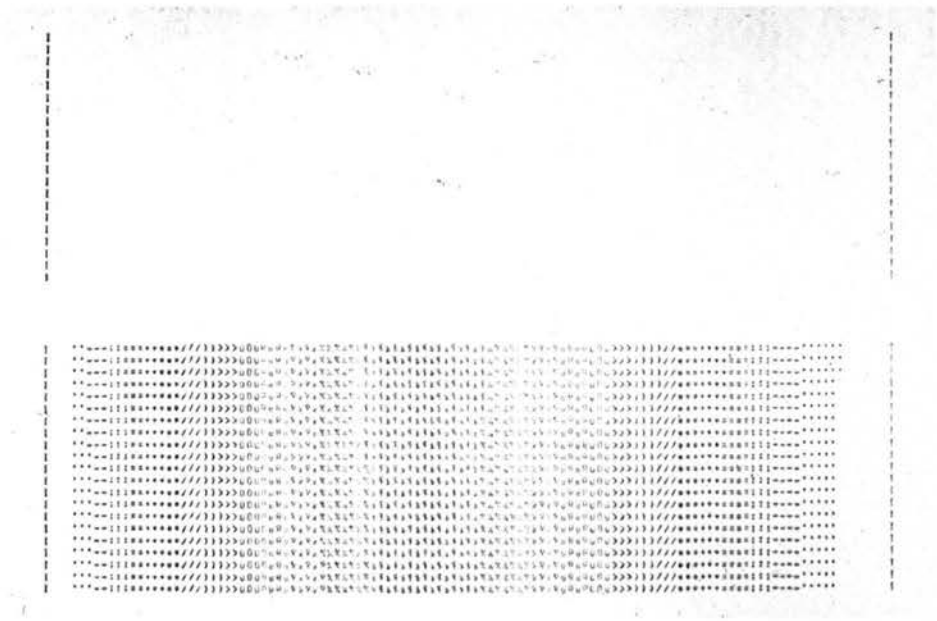

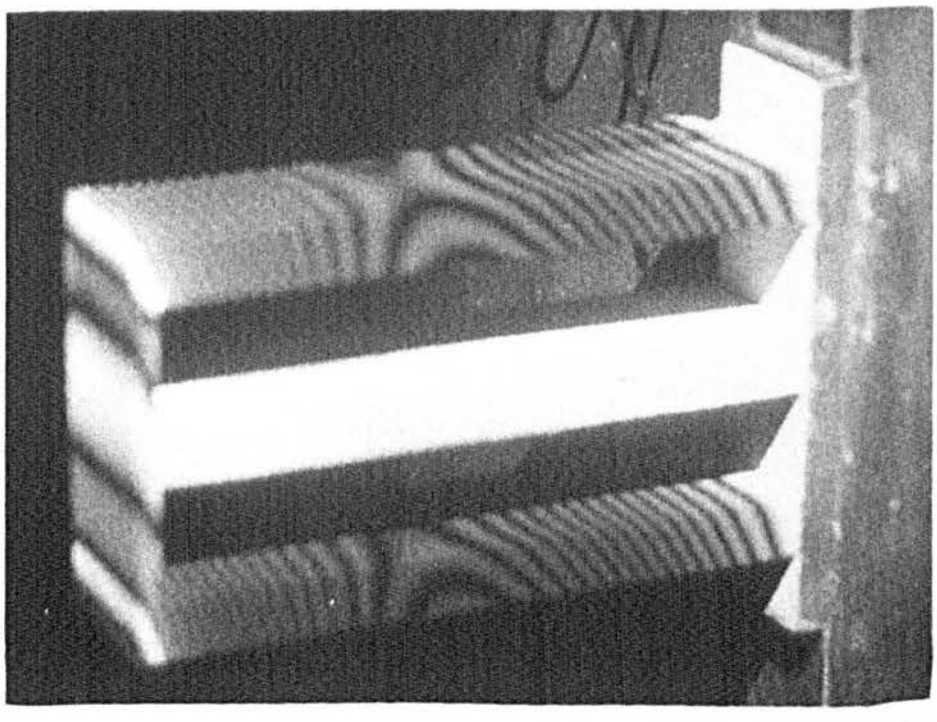

FIGURE 27 : Experimental and Predicted Modes

Model A3

Predicted

5.80 kHz

Second Detached Mode

Experimental

5.51 kHz

FIGURE 28 : Experimental and Predicted Modes

Model A3

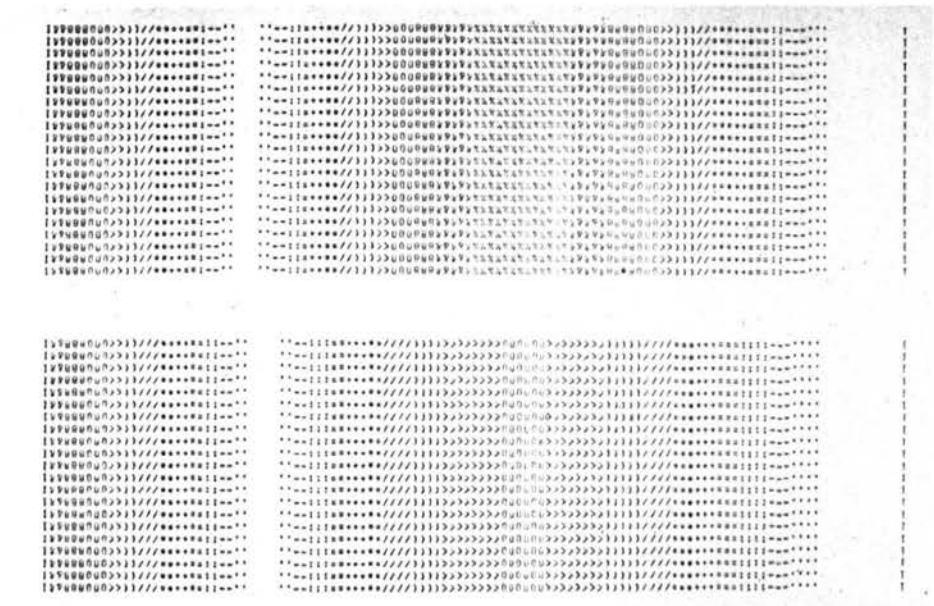

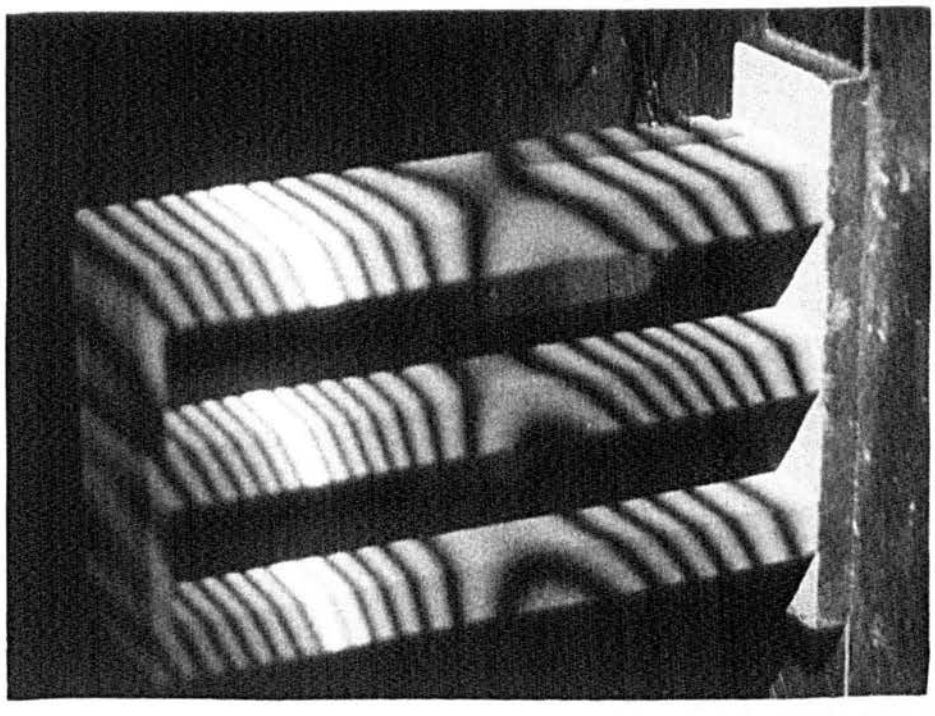

Second Detached Mode

5.80 kHz Predicted

5.51 kHz Experimental

FIGURE 28 : Experimental and Predicted Modes

Model A3

Predicted

11.47 kHz

Experimental

11.21 kHz

FIGURE 29 : Experimental and Predicted Modes

Model A3

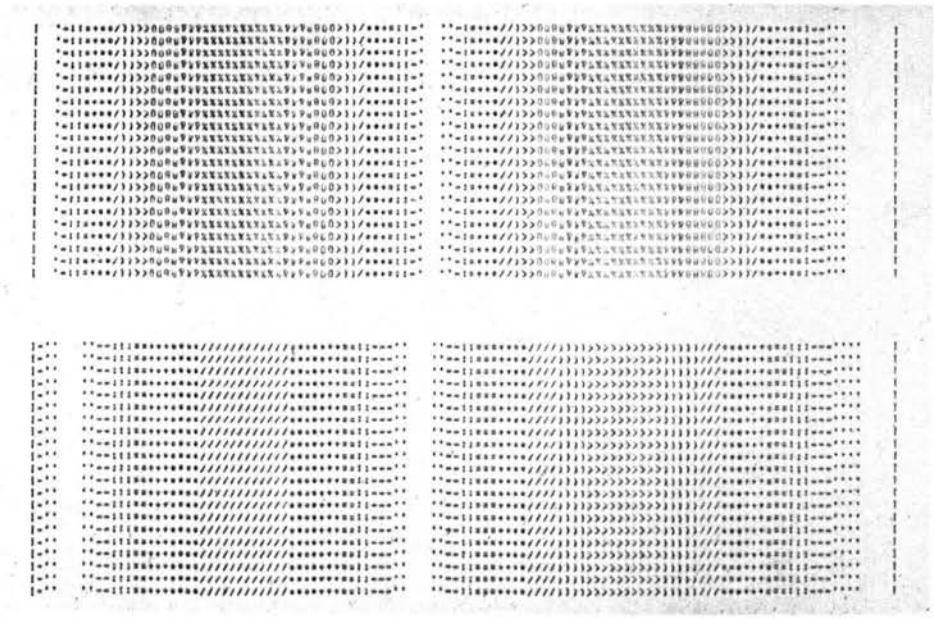

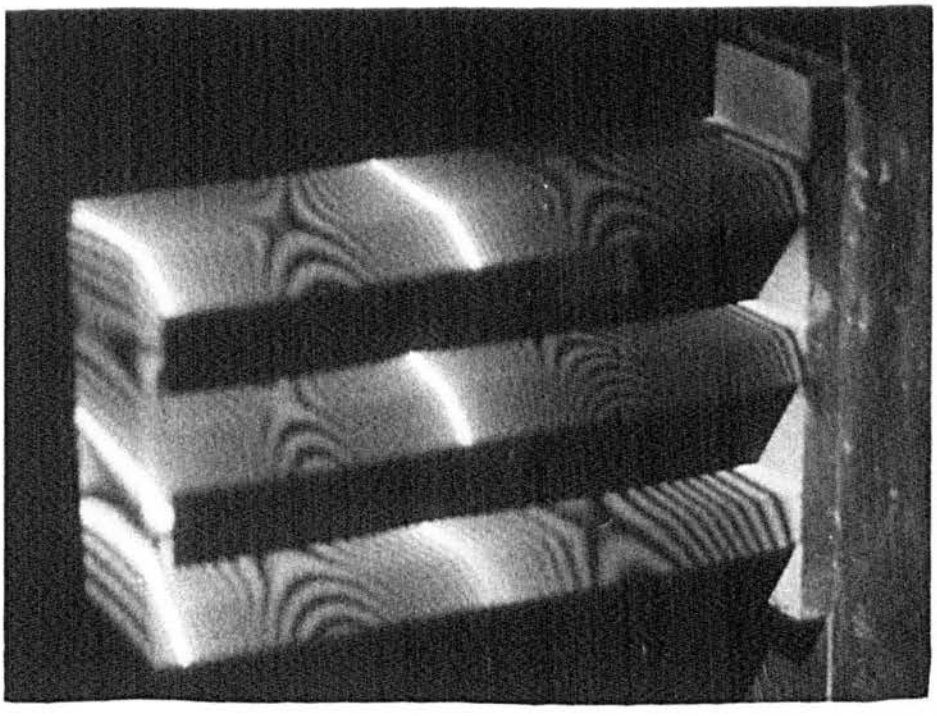

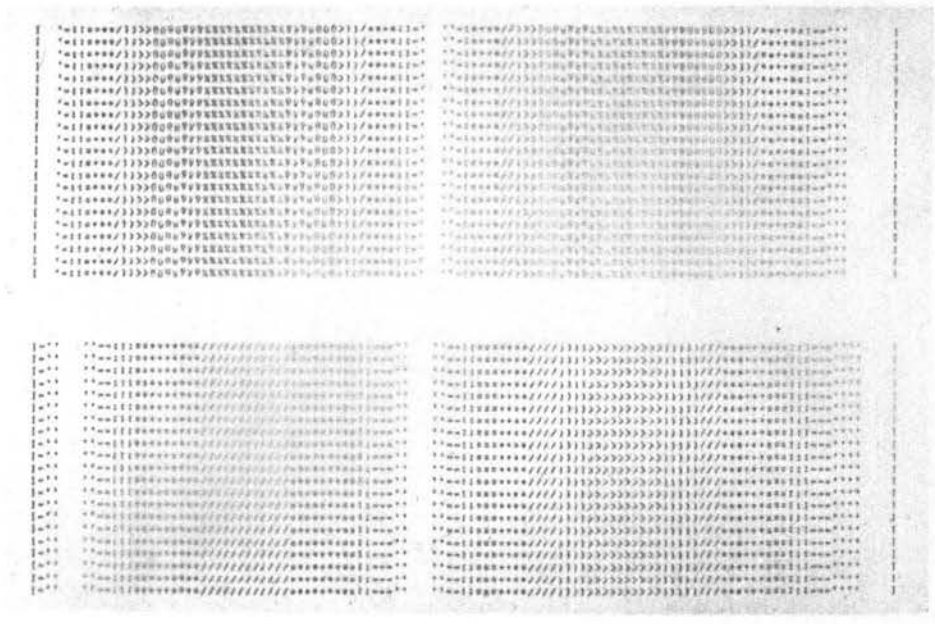

Predicted

11.47 kHz

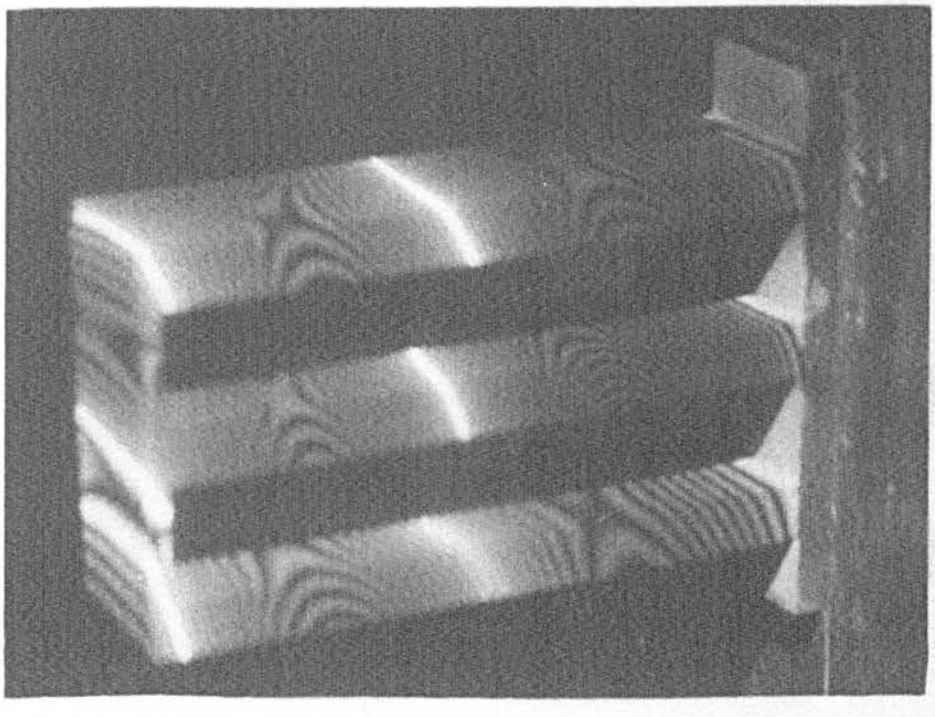

Experimental

11.21 kHz

FIGURE 29 : Experimental and Predicted Modes

Model A3

Predicted

11.51 kHz

Second Antisymmetric Batch Mode

Experimental

11.07 kHz

FIGURE 30 : Experimental and Predicted Modes

Model A3

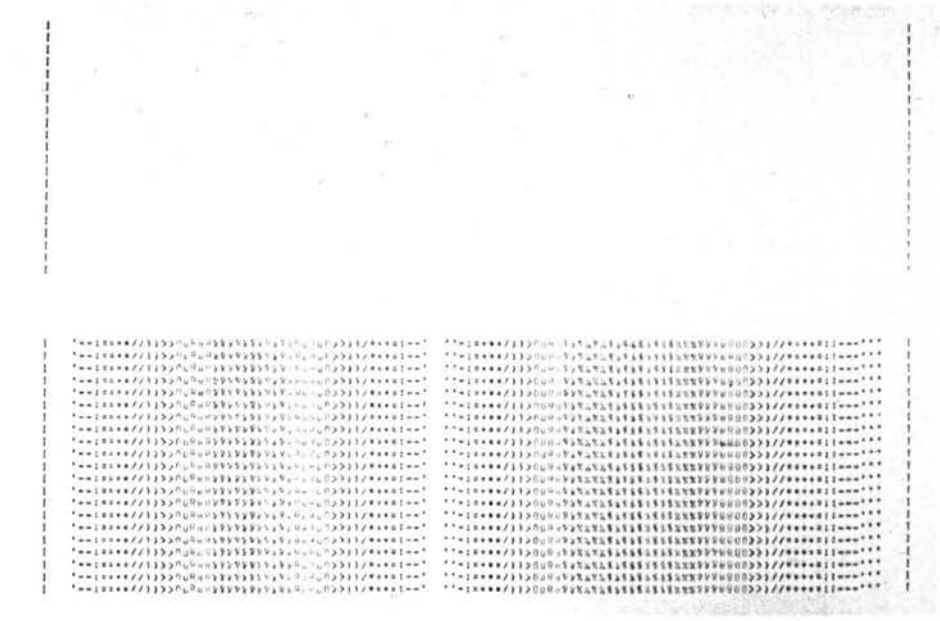

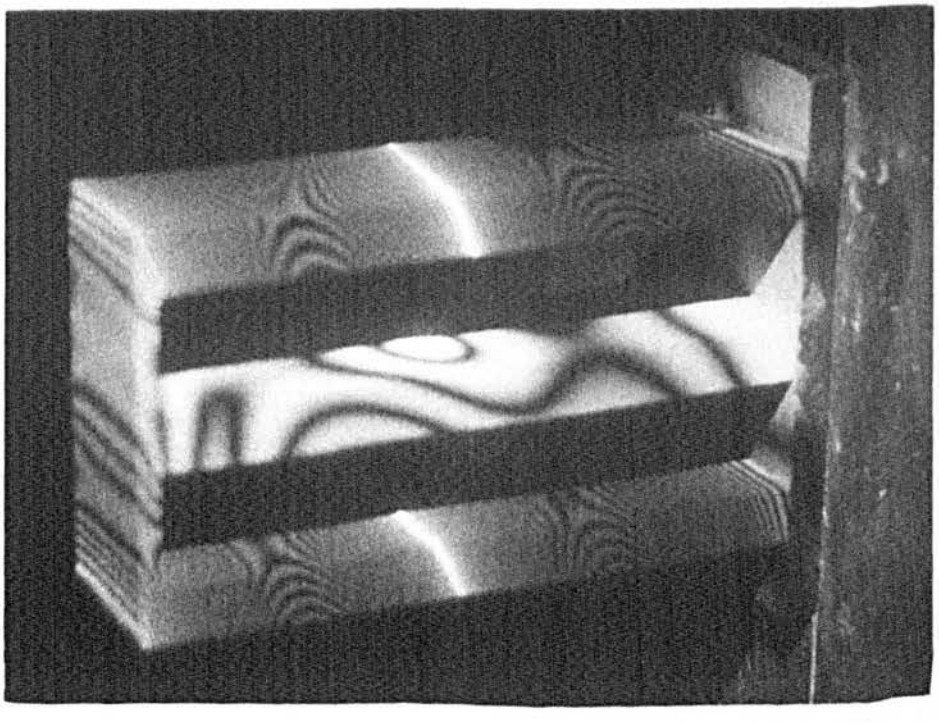

FIGURE 30 : Experimental and Predicted Modes

Model A3

2.260 kHz Experimental 2.834 kHz Predicted (modal shape not shown)

First Edgewise Mode

FIGURE 31 : Experimental and Predicted Modes

Model A3

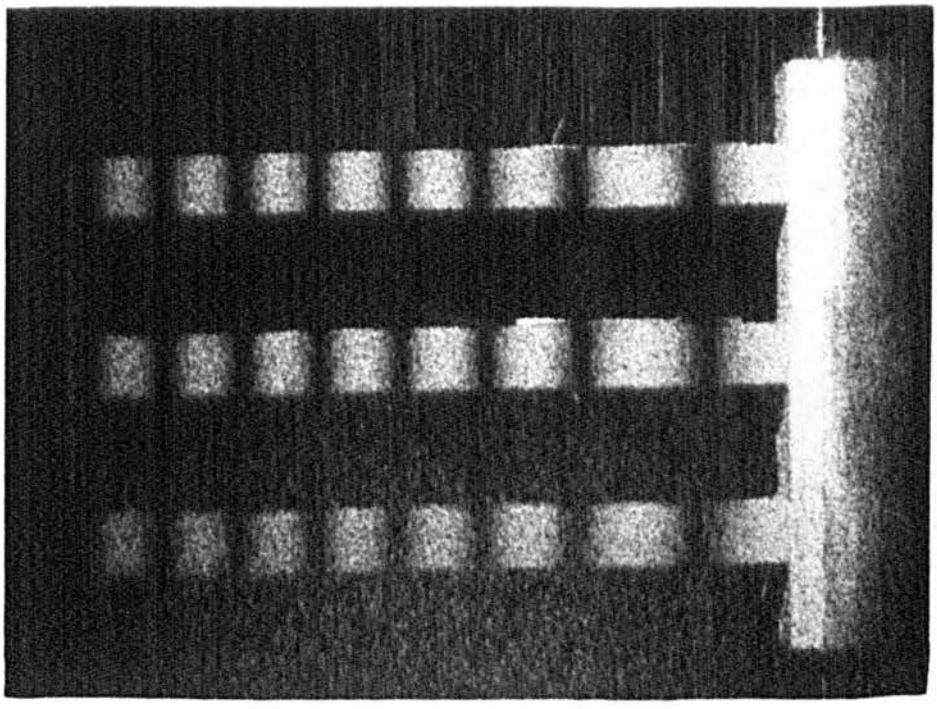

2.260 kHz Experimental 2.834 kHz Predicted (modal shape not shown)

First Edgewise Mode

FIGURE 31 : Experimental and Predicted Modes

Model A3

Predicted

3.481 kHz

First Torsional Mode

Experimental

3.071 kHz

FIGURE 32 : Experimental and Predicted Modes

Model A3

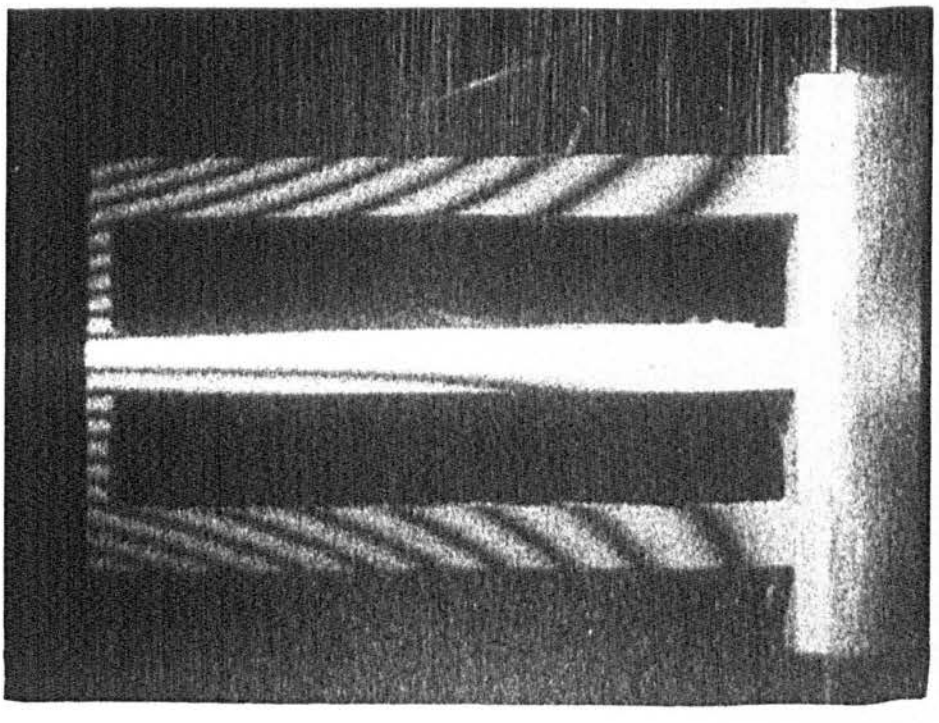

FIGURE 32 : Experimental and Predicted Modes

Model A3

Predicted

1.086 kHz

First Detached Mode

Experimental

1.105 kHz

FIGURE 33 : Experimental and Predicted Modes

Model B3

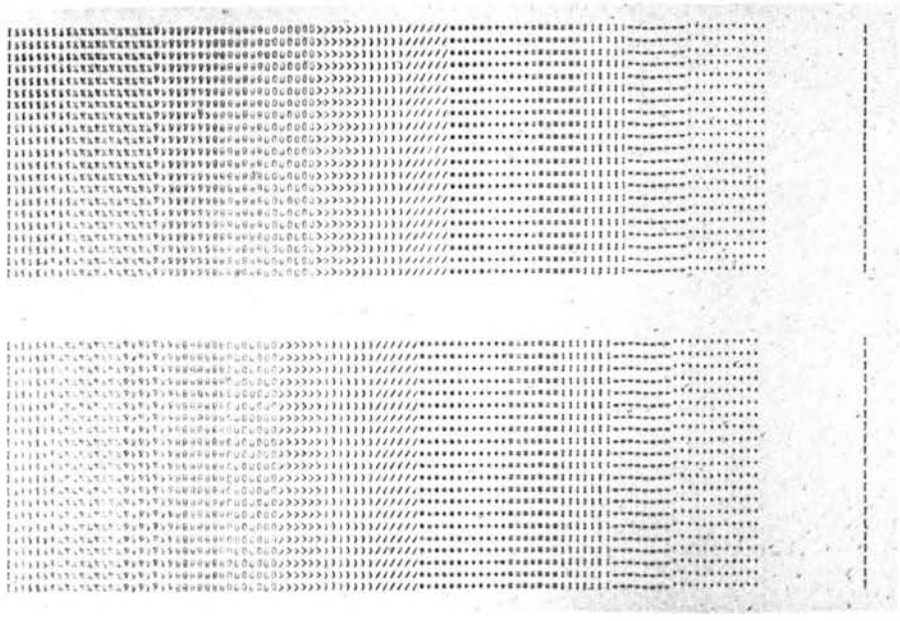

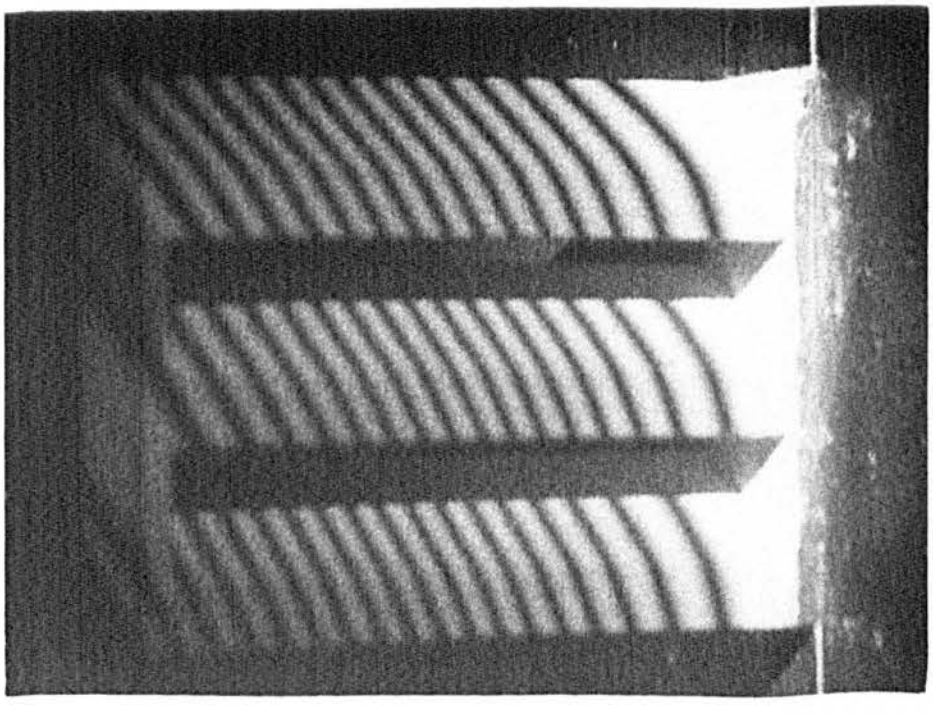

FIGURE 33 : Experimental and Predicted Modes

Model B3

Predicted

3.915 kHz

First Symmetric Batch Mode

Experimental

3.696 kHz

FIGURE 34 : Experimental and Predicted Modes

Model B3

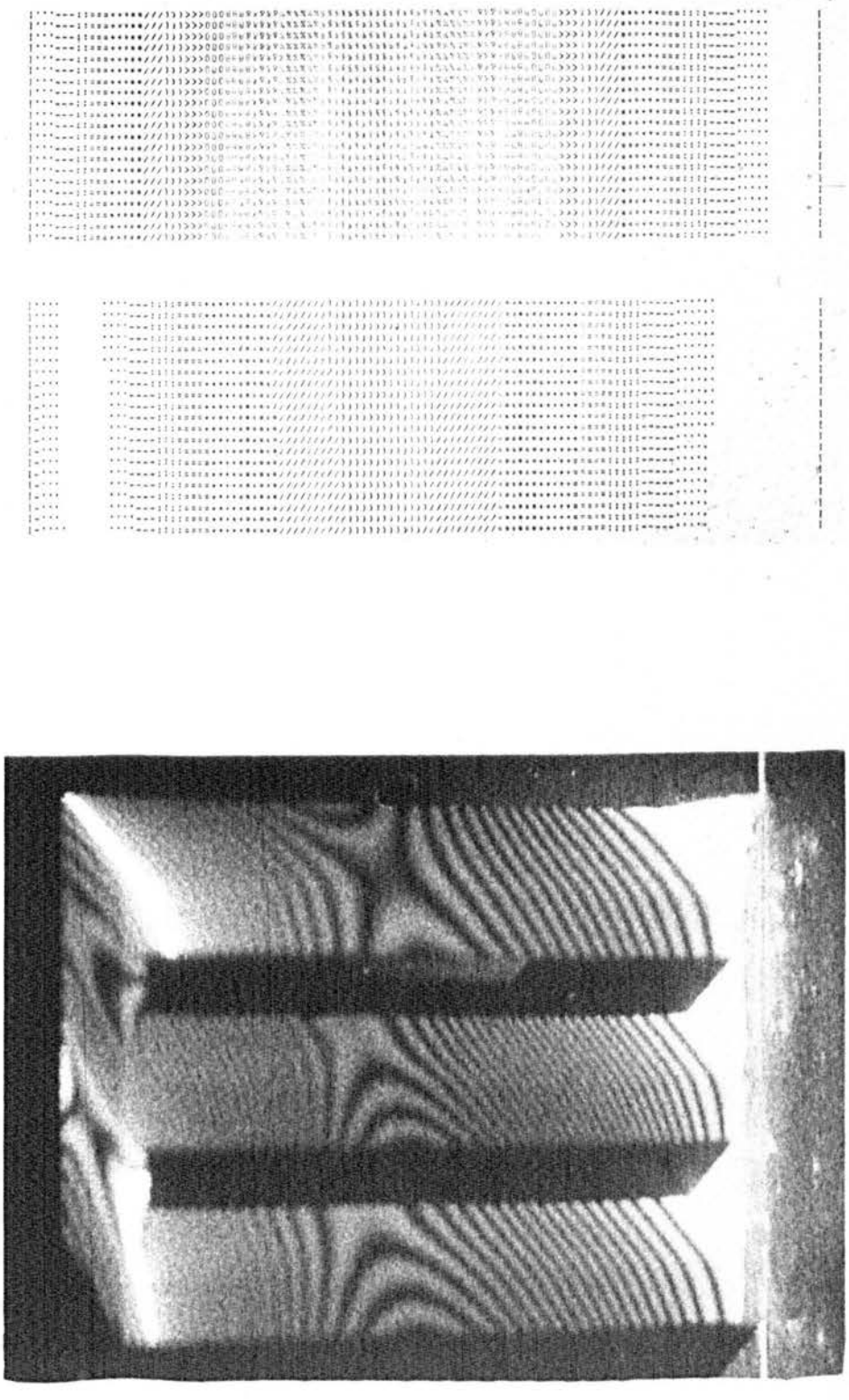

FIGURE 34 : Experimental and Predicted Modes

Model B3

Predicted

4.380 kHz

First Antisymmetric Batch Mode

Experimental

4.135 kHz

FIGURE 35 : Experimental and Predicted Modes

Model B3

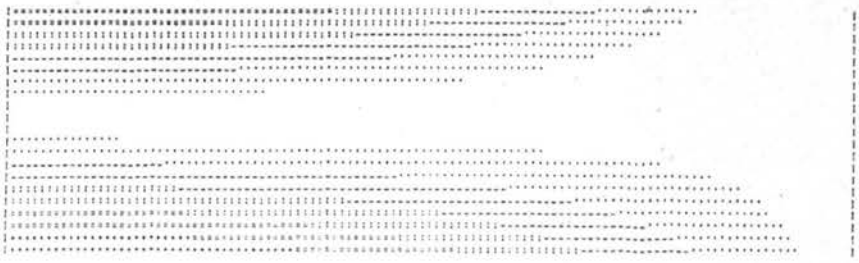

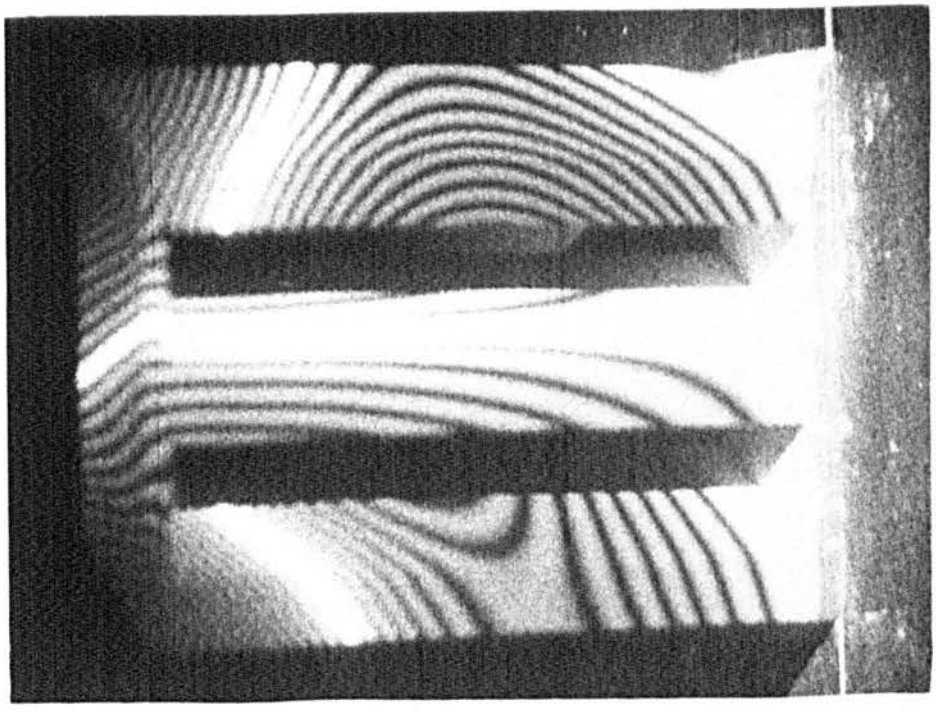

FIGURE 35 : Experimental and Predicted Modes

Model B3

Predicted

5.725 kHz

Second Detached Mode

Experimental

5.280 kHz

FIGURE 36 : Experimental and Predicted Modes

Model B3

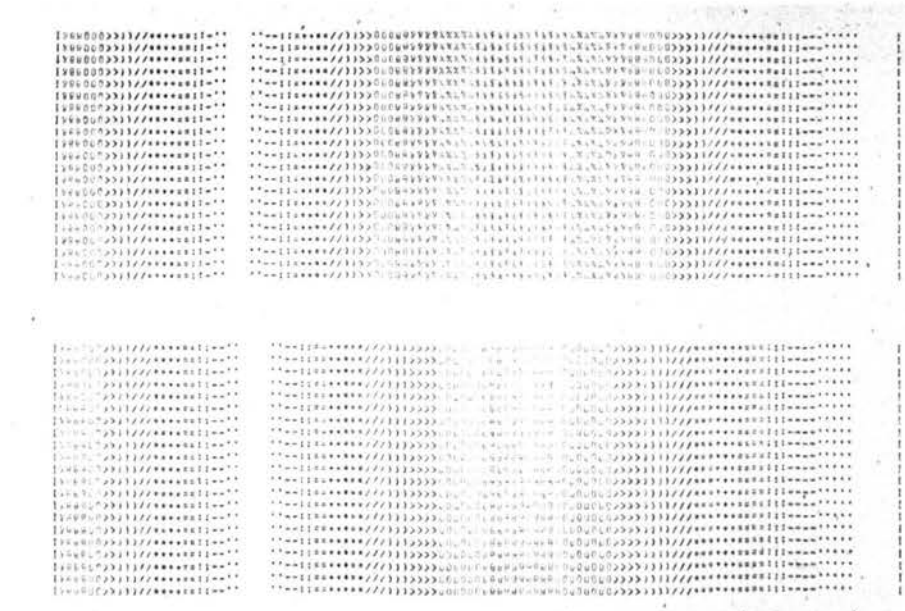

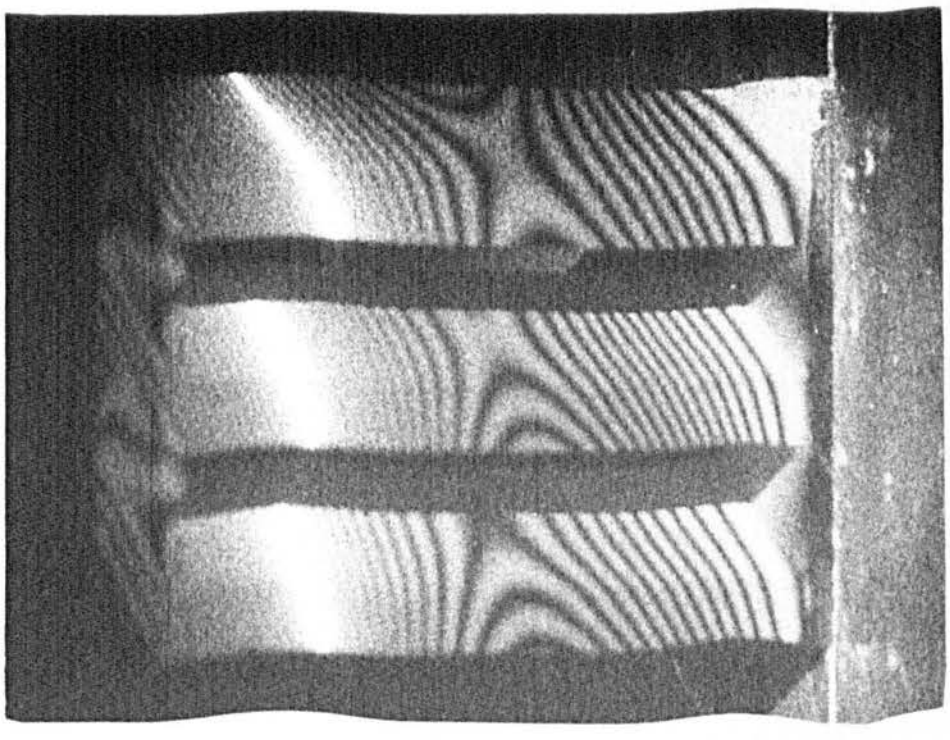

FIGURE 36 : Experimental and Predicted Modes

Model B3

Predicted

11.47 kHz

Second Symmetric Batch Mode

Experimental

10.91 kHz

FIGURE 37 : Experimental and Predicted Modes

Model B3

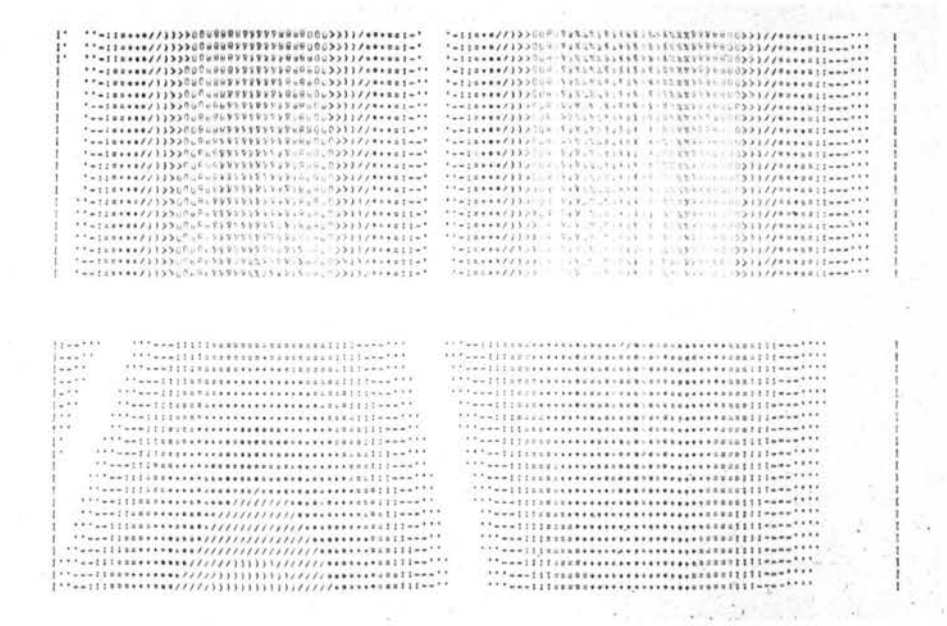

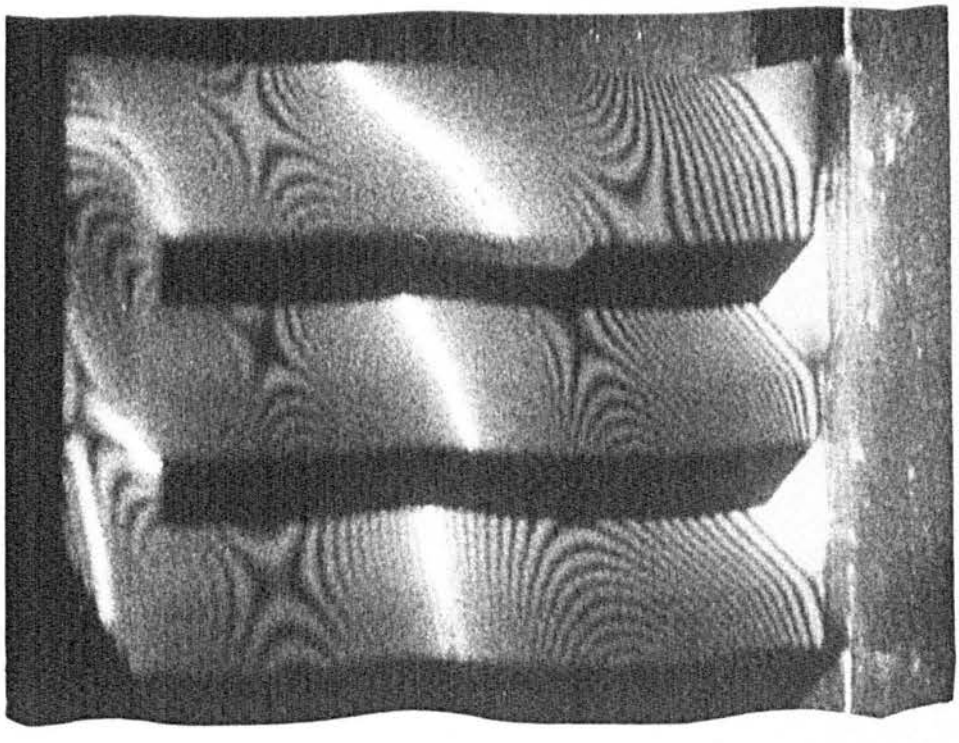

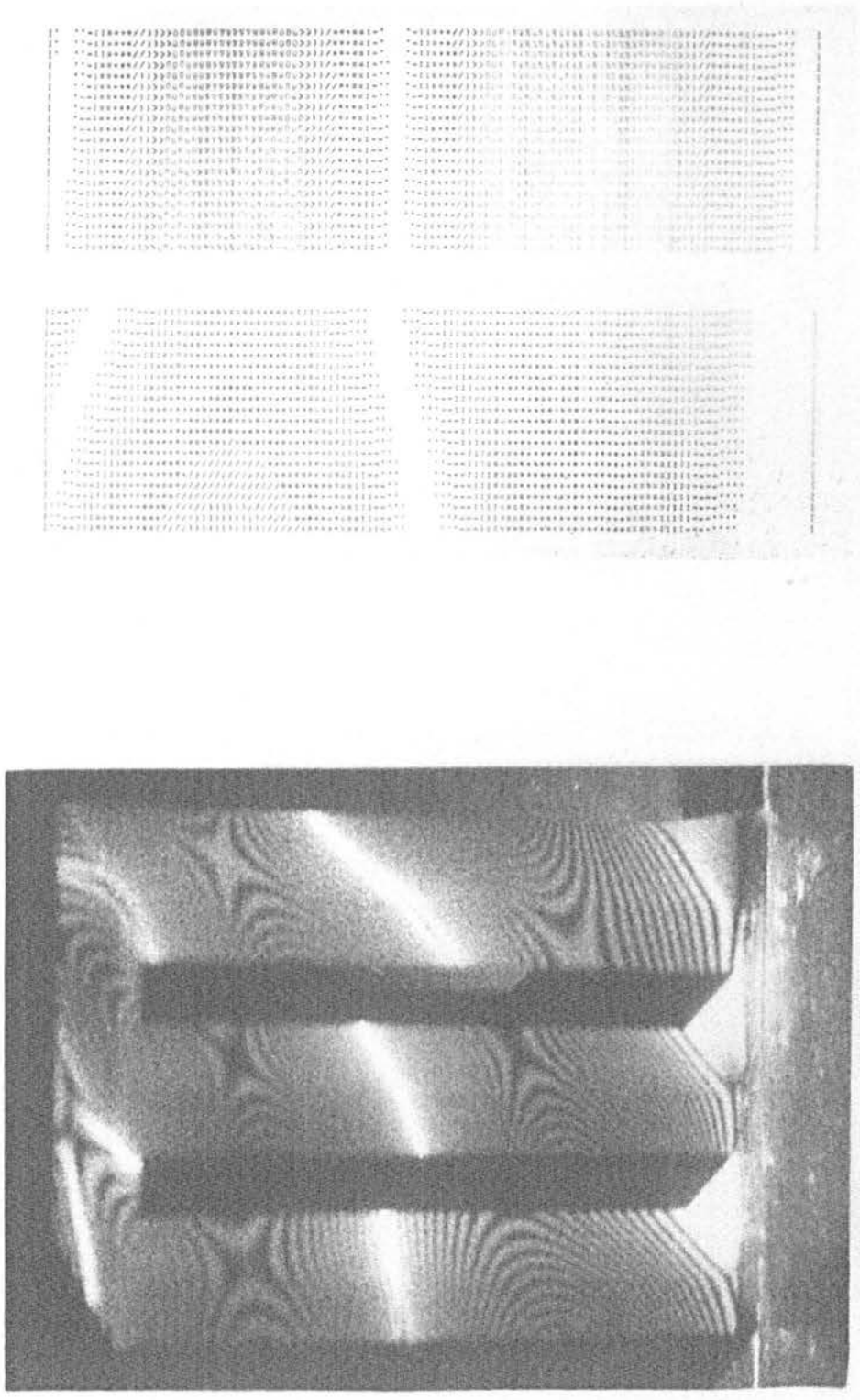

FIGURE 37 : Experimental and Predicted Modes

Model B3

Predicted

11.40 kHz

Second Antisymmetric Batch Mode

Experimental

10.44 kHz

FIGURE 38 : Experimental and Predicted Mode Shapes

Model B3

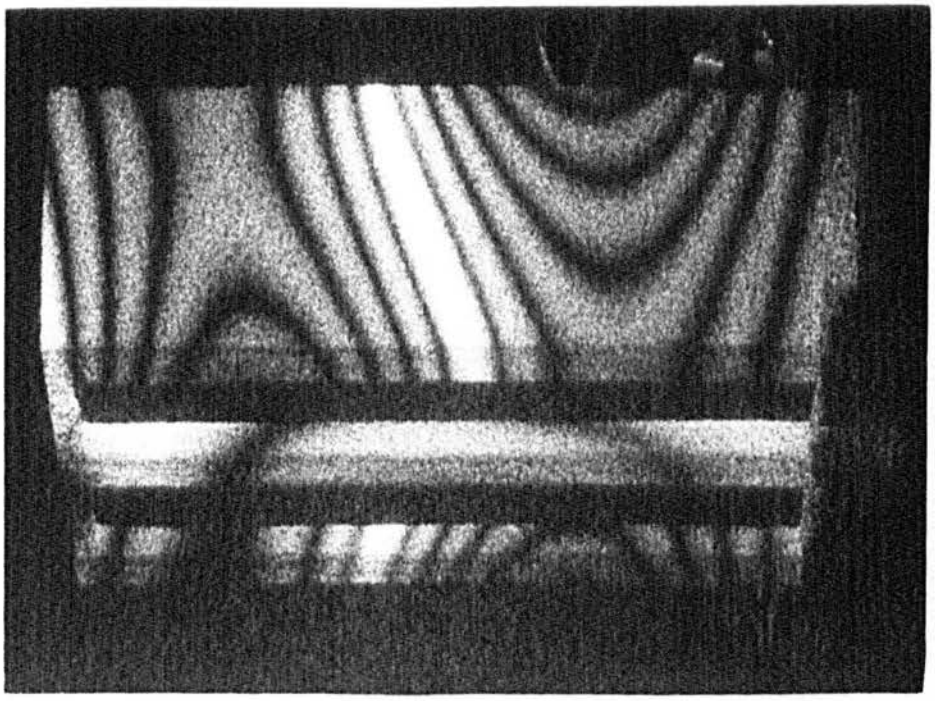

FIGURE 38 : Experimental and Predicted Mode Shapes

Model B3

Predicted

3.108 kHz

First Torsional Mode

Experimental

2.671 kHz

FIGURE 39 : Experimental and Predicted Mode Shapes

Model B3

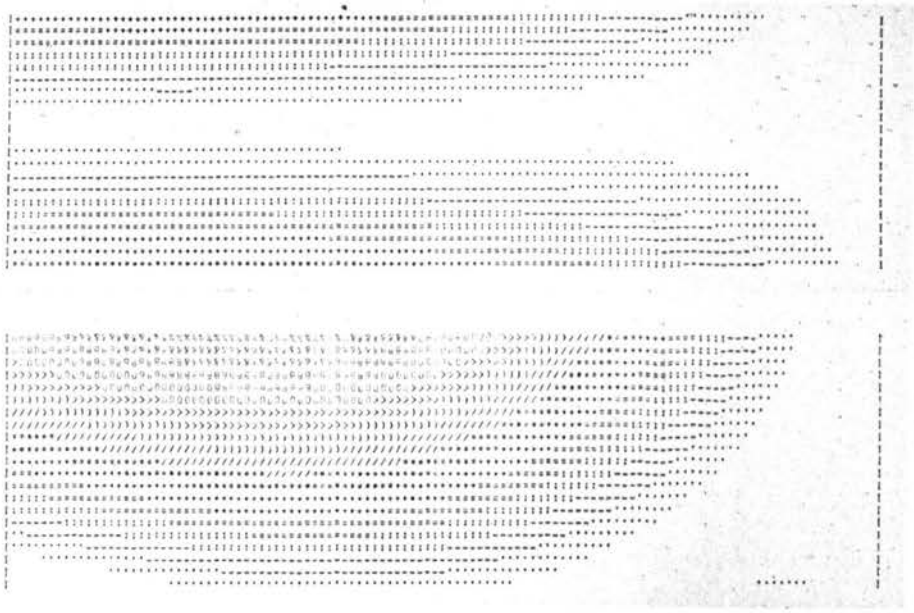

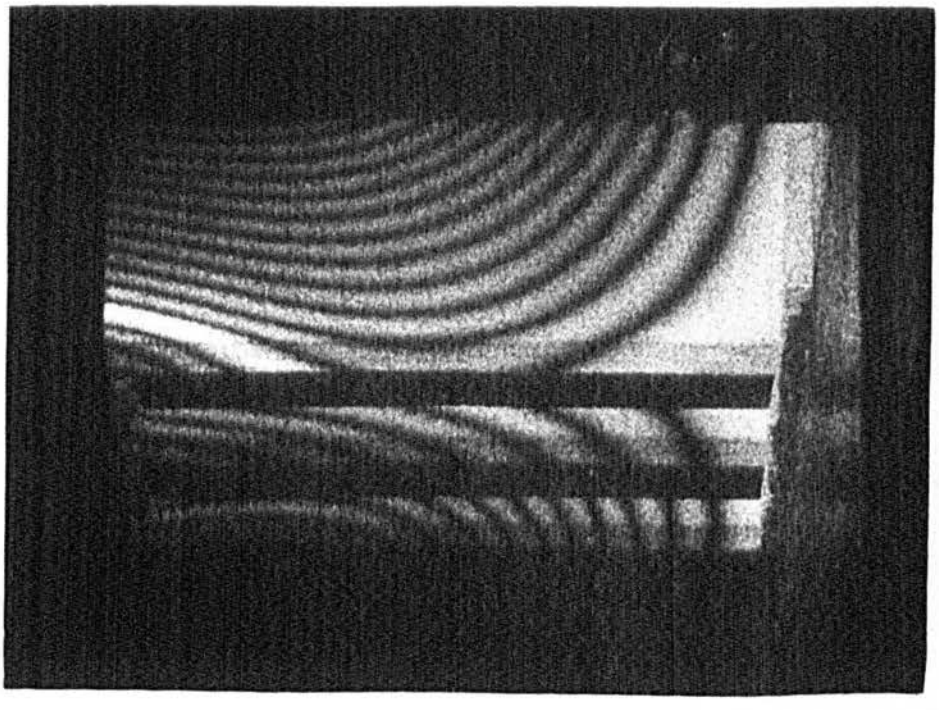

FIGURE 39 : Experimental and Predicted Mode Shapes

Model B3

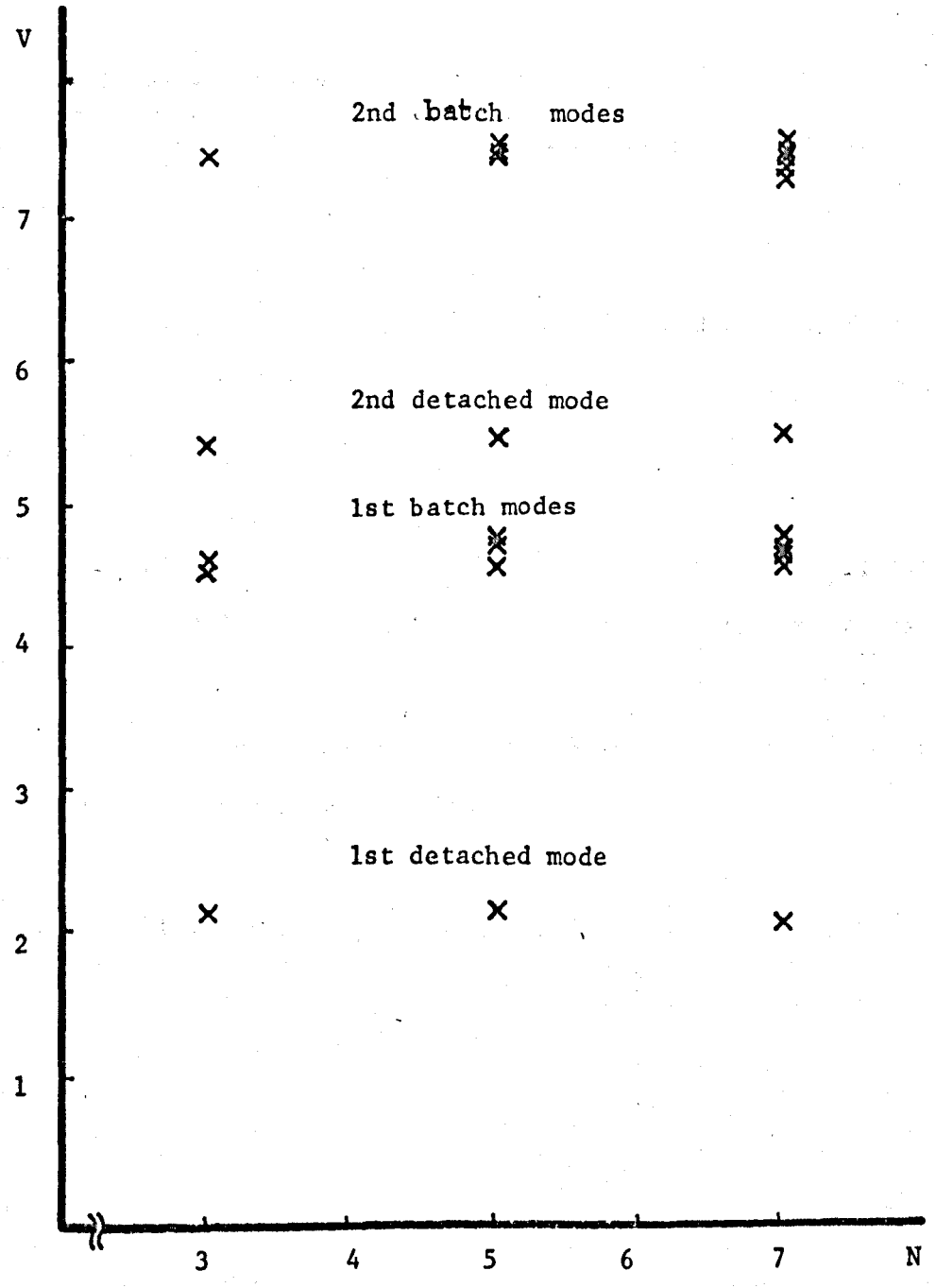

FIGURE 40 : Relationship Between Number of Blades (N) and Batch Frequency Bandwidth (Expressed in Terms of Frequency Parameter (V)

A C K N O W L E D G E M E N T S

The author wishes to express his thanks to the following:

Mr. V. C. Allen (Kingston Polytechnic) and Professor W. D. Carnegie (University of Surrey) for their advice and guidance throughout the study.

Mr. D. I. S. Chisholm (Kingston Polytechnic) and Messrs. E. Archbold and A. E. Ennos (The National Physical Laboratory, Teddington) for their help with the experimental programme.

The staff of the Computer Unit, Kingston Polytechnic for their assistance and for permitting "hands-on" use of the computers.

The Governing Body of Kingston Polytechnic for the provision of facilities for the investigation.

Mrs. P. Williamson for typing the thesis.

APPENDIX 1

Courses of Study Undertaken in Connection with the Research Programme

Courses of Study Undertaken in Connection with the Research Programme

During the period of this research programme a lecture course at Salford University on the matrix analysis of vibration was undertaken in 1974.

The conferences "The Engineering Uses of Coherent Optics" at Strathclyde University (April 1975) and "Laser Holography" presented by the Royal Photographic Society at the Institute of Electrical Engineers in 1975 were also attended.

In addition informal seminars were undertaken, covering the use of finite element methods for the analysis of vibration, at Kingston Polytechnic, and aspects of the use of Laser holography and interferometry at the National Physical Laboratory, Teddington.